8-2019

ROLE OF NUDT21 MEDIATED ALTERNATIVE POLYADENYLATION AND HYALURONAN IN THE DEVELOPMENT OF PULMONARY HYPERTENSION

Scott Dale Collum

ROLE OF NUDT21 MEDIATED ALTERNATIVE POLYADENYLATION AND HYALURONAN IN THE DEVELOPMENT OF PULMONARY HYPERTENSION

by

Scott Dale Collum B.S.

APPROVED:

Harry Karmouty-Quintana, Ph.D.
Supervisory Professor

Darren F. Boehning, Ph.D.

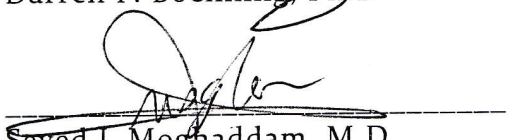

Seyed J. Moghaddam, M.D.

Ann-Bin Shyu, Ph.D.

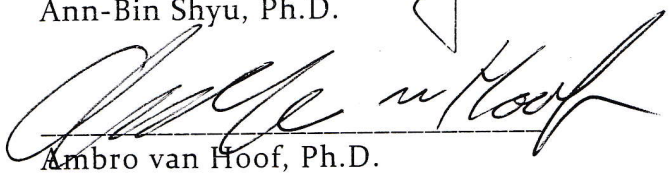

Ambro van Hoof, Ph.D.

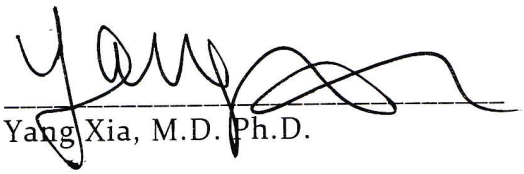

Yang Xia, M.D. Ph.D.

APPROVED:

Dean, The University of Texas MD Anderson Cancer Center UTHealth Graduate School of Biomedical Sciences

ROLE OF NUDT21 MEDIATED ALTERNATIVE POLYADENYLATION AND HYALURONAN IN THE DEVELOPMENT OF PULMONARY HYPERTENSION

A

DISSERTATION

Presented to the Faculty of

The University of Texas

MD Anderson Cancer Center UTHealth

Graduate School of Biomedical Sciences

in Partial Fulfillment

of the Requirements

for the Degree of

DOCTOR OF PHILOSOPHY

by

Scott Dale Collum B.S.

Houston, Texas

June 21, 2019

Copyright

Sections of this dissertation were based on previously published research.

- Collum SD, Amione-Guerra J, Cruz-Solbes AS, DiFrancesco A, Hernandez AM, Hanmandlu A, Youker K, Guha A, Karmouty-Quintana H. Pulmonary Hypertension Associated with Idiopathic Pulmonary Fibrosis: Current and Future Perspectives. *Can Respir J* 2017
    - Authors retain the copyright of their manuscripts, and the article is distributed under the Creative Commons Attribution License.
- Collum SD, Chen NY, Hernandez AM, Hanmandlu A, Sweeney H, Mertens TCJ, Weng T, Luo F, Molina JG, Davies J, Horan IP, Morrell NW, Amione-Guerra J, Al-Jabbari O, Youker K, Sun W, Rajadas J, Bollyky PL, Akkanti BH, Jyothula S, Sinha N, Guha A, Karmouty-Quintana H. Inhibition of hyaluronan synthesis attenuates pulmonary hypertension associated with lung fibrosis. Br J Pharmacol 2017
    - Copyrights for the written article remain with the authors, but the Wiley Publishing Group via the British Pharmacological Society has been granted the exclusive license for use of the article.
- Collum SD, Molina JG, Hanmandlu A, Bi W, Pedroza M, Mertens TCJ, Wareing N, Wei W, Wilson C, Sun W, Rajadas J, Bollyky PL, Philip KM, Ren D, Thandavarayan RA, Bruckner BA, Xia Y, Blackburn MR, Karmouty-Quintana H. Adenosine and hyaluronan modulate lung fibrosis and pulmonary hypertension in combined pulmonary fibrosis and emphysema (CPFE). *Dis Model Mech* 2019.
    - Authors retain the copyright of their manuscripts; the article is distributed under the terms of the Creative Commons BY License.

Acknowledgements

I would like to first acknowledge my advisor Dr. Harry Karmouty-Quintana. His instruction, support and guidance were key to my success in the laboratory and graduate school. His knowledge and expertise were crucial to my progression as a scientist but his accessibility and enthusiastic support helped me through any struggles inherent to research. I would like to thank him for providing me an opportunity when I most need it and the chance to investigate truly interesting science.

The faculty that formed my advisory committees during my studies; Dr. Darren Boehning, Dr. Vasanthi Jayarama, Dr. Seyed Moghaddam, Dr. Ann-Bin Shyu, Dr. Ambro van Hoof and Dr. Yang Xia also deserve thanks for their guidance and feedback during committee meetings and departmental talks. Their advice helped shape the experiments and refined my presentation skills. I would also like to thank Dr. Eric Wagner who advised me during the first three years of my graduate school experience and made me a better scientist.

I would like to thank the current and former members of the Karmouty lab; Dr. Tinne Mertens, Cory Wilson, Dr. Weizhen Bi, Nancy Wareing, Dr. Wang Wei, and Adriana Hernandez for their support and friendship during long experiments and late nights. Their assistance was important for each step of this research from planning to execution. I would also like to thank Dr. Michael Blackburn and the members of his lab for help in experiments and excellent feedback in lab meetings and journal clubs. The faculty and students of the Biochemistry and Molecular Biology department also supported me and gave much needed feedback at talks and poster presentation. The friends here made coming to lab each day enjoyable.

I would like to thank my parents, Dale and Kathy Collum, for their loving support. I would like to thank my Dad for teaching me the right way to live. He also instilled a desire to solve problems and taught me how to approach problems analytically. I would like to thank my Mom for teaching me what is right and to learn. She also instilled in me a voracious need to read and understand. Thank you for encouraging me each step in my life. I would like to thank my brother Matt Collum for exploring the world with me when I were young and for being a great friend as I have both grown up. Everything I did as a family be it traveling or mowing the cemetery made me who I am today. I want to thank my grandparents and aunts and uncles for supporting me and cheering for me in everything I do.

Finally, I would like to thank my wife, Samantha Collum, for her support and companionship in everything. Without you this journey would not have been possible. You are brave, successful and intelligent and encourage me to be the same each day. You challenge me, and indulge me. Thank you for keeping me sane and being my best friend.

ROLE OF NUDT21 MEDIATED ALTERNATIVE POLYADENYLATION AND HYALURONAN IN THE DEVELOPMENT OF PULMONARY HYPERTENSION

Scott Dale Collum

Advisory Professor: Harry Karmouty-Quintana Ph.D.

Pulmonary hypertension (PH) is a progressive disease with serious effects on quality of life and life expectancy of patients. PH is a complex disease that likely develops due to multiple influences, and no curative treatments exist for this disease. It has been shown that alternative polyadenylation (APA) due to depletion of Nudix Hydrolase 21(NUDT21) is involved in several disease states including the chronic lung disease idiopathic pulmonary fibrosis (IPF). Additionally, hyaluronan, an extracellular matrix glycosaminoglycan has been associated with PH. The role and mechanism of NUDT21 and hyaluronan have not yet been described in this disease. My results reveal that NUDT21 depletion and APA in pulmonary artery smooth muscle cells (PASMCs) is associated with phenotypic changes and PH. I I also show that hyaluronan and hyaluronan related genes play important roles in the development of Pulmonary Arterial Hypertension (PAH) and PH associated with IPF and combined pulmonary fibrosis and emphysema. I also identify 4-methylumbelliferone as an inhibitor of PH in this mechanism. These studies provide new mechanisms for understanding the development of PH and potential therapeutic targets.

Table of Contents

List of Illustrations

List of Tables

Abbreviations

4MU	4-Methylumbelliferone
ADA	Adenosine deaminase
AFM	Atomic force microscopy
APA	Alternative Polyadenylation
BALF	Bronchoalveolar lavage fluid
BLM	Bleomycin
COPD	Chronic obstructive pulmonary disease
CPFE	Combined pulmonary fibrosis and emphysema
DaPars	Dynamic analysis of alternative polyadenylation
ECM	Extracellular matrix
HA	Hyaluronan
IPF	Idiopathic pulmonary fibrosis
LVSP	Left ventricular systolic pressure
mPAP	mean Pulmonary Artery Pressure
NUDT21	Nudix Hydrolase 21
PAH	Pulmonary arterial hypertension
PASMC	Pulmonary Artery Smooth Muscle Cell
PDUI	Percent distal usage index
PH	Pulmonary Hypertension
RVH	Right ventricle hypertrophy
RVSP	Right ventricle systolic pressure
UTR	Untranslated region

Chapter 1: Introduction

A portion of this chapter, including figure 1 is adapted from a review published in the Canadian Respiratory Journal. Collum SD, Amione-Guerra J, Cruz-Solbes AS, DiFrancesco A, Hernandez AM, Hanmandlu A, Youker K, Guha A, Karmouty-Quintana H. Pulmonary Hypertension Associated with Idiopathic Pulmonary Fibrosis: Current and Future Perspectives. Can Respir J 2017

Pulmonary hypertension (PH) is a disorder of the lung vasculature. Clinically, PH is defined by an increase in mean pulmonary arterial pressure (mPAP) over 25 mmHg accompanied by a pulmonary artery wedge pressure under 15 mmHg and an elevated pulmonary vascular resistance (1). Physiologically PH includes remodeling and thickening of the pulmonary vasculature walls and a subsequent loss of luminal spaces. This loss of lumen and increase in pulmonary pressures cause an increased load on the right ventricle (RV). As the RV compensates aberrant remodeling occurs in the RV wall leading to hypertrophy and death by right-sided heart failure. The World Health Organization (WHO) classifies PH into five groups based on primary clinical diagnosis and histopathology (2). This study focused on two of the classifications; Group 1 or pulmonary arterial hypertension (PAH) which is not associated with other cardio-pulmonary diagnosis and Group 3 or PH due to lung diseases including interstitial lung diseases such as idiopathic pulmonary fibrosis (IPF) or chronic obstructive pulmonary disease (COPD).

Group 1 PH

Group 1 PH includes several diagnostic groups; heritable pulmonary arterial hypertension, drug and toxin-induced PH, PH associated with connective tissue diseases devoid of lung involvement- and congenital heart disease associated PH. Total annual prevalence of Group 1 PH is estimated to be 40-127 cases per 100,000 in large cohort studies (3-5). Five-year survival rates are 69.4% after initial diagnosis (3). This classification group contains 69.9% females with a mean age of 50 years old (5). While there are no curative treatments for Group 1 PH, several drugs may increase survival time and quality of life in patients. The most common drugs are endothelin receptor antagonists, drugs targeting the nitric oxide pathway such as phosphodiesterase type 5 (PDE-5) inhibitors or soluble guanylate cyclase activators, and prostanoids used as vasodilators (6-8). These treatments are given as monotherapies or in combination as the patient progresses (9). While strides have been made and these drugs may increase 3 year survival rates by up to 70% in some cohorts this disease is still progressive and lung transplantation or death is the final outcome (10). In heritable cases of Group 1 PH a mutation of bone morphogenic protein receptor 2(BMPR2) is found in about 80% of cases while an additional 5% of cases are associated with other members of the transforming growth factor β signaling pathway (11, 12). Many rare mutations are also associated with this heritable disease including mutations in caveolin-1 and activing-like receptor kinase 1. Group 1 PH often presents with more severe pulmonary pressure changes and plexiform lesions than other classifications of pulmonary hypertension (1). Plexiform lesions are vascular structures of the pulmonary artery that are formed of proliferative and potentially phenotypically distinct endothelial cells, myofibroblasts

and smooth muscle cells (13).

Group 2 PH

Group 2 is PH developed due to left heart disease. The prevalence of this group is the highest of the 5 WHO classifications as heart failure is one of the largest public health emergencies with over 23 million cases worldwide (14). It is difficult to establish the exact number of these patients that develop PH as it is often a consequence of progression in heart failure. The pathophysiology of the development of Group 2 PH is unique in that it begins as a mechanical stress due to increased pulmonary venous pressures due to the left heart dysfunction (15). This stress then causes damage to the pulmonary vasculature and only then do I see similar remodeling and vasoconstrictions to other forms of PH and eventual right heart changes (16).

Group 3 PH

Group 3 PH is associated with chronic lung diseases such as IPF and COPD but it also a result of chronic hypoxia, such as that encountered in high altitude environments (1). Overall Group 3 PH is more common than Group 1 PH, true incidence though must be looked at in conjunction with the associated primary chronic lung disease (17). Diagnosis of increased pulmonary artery pressures in patients with chronic lung disease is difficult as right heart catheterization is quite invasive and echocardiography is not as sensitive even with recent advances (18). The prevalence of IPF is estimate to be 14-43 per 100,000 while the prevalence of PH amongst IPF patients

is dependent upon the severity of IPF. In the early stages or when initially diagnosed, PH affects < 10% of IPF patients. However, as IPF advances, the incidence of PH increases markedly. One study of patients awaiting lung transplant, and thus in an advanced stage of IPF, reported prevalence of 32%. Subsequent studies have largely supported or increased this percentage to be between 32 and 50%. However, it is important to mention that the symptoms for PH and IPF are very similar (shortness of breath and exertional dyspnea) and as such it is conceivable for PH to be underdiagnosed in patients with IPF. Furthermore, typically the mPAP of patients with IPF is significantly lower than patients with Group 1 PH. Despite this, the presence of PH in IPF is strongly linked to the increased mortality and efforts aimed at treating PH in IPF may provide much needed therapies to diminish the mortality of IPF. IPF is a disease for which there is no curative treatment outside of transplantation, thus out of proportion PH, which disqualifies patients from transplants, is a serious confounding factor (19). The treatment options seen in Group 1 PH have not proven to be successful in Group 3 PH or have had adverse clinical outcomes (20, 21). This and the strong mortality link make understanding the mechanism of PH development critical to treating patients with a diagnosis of chronic lung disease.

COPD prevalence is much higher than IPF at 7.6% of the population (22). Similar to IPF the prevalence of PH associated with COPD is dependent on the severity of COPD. In early stage COPD as few as 10% of patients may have increased pulmonary pressures (18). In patients awaiting surgical intervention and thus having severe COPD the rates may be near 90% (23). Patients with PH associated with COPD have almost 50% increase in 5-year mortality rate (24). Five-year survival rates for Group 3 PH after

initial diagnosis are 41.4% but the identity and severity of the underlying lung disease obviously has large impacts here (3).

An additional chronic lung disease that is associated with PH is combined pulmonary fibrosis and emphysema (CPFE). This relatively recently defined disease has fibrotic deposition associated with emphysematic destruction of alveoli (25). Alone CPFE has a 5 year survival rate of 55% but when associated with PH 1 year survival rates may be as low as 60% (26). Additionally, up to 90% of CPFE patients will develop PH. As this disease has what on the surface appear to be countervailing mechanisms of fibrotic deposition and destruction of alveoli, it is important to discover the molecular mechanisms that can contribute to both events. While there have been multiple gene mutations associated with CPFE these mutations have not yet been shown to be widespread, as their discovery was part of familial cohorts or case studies (27). Unfortunately, treatment of CPFE or Group 3 PH overall, is limited to controlling symptoms and lung transplantation (28).

A more distinct form of Group 3 PH is associated with hypoxia at high-altitude. This type of PH can both be acute and chronic (29). In acute high-altitude PH patients can develop increased pulmonary pressures very quickly due to an excessive vasoconstriction caused by hypoxia (30). In fact, acclimatization does not appear to reduce increases in pressure but does reduce symptoms, potentially by subtle remodeling of the vasculature to better protect from increased pressures (31). Additionally, changes seen in this group are reversible by returning to low altitudes. Chronic high-altitude pulmonary hypertension is a threat to the more than 140 million people living above 2,500 m elevation. It is estimated that in these populations 5-18% of

residents will develop high altitude PH (32). Healthy residents at high altitude have thickened pulmonary artery walls that may form before birth (33, 34). This remodeling is not the key driver for this PH as even in chronic cases aberrant vasoconstriction appears to be the most important mechanism of increased pressure. Patient with this disease are encouraged to move to low altitude which will manage the disease but many pharmacological interventions have shown promise with none moving to widespread use. Most promising are experiments with fasudil as well as acetazolamide, a carbonic anhydrase inhibitor, which has several larger studies with excellent results (35, 36).

Group 4 PH

Group 4 PH is PH developed due to a chronic thromboembolic disease. Patients that develop a pulmonary embolism, especially those with coagulation disorders or autoimmune disease, are at risk though less than 4% of these patients will develop the chronic disease (37, 38). An unresolved pulmonary embolism causes occlusion of pulmonary vessels causing increased localized pressures and shear stress. This in turn results in remodeling of the affected vessels (38). As this is most often confined to one section of the lung, surgical intervention to remove the blocked vessel is often effective (39).

Group 5 PH

Group 5 PH is PH with unclear multifactorial mechanisms. This classification is a catchall for PH that is associated with disease states not incorporated in the other

groups (2). As this is a diverse group little research links the mechanism of this group. The most well described disease associate with Group 5 PH is sickle cell disease which can lead to PH due to left ventricle dysfunction or vascular stress caused by hemolysis, embolisms or hypoxia (40).

Though the exact number of patients affected by all classifications of PH are hard to calculate, the patients impacted by these diseases have severely reduced quality of life and have much lower life expectancy. With the rise in cases of chronic lung disease in recent decades and the lack of treatment options, it is important to thoroughly understand the molecular and cellular mechanisms that underpin how PH develops. Only by this understanding can novel treatment options be explored.

Disease Mechanism

The primary mechanisms involved in the increase of pulmonary vascular pressures in PH are increased vasoconstriction and sustained vascular remodeling. Many cell types have been shown to be involved in the development and progression of PH including pulmonary artery endothelial cells, fibroblasts, and immune cells such as macrophages. Vascular endothelial cells are the inner most cells of the pulmonary vasculature, as such they are often the first cells damaged by stress events that initiate remodeling seen in PH. Endothelial cells also have strong signaling connections with pulmonary artery smooth muscle cells (PASMCs) through endothelin-1 and nitric oxide signaling as well as many growth factors (41, 42). Vascular inflammation is a key characteristic of PH and as such macrophages have been implicated in multiple roles during the development of PH (43). Blocking macrophage activity or development has

shown efficacy in halting or reversing PH in some model (44, 45).

PASMCs are very involved in both vasoconstriction and vascular remodeling. This makes PASMCs an exciting target for research hoping to understand the underlying molecular mechanisms that contribute to PH. While PASMCs of the proximal pulmonary arteries have a heterogeneous phenotype the cells of the distal pulmonary arteries, which are more involved in PH development, have a more uniform phenotype (46, 47). These PASMCs have a well differentiated phenotype that expresses many factors indicative of a contractile capacity and a low proliferative potential. These cells are key in modulating vascular tone that allows for control of pulmonary artery pressure and changes in flow rate seen during periods of activity (48). In a healthy pulmonary artery, there are three regions when viewed cross-sectionally. The inner layer is the intima comprised of pulmonary artery endothelial cells. Next is the medial layer of PASMCs and finally the adventitial layer which signals the transition to other lung structures, is comprised of other cell types including fibroblasts. In a PH artery, the intima may be infiltrated by smooth muscle cells, the medial smooth muscle cells will proliferate and hypertrophy while the adventitial layer will have increase in fibroblasts and macrophage infiltration (40). These changes contribute to the main pathological signs of PH, medial hypertrophy leading to reduced lumen in previously muscular arteries and increased abundance of muscular arteries due to muscularization of peripheral arteries and potentially plexiform lesions (1).

PASMCs undergo many phenotypic changes during the initiation and development of PH. Early in the development it has been shown by many experimental models that there is an increase in proliferation. This was first seen in the rat hypoxia

model in which there was a small amount of medial PASMC proliferation increase and confirmed in the monocrotaline rat model where there was observed a more robust increase in proliferation (49, 50). The hypoxia model of rat pulmonary hypertension treats the rats with 14 days of hypobaric hypoxia (49). In the monocrotaline model rats are treated with a single dose of monocrotaline which causes pneumotoxicity. After 14 days the pulmonary arteries are very inflamed and PASMCs are contracted and by day 22 there are right ventricle dysfunctions (51). Of interest is that despite the differences in these two models in showing a change in medial PASMC proliferation both models show a very significant increase in the number of muscularized vessels indicating not just a concentric increase in PASMC but also spreading of these cells to more distal portions of the arteries (52). As more models of PH have been developed, these changes in proliferation have been more precisely studied. More recent studies have confirmed the early increase in proliferation seen but indicate that this proliferative capacity decreases as the model continues and the cells potentially progress into a second phenotype change (53). This has been observed in the mouse Schistosomiasis model and in one of the more utilized models of PAH, the hypoxia-sugen rat model (53, 54). The Schistosomiasis model involves inoculating mice with *Schistosoma mansoni* and then a second hit with i.v. administration of *S. mansoni* eggs. Seven days after administration of the eggs, PH develops in an IL-13 dependent mechanism (54). The hypoxia-sugen model treats mice with 28 days of 10% oxygen and four treatments with a vascular endothelial growth factor inhibitor leads to increased pulmonary pressures and remodeling (55). PASMC proliferation provides for the medial thickening seen in the development of PH and provides an increased pool of PASMCs to participate in the

other abnormal phenotypes that are introduced below.

Another phenotypic change seen in PASMCs during the development of PH is an increase in cellular tone. During exercise the cardiac output of the right ventricle will increase to provide for more oxygen delivery (56). To minimize the increase in pulmonary artery pressure due to this increase in right heart effort the pulmonary arteries relax, allowing for a reduction in pulmonary vascular resistance. In fact, in a multi-study analysis it was seen that the slope of the relationship between mPAP and cardiac output in an individual can vary by as much as 6 fold when a stable linear relationship would be seen in a non-contractile system (57). If this relaxation does not occur then pulmonary pressures will increase as seen in PH. As with many other key cellular signaling events, Ca^{2+} activated response controls the contractility of PASMCs (58). Since Ca^{2+} signaling has other outputs, many studies have worked to understand the signaling necessary for the contractile response in PASMCs. A key phosphorylation event is the phosphorylation of myosin regulatory light chain (59). The levels of this phosphorylation are controlled by the interplay of calcium-calmodulin dependent myosin light chain kinase and the MLC phosphatase (60). PASMC contractility is not controlled by a change in Ca^{2+} but by a calcium sensitization caused by the Rho-kinase (ROCK) dependent phosphorylation of myosin targeting phosphatase subunit (60). ROCK is previously activated by Ras-homology A(Rho) in its GTP bound state (60). This sensitization ends when regulatory proteins cause RhoA to cleave GTP (61). These proteins and the nucleotide exchange factors are under tight control, allowing for multiple upstream pathways to control PASMC contractility (62). As there are many signaling pathways controlling PASMC contractility it is of no surprise that in PH many

pathways and signaling mechanisms can lead to increased vascular tone. One of the mediators involved is endothelin. Endothelin-1 is released from pulmonary artery endothelial cells due to stress and signals through the Endothelin receptor B (63). This signaling leads to Ca^{++} dependent signaling changes through IP_3 (64). This complex control of contractile response in PASMCs allows for fine tuning of the vascular resistance in healthy individuals and maintains a suitable pulmonary artery pressure but allows for changes in signaling in a disparate set of pathways to abnormally control this contraction in the development of PH.

An additional change seen in PASMCs is an increase in the production of extracellular matrix (ECM). The ECM is a combination of proteins and polysaccharides surrounding the cells of every tissue. The exact make up of ECM in each tissue varies and ECM is dynamically produced and degraded (65). The ECM does not only provide a structural lattice for cellular components of tissues but also plays an important role in signaling many cellular activities including proliferation, migration and cellular distribution through interactions with many signals including growth factors (66). The main protein component of all tissue and of the ECM is collagen, a protein whose many functions and interactions are only rivaled by the many classifications and variants expressed. Collagen provides tensile strength, cell interactions, migration and tissue polarization cues. A second ECM protein is elastin, a highly crosslinked protein that helps provide stretch and recoil to tissues. The third major protein in ECM is, in concert with collage, which is very important in the development and presentation of many chronic lung diseases including PH and IPF is fibronectin (FN). FN has been implicated in a feedback loop that keeps PASMCs in a synthetic phenotype with increased

proliferation (67, 68). The other molecule type that composes a large portion of the ECM are glycosaminoglycans. These polysaccharides are usually found covalently bound to a variety of ECM proteins and provide interactions and help provide a strong and hydrated matrix (69). These proteoglycans often are helper proteins in cell surface receptors (70). One exception to extracellular glycosaminoglycans being covalently bound to proteins is hyaluronan (HA). This molecule instead binds to many ECM proteins and cell surface receptors such as CD44 through specific binding motifs called Link domains, though as the catalogue of HA binding proteins expands some lack this domain (71). This molecule will be further introduced later in the thesis. During the development of PH, a population of PASMCs may switch into a synthetic phenotype which can deposit these ECM components. This deposition allows for multiple effects. The modified ECM can feedback into the PASMCs maintaining an abnormal phenotype (67). The new ECM can provide a foundation for cell adhesion and immune cell infiltration into the vasculature (72). Finally, the excessive ECM can cause mechanical stiffening to the pulmonary vasculature and physical block to gas exchange (73). Together these PASMC dependent ECM changes contribute to many of the other phenotypic changes seen in the development of PH and provide an important research subject.

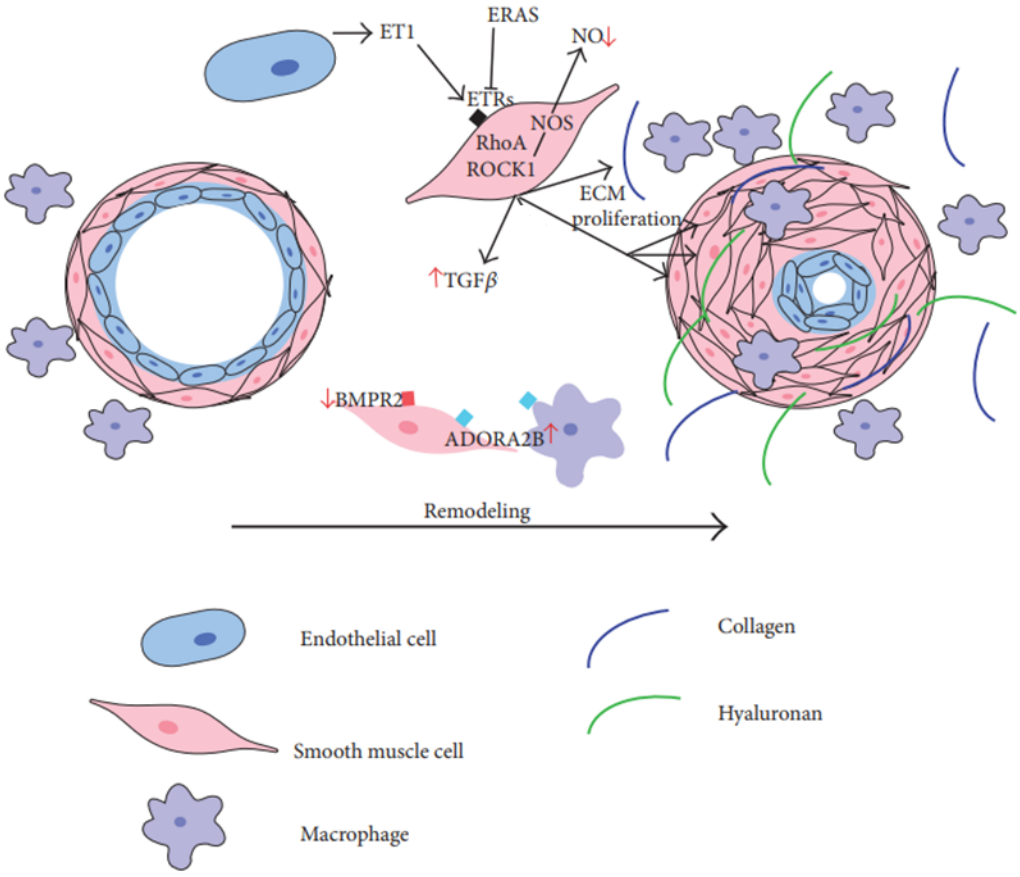

Figure 1 Vascular Remodeling

Adapted from Pulmonary Hypertension Associated with Idiopathic Pulmonary Fibrosis: Collum SD, Amione-Guerra J, Cruz-Solbes AS, DiFrancesco A, Hernandez AM, Hanmandlu A, Youker K, Guha A, Karmouty-Quintana H. Pulmonary Hypertension Associated with Idiopathic Pulmonary Fibrosis: Current and Future Perspectives. *Can Respir J* 2017

Chapter 2: Background

RNA Processing

Transcription of protein coding mRNAs by RNA polymerase II is the first step in turning genetic information in the DNA of cells into molecules that can maintain the homeostasis of the cells, decide cell fate, and provide the functional capacity for this fate. It is not surprising then that transcription is a process involving many steps each of which is complex and must be tightly regulated. To properly discuss the final step in transcription, cleavage and polyadenylation, it is useful to briefly discuss the transcriptional processes that precedes it. The basic structure of a viable, stable and translatable mRNA is to contain a 5' m7G cap, a 5' untranslated region (UTR), the coding sequences containing a start codon and a final stop codon, a 3' UTR and finally a poly(A) tail of many adenosine monophosphates.

The first step of transcription is initiation. During this process five general transcription factors assemble with RNA pol II to form the preinitiation complex. This complex recognizes the DNA regions that most eukaryotic RNA pol II genes contain called the TATA-box and the TFIIB recognition element. These sites are about 30 bases upstream of the transcription start site and allow for proper positioning of the transcription complex. This site recognition can be modified by transcription cofactors and enhancer regions and the proteins that bind them called activators and repressors. Control of transcription initiation is provided by large protein complexes interacting with each other and DNA over 100 Mb away (74). After initiation of a stable complex the RNA pol II begins elongation adding nucleotides sequentially to the 3' of the nascent

mRNA. After 25-30 nucleotides the capping enzyme is recruited by a phosphorylated serine on the RNA pol II and carries out three enzymatic steps to cap the mRNA. The final step in this cap addition, the methylation by RNA guanine-N7 MTase can be also controlled in a cell cycle manner by CDK1-cyclin BI (75). Another co-transcriptional mRNA processing event that begins during elongation is splicing. Similar to the recruitment of the capping enzyme by RNA pol II the spliceosome, a large complex of proteins and small nuclear ribonucleoproteins, is recruited by a C-terminal domain phosphorylation (76, 77). The spliceosome then recognizes splice sites within the pre-mRNA and removes intervening sequences that do not form a portion of the mature RNA (78). Splicing was discovered to not be a constitutive process but to have many variations and controls. In fact alternative splicing has helped to explain the disconnect between the number of putative genes and mature proteins that are produced, as it has been discovered that at least 70% of human genes undergo alternative splicing in tissue or developmental regulated manner (79). It is also calculated that up to 60% of human heritable diseases involve a splicing change due to mutation (80). Splicing provides yet another process to control mRNA processing. The final step in transcription and maturation of RNA pol II mRNAs is cleavage and polyadenylation. This process involves the recognition and enzymatic cleavage of a cleavage site and then the addition of a poly(A) tail, this is known as cleavage and polyadenylation.

Cleavage and polyadenylation

Cleavage and polyadenylation is carried out at a location of the pre-mRNA

defined by a set of sequence signals of which are relatively well conserved with potential activity with major mutations and a set of more diffuse and weaker signals that stabilize the more conserved signals (81). These signals do vary by species so here is described the signal elements for mammals. The first and strongest signal is a hexamer sequence AAUAAA just upstream of the cleavage site. Other similar hexamers have much reduced processing activity while AUUAAA and AGUAAA retain 80% and 30% respectively (82). The first synthetic poly(A) site consisted of this hexamer and a U/GU rich sequence 22 nucleotides downstream (83). Besides these strong signals there is an U-rich region within 100 nucleotides upstream and downstream as well as potential G-rich elements more than 30 nucleotides downstream (84). The RNA sequence UGUAN can also act as a strong promotor of cleavage and polyadenylation and is often found upstream of the PAS (85). Cleavage and polyadenylation is carried out by a protein complex that is known to have greater than 80 associated factors. Of these associated factors 19 proteins make up the core of the machinery (86). The cleavage and polyadenylation specificity factor (CPSF) is a sub-complex made of six required proteins; WDR33, CPSF30, CPSF160, hFip1, CPSF100, and CPSF73. WDR33 is the protein that binds the AAUAAA hexamer while CPSF30 and CPSF160 assist in this recognition and binding (87, 88). While both CPSF100 and CPSF73 contain metallo-β-lactamase and β-CASP domains it is CPSF73 that cleaves pre-mRNAs (89). The CstF complex is a trimeric complex that recognizes downstream elements in the PAS. It consists of CstF64, CstF77, and CstF50 (90). Together these proteins recognize U/GU rich regions as well as modulating some protein interactions outside the cleavage and polyadenylation machinery (91, 92). Symplekin is a protein that acts as a scaffold for the arrangement of several of the

subcomplexs of the larger cleavage and polyadenylation complex (93). The mammalian cleavage factor I is made of 3 proteins, Nudix Hydrolase 21 (NUDT21), CPSF6 with two splicing isoforms, and CPSF7 (94). NUDT21 binds the UGUAN while forming a dimer with itself and potentially a tetramer with a dimer of one of its complex partners (94). When in this tetramer with CPSF6 it is known that this binding to RNA can cause a looping which is theorized to be important in recognition of a proper cleavage and polyadenylation site and alternative polyadenylation (APA) (95, 96). The mammalian cleavage factor II complex contains up to 20 proteins but only (Cleavage and Polyadenylation Factor Subunit 1 (Clp1) and Pcf11 have been well characterized. Clp1 appears to assist in the assembly of CFIm and CPSF while Pcf11 is essential for degradation of the remaining nascent RNA after cleavage (97, 98). The final proteins considered part of the core cleavage and polyadenylation machinery are Poly(A) Polymerase Alpha (PAP) and Poly(A) Binding Protein Nuclear 1 (PAPBN1) which add the poly(A) tail. PAP catalyzes the reaction adding adenosines in a template-independent manner while PABPN1 binds the tail as it is added and increases the catalytic rate of PAP (99, 100). Additionally the C-terminal domain of the RNA pol II is again key in recruiting the factors discussed here (101).

Alternative Polyadenylation

Alternative polyadenylation is a process in which an pre-mRNA with multiple poly(A) signals may use a non-canonical site. While this mechanism of regulating mRNAs was first proposed and discovered in a few specific cases in the 1980s, amongst others the IgM heavy chain and dihydrofolate reductase, it was not until more

sophisticated techniques in the modulation of protein levels and RNA quantification were developed that the true scope of this process could be recognized (102, 103). With the advent of next generation RNA sequencing technology the ability to identify APA events as a result of many diseases or manipulated protein levels showed that at least 69.1% of human genes have multiple poly(A) sites (104). There are four basic types of APA as grouped by the location of the non-canonical poly(A) site. The first and most easy to visualize is tandem 3'UTR APA which occurs when there are additional poly(A) sites within a single 3'UTR. Tandem 3'UTR APA is the only type which generates an identical protein coding sequence and thus this form of APA has a more difficult effect to study (105). Alternative terminal exon APA creates a new terminal exon and 3'UTR while intronic APA is similar but also retains a canonically spliced intron (105). Finally is internal exon APA which maintains the typical splicing pattern but cleavage recognizes a typically ignored sequence within one exon which is the most rare of APA events (106). The rest of this thesis will focus on Tandem 3'UTR APA as while this type does not affect the coding sequences changes in the 3'UTR length can affect the stability, translation efficiency, and cellular localization of mRNAs through loss of miRNA binding sites and RNA binding protein sites (Figure 2). These changes will affect signaling, disease processes, and development.

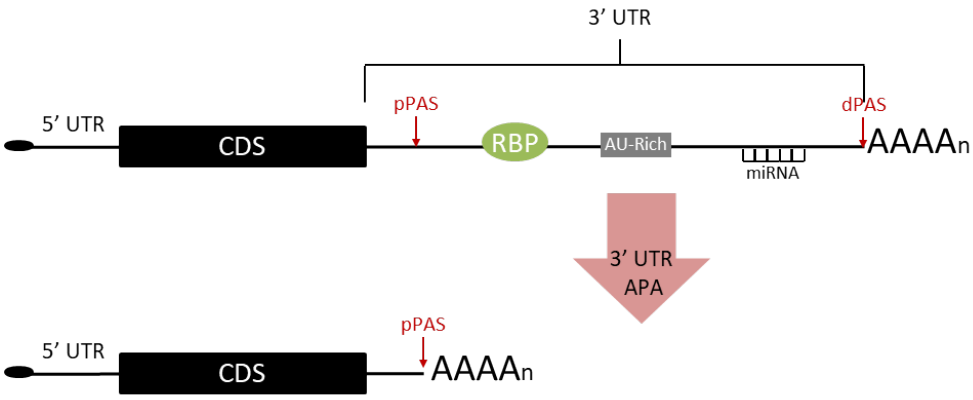

Figure 2 3'UTR APA

Regulation of APA

As can be seen by the large number of complexes that interact during transcription and cleavage and polyadenylation, it is not surprising that many factors can modulate the occurrence of APA events. APA can be controlled by simple kinetics of transcription where pausing increases nearby poly(A) site usage (107). Additionally the efficient recruitment of cleavage and polyadenylation complex by RNA pol II and transcriptional activating proteins early in transcription can influence poly(A) site usage (85). Many RNA binding proteins also regulate APA events. Two examples are SR proteins Serine and Arginine Rich Splicing Factor 3 (SRSF3) and Serine and Arginine Rich Splicing Factor 7(SRSF7) were first discovered to regulate splicing but have also been observed to lengthen and shorten 3'UTRs of mouse cells (108). Splicing is also linked to the control of APA. To avoid premature cleavage and polyadenylation U1 snRNP inhibits poly(A) site usage in introns in a process termed telescripting (109). Telescripting may also play a role in APA of genes during periods of transcriptional upregulation (110). Of great interest is the effect of the cleavage and polyadenylation

complex levels on APA. Changes in the levels of each of the core components appear to have different effects. Increases in CSTF64 was seen to increase CSTF complex and increased the usage of a proximal poly(A) while downregulation of expression leads to global lengthening in HeLa cells (102, 111). This suggests that the CstF complex may follow this trend.

In stark contrast to APA changes seen by modulating levels of CSTF64, down regulation of CFIm complex members leads to a strong shortening on a global level (112). Of note the most robust 3'UTR shortening seen is with the knockdown of NUDT21 (113). This change has now been seen to play a role in multiple disease states.

NUDT21 Regulated APA and Disease

As the role of CFIm complex members in controlling APA was being discovered, multiple diseases were found in which levels of NUDT21 were modified as was global poly(A) site usage. One of the first studies that linked NUDT21 to a disease was by Masamha et al. which described the role of CFIm25 (NUDT21) in glioblastoma tumor suppression (113). In this paper it was described that in cell culture human glioblastoma cells had lower levels of NUDT21 and that this directly contributed to a more proliferative phenotype as well as a more aggressive tumor in a xenograft mouse tumor model. This study also identified 1450 genes that underwent APA with NUDT21 knockdown. An additional disease in which NUDT21 was found to play a role was pulmonary fibrosis (114). In this study by Weng et al. reduced NUDT21 induces APA in many genes in lung fibroblast and leads to worsening fibrosis in the bleomycin mouse model. Additionally, a knockout of NUDT21 contributed to increased expression of

collagen fibronectin and TGF-βR1. APA induced by NUDT21 level changes has been implemented in many changes in other cancers including hepatocellular carcinoma in which cellular migration and invasion are increased with depleted level as well as in osteosarcoma in which similar changes are seen (115, 116). NUDT21 copy number changes also play a role in the neuropsychiatric disease Rett syndrome by controlling levels of the protein MeCP2 (117).

NUDT21 regulated APA has been shown to play a role in several diseases including the chronic lung disease IPF. This APA is also associated with changes in cell proliferation and cell migration as seen in the study on glioblastoma. These changes in cell phenotype may resemble changes seen during the initiation and development of PH and provide a unique opportunity to discover a mechanism of disease progression. This thesiswill describe a role for NUDT21 in PH.

Hyaluronan

Hyaluronan is a non-protein component of the ECM with a repeating disaccharide structure of N-acetyl-glucosamine and glucuronic acid. HA is produced in mammals by three hyaluronan synthases (HAS), 1-3. These synthases produce HA in a broad range of molecular weights, generally above $2x10^5$ Da with HAS2 generally producing at molecular weights an order of magnitude higher than the other enzymes. HAS2 is an essential gene for mouse embryonic development but a double knockout of the other enzymes is viable with abnormal wound healing. Offsetting these HA producing enzymes are four hyaluronidase isoforms (Hyal1-4). Of these, Hyal2 has shown to be the most necessary with deficient mice accumulating HA in the heart and

developing severe cardiac phenotypes (118). Hyal1 and Hyal3 deficient mice show minor changes in skin dendritic cells and alveolar structure respectively (119). While some of the effects may seem minor, Hyal are quite important as in humans one third total HA is turned over each day, either absorbed by cells by endocytosis or cleared from the blood by liver endothelial cells (120). HA can also be degraded in an uncontrolled manner by reactive oxygen species (121). As with other ECM components, HA is bound by many proteins including proteoglycans. This forms a complex mesh that may play a role in organizing activities and signaling in the ECM in a structure referred to as pericellular matrix or glycocalyx (122). HA conformational changes by TSG-6 through heavy chain transfer from inter-α-inhibitor, as well as binding to versican and aggrecan may modify this structure (123). This higher order structure also plays a role in development and in cancer cell survival (124, 125). One of the most described HA receptors is CD44. This receptor also binds other ECM components such as collagen and fibronectin but has HA dependent activity that results in cell motility and inflammation changes as well as HA clearance (126). Another important receptor of HA is Receptor for HA-Mediated Motility (RHAMM) which has been linked to proliferative responses and motility in smooth muscle cells as well as participating in acute lung injury (127, 128). Additionally Hyaluronic Acid Receptor for Endocytosis (HARE) and Layilin act as HA receptors in certain cell types where they are associated with endocytosis activation and epithelial barrier function respectively (129-131). HA plays a role in many biological functions by interacting with special domains in cell surface receptors and other ECM components. These functions include cell fate and organ development, injury response, cell migration including cancer progression, as well as

playing an important role in maintaining a well hydrated matrix (120). However, depending on the context HA seems to have contradicting effects. One of these contradicting effects in the seeming opposing forces of high molecular weight(HMW) HA in an anti-inflammatory activity and low molecular weight(LMW) HA in a pro-inflammatory activity (132). While it is suggested that receptor interaction changes due to molecular weight could play a role here, it is also indicated that inter-α-inhibitor modification of HMW HA is reversible while LMW modification is not reversible (133). This is important because inter-α-inhibitor modification greatly increases inflammatory cell recruitment by HA (134). Early studies on the effect of HA on proliferation showed a marked decrease in cellular proliferation when treated with HA (135). As studies began to look at more cell types and cells in different conditions it was found that HA can robustly increase proliferations in other circumstances (136, 137). While it has been shown that this is at least partially due to differences in molecular weight, it is also linked to differences in receptor recognition and downstream signaling (136). Additionally, LMW HA is strongly linked to angiogenesis through the ephrin receptor A2 (138). Refer to (Figure 3) for an illustration of the HA pathway.

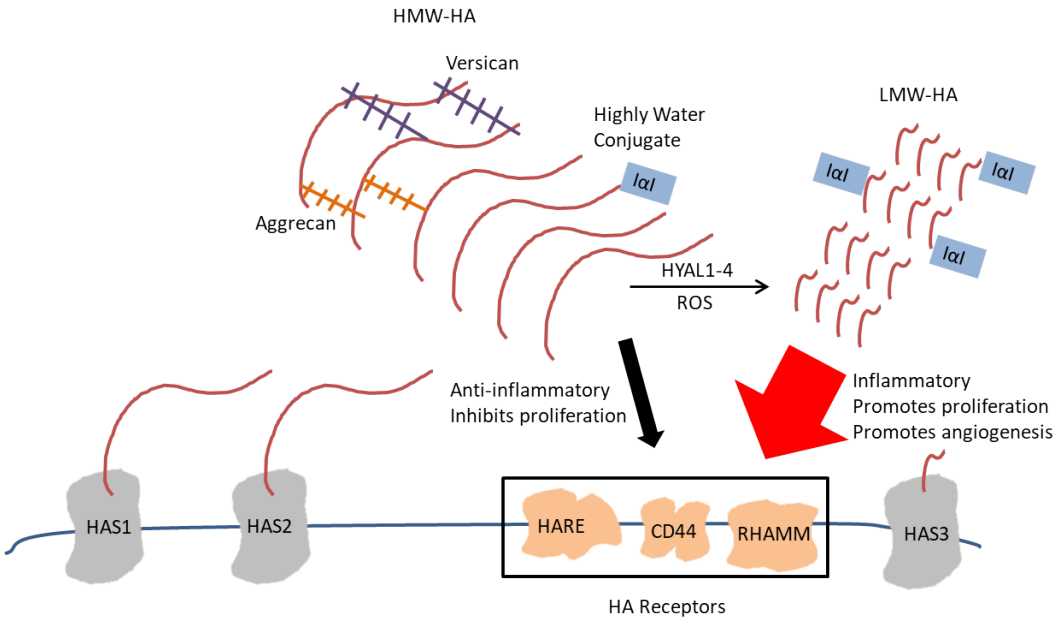

Figure 3 Hyaluronan Enzymes and Interactions

Hyaluronan and Disease

Altered Hyaluronan production and degradation have been associated with various diseases. Extensive research has shown that HA and HA related enzymes play important roles in cancer, especially in cell survival, proliferation, and metastasis (120). Colon and breast cancer lines express high levels of Hyal1 and Hyal2 as well as CD44 and depletion of HAS2 resulted in reduced cancer phenotypes (139-141). HA levels in the serum of diabetic patients are raised and adipose CD44 signaling has also been associated with this disease (142, 143). HA overexpression in mouse models of atherosclerosis leads to increased plaque formation, potentially through CD44 signaling in macrophages and smooth muscle cells (144, 145).

HA has been found to play an important role in multiple lung diseases. As HA regulates inflammation, it is not surprising that HAS2 mutations have been found to be associated with asthma (146). Additionally, HA is elevated in asthma patients and increased HA is related to worsened symptoms (147). Cells isolated from patients have elevated HAS2 levels and produce lower molecular weight HA than cells from healthy patients (148). HA level changes are associated with COPD, where augmented levels of HA and HAS2 expression has been reported (149). Some groups looking at specific subsets of COPD patients or looking specifically at airway smooth muscle cells have reported reduced levels of HA, HAS1 and HAS2 (150, 151). Increased HA deposition is also associated with IPF. Patients with IPF have increased HA in the bronchoalveolar lavage fluid compared to healthy individuals (152). Additionally, fibroblast cultured from these patients show increased HA deposition with increased HAS2 expression (153). The bleomycin mouse model also shows increase HA deposition while HAS2

knockout mice show improvements in fibrosis (153). Exogenous hyaluronidase treatment in this model has been shown to attenuate fibrosis (154). Of note, increased HA levels have been observed in patients with Group 1 PH, associated with increased HAS1 and HYAL1 expression (155). Excessive HA has also been observed in the plasma of patients with PH associated with congestive heart failure and COPD (156). This association has also been observed in the rat monocrotaline model as well as the adenosine deaminase (ADA) deficient mouse model of lung injury (157, 158). This evidence along with the role of HA in eliciting cellular response similar to those seen in PASMCs in PH indicates that the role of HA in PH should be further investigated. This thesis will untangle some of this pathway in PH.

Dissertation Overview

PH is a chronic lung disorder with increasing prevalence which has a great impact on the quality of life and mortality of hundreds of thousands each year (1, 5). PH patients typically have 5 year survival rates below 70% and PH is a common and significant comorbidity with other chronic lung disease, serving as one of the most significant indicators of poor prognosis (3). One of the patient groups greatly affected by PH is those that also present with chronic lung diseases such as IPF or COPD (1). Within this cohort of patients with chronic lung diseases, patients presenting with a rare presentation of combined pulmonary fibrosis and emphysema (CPFE) have a higher prevalence of PH (19). Up to 90% of CPFE patients develop PH and this diagnosis reduces the survival rate from 55% for 5-year to 1-year survival rates of only 60% (159). Understanding the molecular and cellular mechanism that give rise to these diseases is important as few therapies exist and no curative treatments are available outside of lung transplantation (7). This thesis explores two such mechanisms; NUDT21 induced APA and increased HA deposition.

Previous studies have indicated that APA is an important regulatory mechanism during the transcription of mRNAs (105). APA events induced by reduced level of NUDT21 have been implicated in cancers and IPF (113-115). In some diseases NUDT21 depletion correlated with increased proliferation and changes in cell migration similar to those seen in the PASMCs during PH progression (113). The role of NUDT21 in controlling the phenotype of PASMCs has not been described and no link to PH has yet been proven.

HA is a glycosaminoglycan that makes up a large portion of the lung ECM. This molecule is an important structural component linking many proteins together and often controlling cell adhesion, while also being an important signaling molecule binding several receptors including CD44 and RHAMM in vascular smooth muscle (127, 160). In disease states such as IPF, HA synthesis and degradation are dysregulated and increased levels of HA have been measured in patients and animal models of PH and secondary to fibrosis and other lung injuries (153). A complete understanding of the role of HA and the many enzymes involved in its production, degradation, and signaling in PH has not been gained. **This project hypothesizes that NUDT21 depletion and aberrant HA accumulation are important drivers of PH through changes in PASMC phenotype**

Specific Aim 1: Determine the role of NUDT21 depletion and subsequent APA in the development of PH.

Patient samples and healthy controls were measured for NUDT21 and other CFIm complex member levels by immunohistochemistry staining and western blotting showing decreased levels. Using the hypoxia-sugen mouse model and the NUDT21$^{F/-}$ Tagln-CreKI mouse line it was shown that depletion of NUDT21 contributes to worsened PH symptoms. In cell culture of healthy and PH PASMCs it was shown that low NUDT21 levels are associated with increased proliferation and reduced migration in a Boyden chamber assay. The results of this aim are presented in **Chapter 3**.

Specific Aim 2: Determine the role of hyaluronan in the development of pulmonary hypertension.

I show that 4-Methylumbelliferone (4MU), a drug that inhibits HA production, is sufficient to reduce PH symptoms in the hypoxia-sugen model of PH and bleomycin model of lung fibrosis and PH. It was also shown that deletion of HAS2 from the PASMCs of mice in the hypoxia-sugen model reduces PH. HA, HAS1 and HAS2 levels were seen to be associated with PH by western blot and RT-PCR. These results were recapitulated in the bleomycin model of lung fibrosis and PH. PASMCs treated with small fragments of HA present with increase proliferation, migration and stiffness, all hallmarks associated with PH. These results are presented in **Chapter 4**.

Specific Aim 3: Determine the role of HA in PH associated with CPFE.

CPFE is complicated disease in which PH plays an important and deadly role. Patient samples of this disease show an increase in HAS3 expression and HA accumulation. A novel model of CPFE, adenosine deaminase ($ADA^{-/-}$) deficient mice, confirmed these findings. Here I show that 4-MU reduced HA levels in the $ADA^{-/-}$ mouse model of PH. These findings were associated with a reduction in fibrotic deposition and PH, though no changes in airspace enlargement were seen. As the $ADA^{-/-}$ model recapitulates adenosine accumulation and signaling seen in CPFE patients, I showed that HAS2 and HAS3 are upregulated in an adenosine A2B receptor dependent manner in vitro. The results of this aim are presented in **Chapter 5**.

Identifying novel mechanisms that contribute to the development and progression of PH will lead to increased understanding of the pathogenesis of disease and eventually newly targeted therapies for the treatment of PH. The pathways described here are exciting new mechanisms that control the phenotype of PASMC and may be directly responsible for a portion of the vascular remodeling seen in PH as well as one of the first mechanisms described for the progression of CPFE.

Chapter 3: Loss of NUDT21 links APA with PH

Introduction

The vascular changes associated with PH include aberrant proliferation, cell growth and abnormal vasoconstriction and the development of complex vascular lesions (161). These changes in cell phenotype happen in several cell types but here I will focus on PASMCs as they form the large medial section of pulmonary arteries and can provide multiple mechanisms of vascular changes (162). Understanding the molecular pathways that lead to changes in PASMC phenotype is important in understanding the initiation and development of this disease. As APA has been recently described as a driver of multiple disease states, most provocatively in cancer and IPF, I hypothesize that NUDT21 loss and resulting APA may contribute the the development if PH by altering the PASMC phenotype (114, 163).

The addition of poly(A) tails is a key process in the maturation of mRNA. An mRNA containing multiple polyadenylation sites in the 3'UTR may undergo a process known as 3' UTR APA, in which the non-canonical polyadenylation site is used, leading to an alternate transcript (164). As these alternate polyadenylation sites often occur early in the 3'UTR a hallmark of this APA is 3'UTR shortening that leads to loss of binding sites for regulatory elements such as miRs allowing transcripts to escape mRNA regulation resulting in heightened levels of affected transcripts as well as allowing for changes is translation efficiency(112). Depletion of NUDT21, a RNA binding protein in the CFIm complex, is an important driver of 3'UTR APA (113, 165). This type of APA has been found to drive cell proliferation and invasion in cancer (113). While NUDT21

depletion can cause a few examples of other types of APA introduced in Chapter 2, this research will focus on 3'UTR APA (112). As many of the hallmarks of cancer, including; sustained proliferation, resistance to cell death, angiogenesis, and invasion, are recapitulated in the cells of patients with PH, especially PAH, I focused on the role of NUDT21 driven APA to control the phenotype of PASMCs and contribute to PH (166).

My results reveal that NUDT21 is depleted in isolated PASMCs of patients with PH, both Group 1 and IPF + PH. This depletion was also recapitulated in a model of Group 1 PH, the hypoxia-sugen mouse. Additionally, mice with heterozygous removal of NUDT21 in PASMCs had increased PH symptoms over control mice. I also report a phenotypic change in human PASMCS with depletion of NUDT21 associated with an induction of proliferation and reduced migratory capacity. I also report several pathways which are enriched in APA events after NUDT21 depletion, including a shortening of the HAS2 gene and concomitant increases in HAS2 mRNA levels. These results show evidence for a novel role for NUDT21 regulated APA to control cell phenotype and contribute to disease progression in PH.

Results

NUDT21 is depleted in patients with Group 1 or Group 3 PH

I first stained lung sections from healthy donors and patients diagnosed with PAH or IPF + PH for αSMA and NUDT21 expression. Serial sections were stained for NUDT21 and αSMA or DAPI and αSMA. I then quantified the cells that were αSMA positive with either NUDT21 staining or DAPI positive nuclei. This showed that patients with PAH or IPF + PH have reduced nuclear NUDT21 in remodeled vessels compared to

healthy vessels (Figure 4A-B). I then used flash frozen tissue samples to measure levels of CFIm complex members in the pulmonary artery of patients with PAH compared to control by western blot. Here I see a depletion in the level of NUDT21, CFIm59, and CFIm68 (Figure 4C-D). CPSF73 is an important part of the cleavage and polyadenylation machinery but is not a part of the CFIm complex and also does not change in level in PAH samples (Figure 4C-D). Subsequently, I performed a western blot on samples from healthy pulmonary arteries, arteries from lungs with IPF and arteries from lungs with IPF + PH. Interestingly here, I only saw a change in NUDT21 in the IPF and IPF + PH with no further depletion between IPF and IPF + PH. Meanwhile, CFIm59, CFIm68, and CPSF73 have no significant change (Figure 4E-F). Taken together this suggests that NUDT21 depletion is associated with PH.

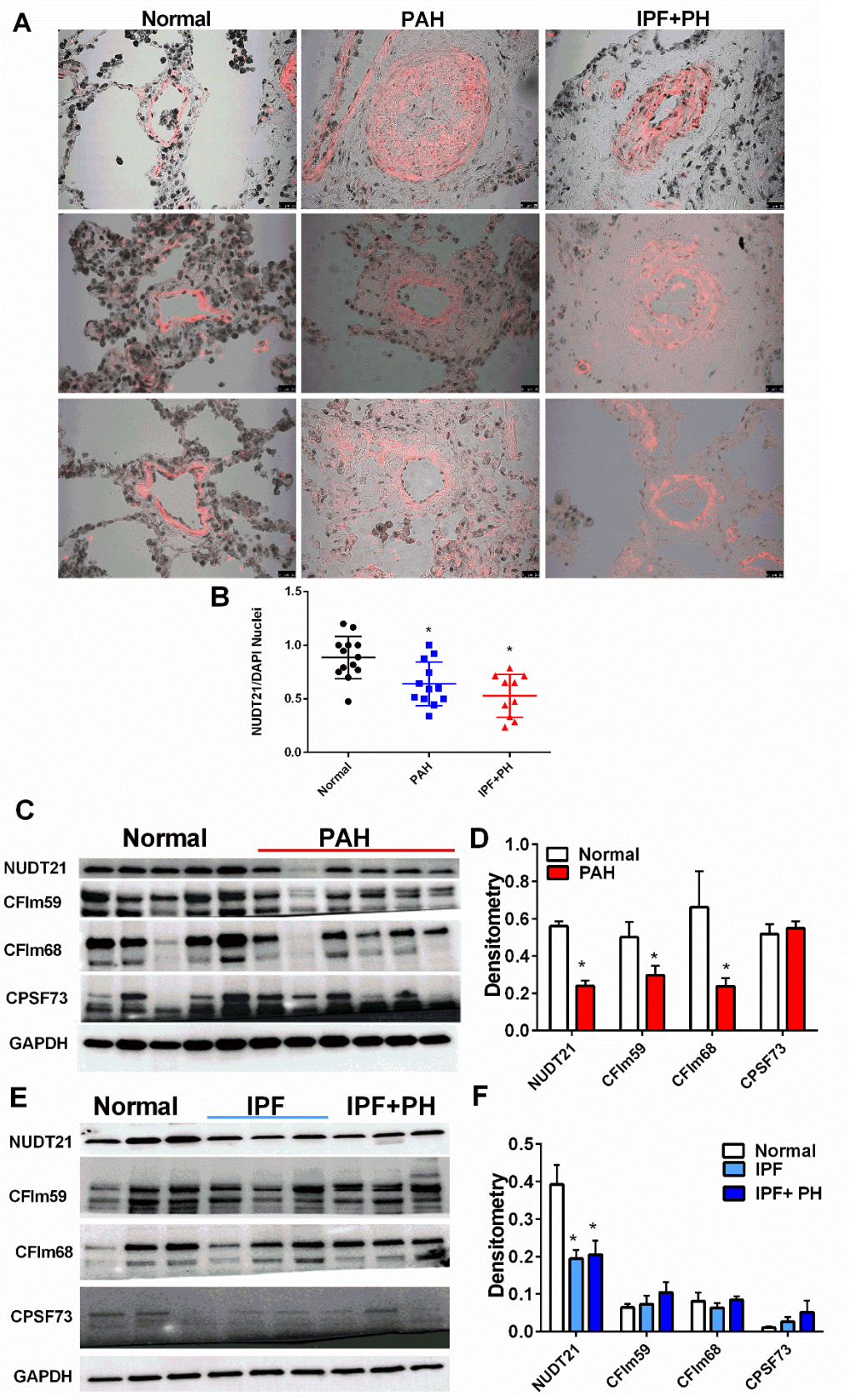
A
Normal
PAH
IPF+PH
B
NUDT21/DAPI Nuclei
1.5
1.0
0.5
0.0
Normal
PAH
IPF+PH
C
Normal
PAH
NUDT21
CFIm59
CFIm68
CPSF73
GAPDH
D
Densitometry
1.0
0.8
0.6
0.4
0.2
0.0
Normal
PAH
NUDT21
CFIm59
CFIm68
CPSF73
E
Normal
IPF
IPF+PH
NUDT21
CFIm59
CFIm68
CPSF73
GAPDH
F
Densitometry
0.5
0.4
0.3
0.2
0.1
0.0
Normal
IPF
IPF+ PH
NUDT21
CFIm59
CFIm68
CPSF73

Figure 4 NUDT21 depletion in PH.

Sequential lung sections double stained for α-smooth muscle actin (α-SMA; red signals) and NUDT21 (brown signals) from normal lungs (left) or patients with PAH (middle) or IPF + PH (right) (A). Quantification of NUDT21 positive nuclei in α-SMA positive cells and sequentially stained DAPI (ratio NUDT21 positive nuclei to DAPI) (B). Immunoblots for NUDT21, CFIm59, CFIm68, CPSF73 and GAPDH from Normal and PAH pulmonary arteries (C). Densitometries from C normalized to GAPDH(D). Immunoblots for NUDT21, CFIm59, CFIm68, CPSF73 and GAPDH in Normal and IPF and IPF + PH pulmonary arteries (E). Densitometries from E normalized to GAPDH(F). The N used for panel B 13 (Normal); 12 (PAH); 10 (IPF+PH). Data are shown as mean ± SD.* $P \leq 0.05$

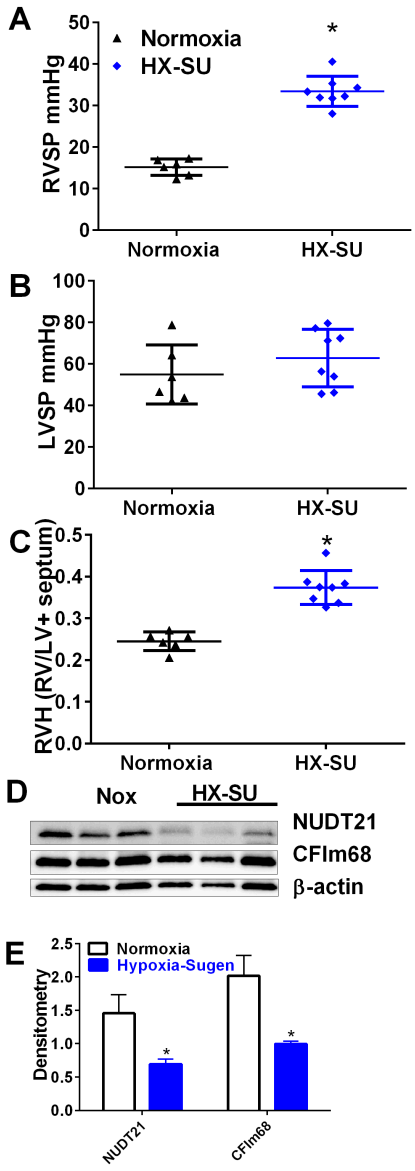

Figure 5 Hypoxia-sugen model of PH shows reduced pulmonary artery NUDT21.

Right Ventricle Systolic Pressure (RVSP) (A); Left Ventricle Systolic Pressure (LVSP)(B); Fulton index determined from measuring dry weights of RV and LV + septum (C). Immunoblot for NUDT21, CFIm68 and βactin (D). Densitometries of D normalized to βactin (E). The N number used for these studies are 6 (Normoxia); 8 (HX-SU). Significance level * $P \leq 0.05$

NUDT21 in the hypoxia-sugen model of PH

I next wanted to verify that the depletion of NUDT21 seen in patient samples is recapitulated in a model of PH. In this experiment I used the hypoxia-sugen mouse model. Here mice of ~8 weeks are exposed to hypoxic condition of 10% O_2 for 28 days. To further the model and prevent vascularization the mice are also treated weekly with 20mg/kg of Sugen 5416, IP a vascular endothelial growth factor receptor antagonist. At day 28 hemodynamics of the mice are measured and the mice are sacrifice to obtain samples. These mice have a significant rise in Right Ventricle Systolic Pressure (RVSP), a measure similar to mPAP of patients (Figure 5A). The Left Ventricle Systolic Pressure (LVSP) is not elevated in this model indicating no change in systemic blood pressure. These mice also have significant Right Ventricle Hypertrophy (RVH) (Figure 5C). My study showed that NUDT21 is depleted in the isolated pulmonary artery of these mice (Figure 5D-E). I also see depletion of CFIm complex member CFIm68 (Figure 5D-E). This indicates that this model is relevant for studying NUDT21 induced APA and PH.

NUDT21 deficient mice are more susceptible to PH

The Cre-Lox system is a very powerful tool for the genetic manipulation of mice. I acquired the NUDT21-Flox mouse line and crossed it with the Tagln-CreKI mouse line (114, 167). The Tagln-CreKI expresses cre recombinase from a knock in transgene at the transgelin gene locus. This allows for recombination of loxp sites that were introduced surrounding several exons of the NUDT21 gene in the NUDT21-Flox line. This allows for the specific deletion of NUDT21 from vascular smooth muscle cells. Unfortunately, the homozygous NUDT21-Flox Tagln-CreKI animals are embryonic lethal so I continued

with only a heterozygous knock out. In addition, there are no available mice with inducible expression of Cre in vascular smooth muscle cells. I then exposed these animals to the hypoxia-sugen model and measured hemodynamics and NUDT21 expression. I show that even in normoxic conditions NUDT21 heterozygous KO is sufficient to increase the RVSP significantly, but when exposed to hypoxia-sugen these mice develop an augmented increase in RVSP (Figure 6A). Hypoxia in control mice was able to reduce NUDT21 levels by nearly half, a similar level to the heterozygous KO mice in normoxic conditions (Figure 6C-D). This data suggests that NUDT21 is a causative agent in PH and that understanding the mechanism is important for understanding this disease.

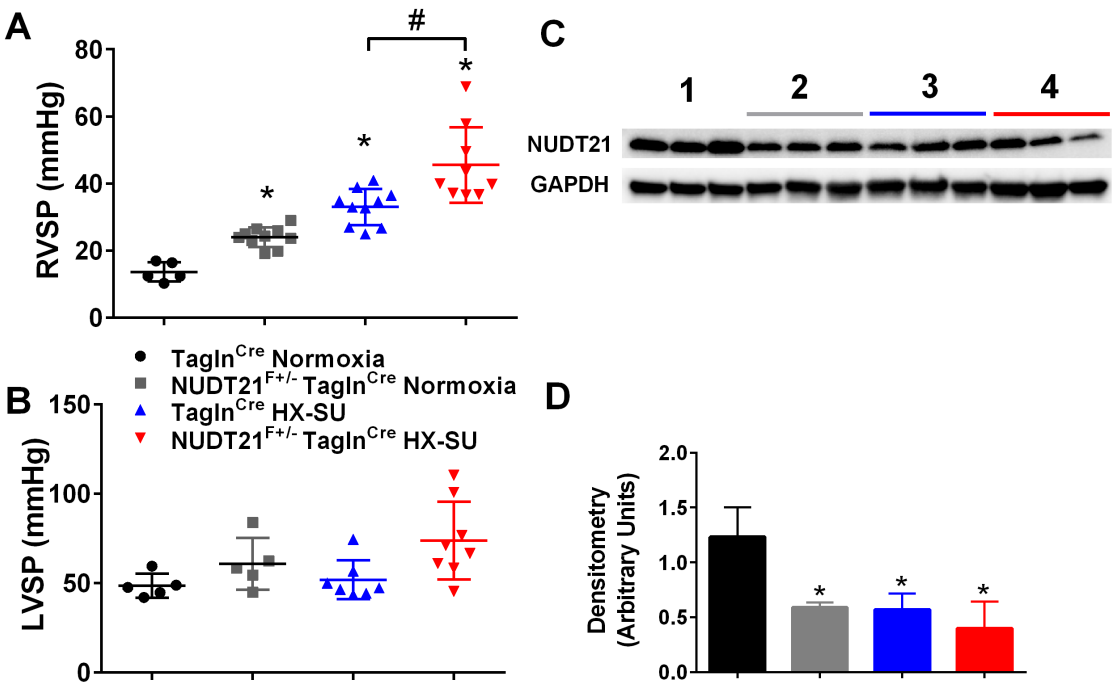

Figure 6 PASMC KO of NUDT21 worsens pulmonary hypertension.

Tagln^{Cre} Normoxia, Nudt21$^{f/+}$ Tagln^{Cre} Normoxia, Tagln^{Cre} Hypoxia-sugen, Nudt21$^{f/+}$ Tagln^{Cre} Hypoxia-sugen. RVSP (A); LVSP(B); Immunoblot for NUDT21 and GAPDH(C). Densitometries of C normalized to GAPDH (D). The N used for these studies are 5 (Tagln^{Cre} Normoxia); 10 (Nudt21$^{f/+}$ Tagln^{Cre} Normoxia); 10 (Tagln^{Cre} Hypoxia-sugen); 9 (Nudt21$^{f/+}$ Tagln^{Cre} Hypoxia-sugen) for panel A and 5 (Tagln^{Cre} Normoxia); 5 (Nudt21$^{f/+}$ Tagln^{Cre} Normoxia); 7 (Tagln^{Cre} Hypoxia-sugen); 8 (Nudt21$^{f/+}$ Tagln^{Cre} Hypoxia-sugen) for B. Variations in N are due to violation of a predetermined criteria: heart rate below 250 BPM at the time of LVSP.

NUDT21 controls the phenotype of PASMCs

To determine the role that NUDT21 played in controlling PASMC phenotype, I harvested and cultured these cells from healthy donors and lungs from patients with PAH. I first measured the proliferative capacity of the healthy PASMCs by starving them for 72 hours followed by treatment with control or NUDT21 siRNA. I then stimulated the cells with vehicle or 25μM PDGF for 48 hours and then measured proliferation using the WST1 assay. This demonstrated that depletion of NUDT21 increased PASMC proliferation after 25μM PDGF (Figure7A). I then measured the proliferative phenotype of cells isolated from PAH patients. These results demonstrate that PASMC derived from patients with Group 1 PH present with an enhanced proliferative response to PDGF. Interestingly, overexpressing of NUDT21 from the pcDNA3.1 plasmid attenuated the enhanced proliferative phenotype of PAH-derived PASMC (Figure 7A). I used these same groups to examine migratory ability. Here I used Boyden chambers with 8μm pores (168). These allow cells to pass through but do provide a resistance. Then I implement either a control or serum gradient to induce migration. In this experiment I see reduced migration in the healthy cells when NUDT21 is reduced by siRNA (Figure 7B). Overexpression of NUDT21 in PH PASMCs showed no change in migration due to sample variability.

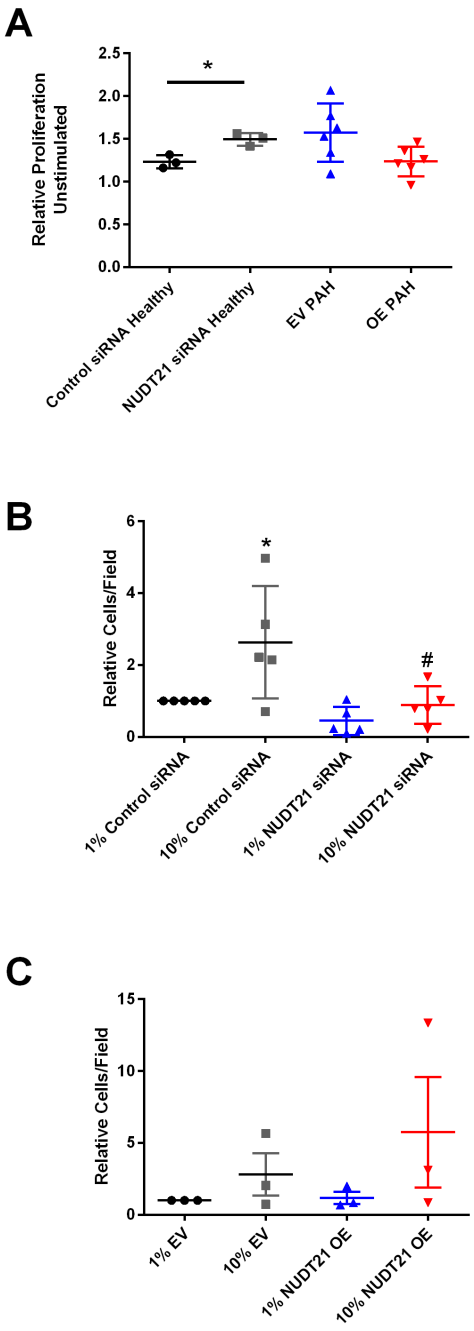

Figure 7 Changes in NUDT21 level induces phenotype changes in PASMCs

PASMCs isolated from healthy donors with control siRNA or NUDT21 siRNA are stimulated with 25mM PDGF, PASMCs isolated from PAH patients with Empty Vector (EV) or NUDT21 over expression vector (OE) are stimulated with 25mM PDGF, WST-1

proliferation assay relative to unstimulated (A). PASMCs isolated from healthy donors with control siRNA or NUDT21 siRNA in a Boyden chamber assay 1% is no serum gradient, 10% is serum gradient (B). PASMCs isolated from PH patients with Empty Vector (EV) or NUDT21 over expression vector (OE) in a Boyden chamber assay 1% is no serum gradient, 10% is serum gradient (C). Data are shown as mean ± SD.* $P \leq 0.05$ # $P \leq 0.05$

Pathways controlled by NUDT21 mediated APA in PASMCs

After showing the phenotypic alterations caused by NUDT21 loss I sought to understand the pathways that could be driving this change. To do this I utilized human PASMCs (Lonza CC-2581) in culture. I used a siRNA to deplete NUDT21 in these cells and harvested RNA. This RNA was then put through a library preparation procedure for Illumina MiSeq. The sequencing was then performed and the bioinformatics technique dynamic analysis of alternative polyadenylation (DaPars) was used to analyze the data (169). This algorithm identified 664 shortened transcripts and 350 lengthened transcripts (Figure 8A). My next step was to identify the functional pathways that are enriched in the shortened data set. To do this I utilized the ConsensusPathDB that not only defines pathways by gene product activity but also by protein-protein interactions and regulatory interactions (170). In doing this the pathways with the most hits were metabolism related genes, extracellular matrix, and cell proliferation (Figure 8B). To visualize the changes discovered by the DaPars algorithm the RNA-seq traces for VMA21 are shown here (Figure 8C). VMA21 is very consistent in its shortening during reduced levels of NUDT21 making it an excellent control for NUDT21 mediated 3'UTR APA. Finally, I show the confirmation of NUDT21 depletion by siRNA as well as showing that this change is sufficient to induce the expression of Col1 and Fn in cell culture (Figure 8D).

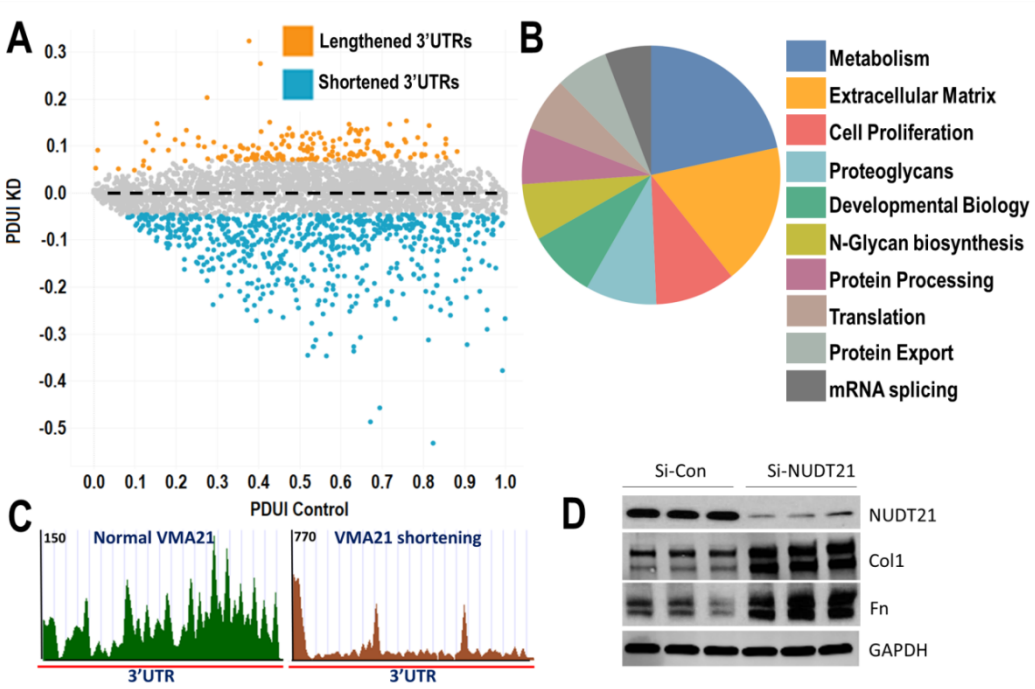

Figure 8 RNA-seq exposes global APA changes in PASMCs after NUDT21 depletion

Plot of Percent Distal Usage Indexs(PDUI) of control vs change in PDUI in NUDT21 siRNA treated cells, shortened transcripts blue lengthened orange(A). ConsensusPathDB pathways enriched in shortened transcripts (B). Example trace or shortened trace, VMA21 (C). Immunoblot of NUDT21, Col1, Fn, and GAPDH from si-con and si-NUDT21 treated cells (D).

Confirmation of NUDT21 mediated APA by RT-PCR

I then wanted to confirm the shortening events seen in the RNA-seq data. The best way to confirm this is by RT-PCR to determine distal polyadenylation site usage. To do this two RT-PCR primer sets are designed, one primer set in the coding sequence which will measure both a short and long transcript, and one primer set distal of the first major poly(A) site which will only measure the distal transcript. The $\log_2$ of the difference of the Ct value of these primers gives the fold change in dPAS usage. Here I verify VMA21 dPAS usage as well as one of the identified shortening targets within the ECM pathway from the ConsensusPathDB, HAS2 (Figure 9A). This negative dPAS usage indicates a shift from distal to proximal poly(A) usage and shortening of the mRNA transcripts. VMA21 showed very robust shortening, as expected, while HAS2 presented with a more moderate but nearly a 50% change in dPAS usage. I then measured total transcript levels of these genes and demonstrated that both VMA21 and HAS2 are significantly increased (Figure 9B). Next, I purified RNA from the isolated pulmonary artery of healthy donors and patients with PAH to measure APA. I show that there is a trend towards shortening in these samples in both VMA21 and HAS2 (Figure 9C). This shortening is also accompanied by increases in total transcripts though VMA21 change is non-significant (Figure 9D). These data confirm that NUDT21 depletion leads to shortening in select transcripts in PASMCs in culture. While these shortening events are not seen in these human samples due to biological variation, transcript levels are significantly increased.

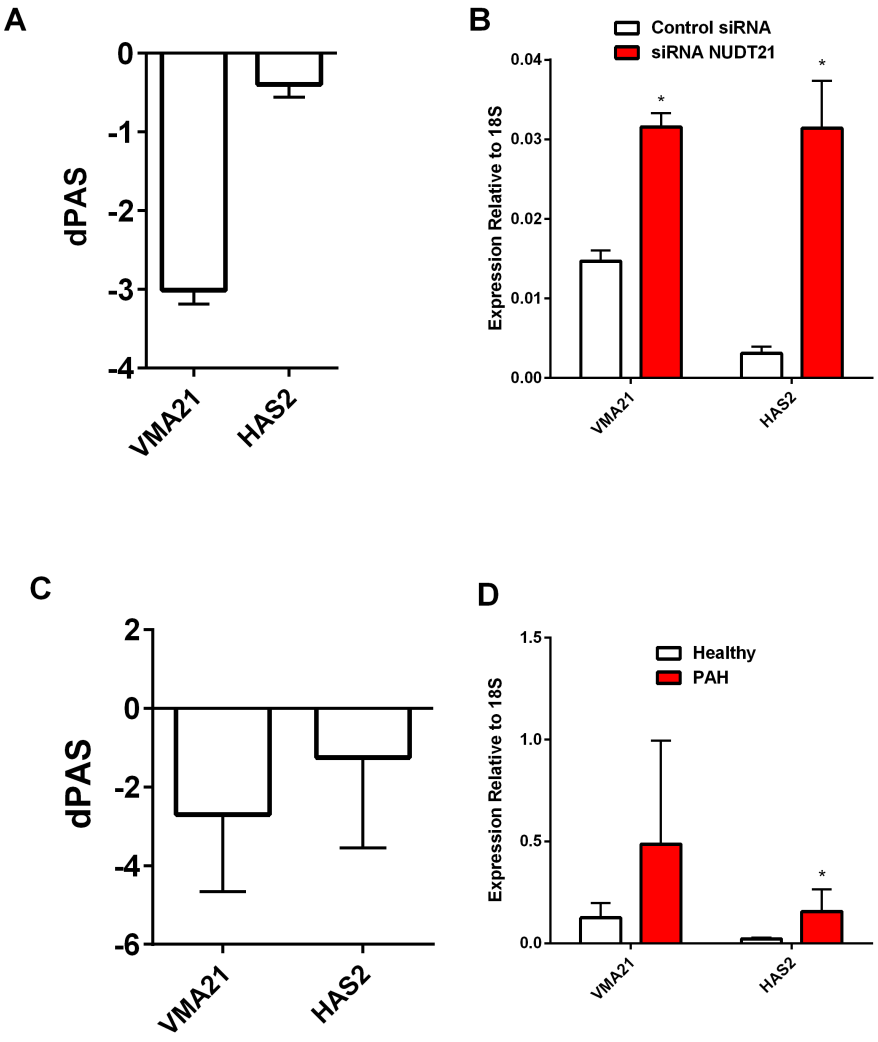

Figure 9 RT-PCR verification of shortening in PASMCs

DPAS usage in VMA21 and HAS2 transcripts after NUDT21 siRNA treatment normalized to control siRNA treatment (A). Expression levels of VMA21 and HAS2 using 18S rRNA as a control (B). dPAS Usage of VMA21 and HAS2 from PAH pulmonary arteries normalized to healthy pulmonary arteries(C). Expression levels of VMA21 and HAS2 normalized to 18S (D).

Discussion

A major finding of my research is that NUDT21 levels are reduced in PH patients and that depletion of NUDT21 drives the development of PH experimentally. This reduction is consistent with the hypothesis that NUDT21 depletion leads to 3'UTR APA and changes in mRNA transcripts that lead to PH. In fact, my finding that heterozygous deletion of one copy of NUDT21 in mice PASMCs increases the PH that these mice acquire in the hypoxia-sugen model is a strong indicator that this mechanism plays an important role in the worsening of this disorder. This adds PH to the list of diseases that have recently been shown to be partially or whole driven by APA, including several in which NUDT21 level are key (112, 114). The results are highly important as they give a new target for research and drug development in a disease that is not well controlled with current therapies and lacks a curative treatment without transplantation.

NUDT21 is depleted in glioblastoma tumors and reduced levels of NUDT21 have been reported in fibroblast from patients with IPF (163). In these fibroblast, NUDT21 reduction leads to increased TGFβ and Wnt signaling by altering gene expression through APA. These changes result in a more fibrotic phenotype with the increases of collagen and fibronectin expression. IPF fibroblast in culture also showed this synthetic phenotype but resembled healthier fibroblast with the addition of exogenous NUDT21 (114). This change in phenotype encouraged me to explore the changes in cell phenotype seen in PH and investigate the role of NUDT21 induced APA. My findings indicate that healthy PASMCs, with reduced levels of NUDT21 by siRNA have an increased proliferative potential when induced by PDGF. This high level of proliferative potential matches that seen in PASMCs from patients with PH. This finding is consistent with the

proliferative phenotype of patient cells seen in other studies (171). Alternately, migratory capacity appears to be reduced with reduced level of NUDT21 in a Boyden chamber assay with and without serum gradient. This is an unexpected result as I hypothesized that increased migration would occur to accompany increased proliferation as was seen in glioblastoma cell lines and is often seen in PASMCs exposed to hypoxia (113, 172). It may be though that proliferation increased to such a speed that migration was inhibited by the necessity of continued growth. An alternative explanation is that NUDT21 depletion leads to increased ECM deposition, precluding cell migration. Evidence for this is present from PASMCs where increased Fn and Col1a1 expression was observed following NUDT21 KD. This would indicate a potential intermediate phenotype with increased proliferation and synthesis but reduced migration. These results show that NUDT21 depletion regulates the phenotype of PASMC inducing changes similar to PASMCs isolated from patients with PH. This is consistent with previous findings of increased proliferation in PASMCs in PH (173).

In PASMC derived from patients with PH, rescuing expression of NUDT21 reversed their hyper-proliferative phenotype. This indicates that NUDT21 is a highly promising target for pharmacological inhibition of PH. One of the challenges of targeting NUDT21 is that it is a core member of the cleavage and polyadenylation machinery and that activity of this complex is necessary for proper cellular survival. To circumvent this problem I have two options, target specifically the pulmonary artery cells or look to the interactions within the CFIm complex.

Increasing expression of NUDT21 in the PASMC would be an excellent therapeutic target if it can be done very selectively and subtly. Recent advances in

nanoparticle deliver could allow for treatment of PASMCs with a small oligonucleotide (174). This was successfully used to target miR-145, which is associated with PAH, in the hypoxia-sugen mouse rat model (175). Targeting a miRNA which regulates NUDT21 or depletion of an upstream effector with RNAi through this delivery mechanism is a potential therapeutic approach for PH.

An interesting finding was that in PAH all three CFIm complex members are downregulated in in the pulmonary artery. Conversely, I see no such change in CFIm59 or CFIm68 in IPF or IPF + PH samples. This difference could point to a key separator in the development of PAH when compared to Group 3 PH. If this is the case it is important to further investigate these findings to understand potential interventions. Additionally, understanding the role of each CFIm member allows me to target interactions within the complex to make more subtle changes to the APA landscape. While the exact role of CFIm59 and CFIm68 are unknown, some hypothesize that they convey specificity in RNA binding to the complex during the formation of a tetramer (176). If this is true, drug screens for NUDT21 mediated APA will likely target the protein interactions that bind this complex.

NUDT21 regulated APA is a broad mechanism that changes the transcriptional landscape in a cell. These changes can cause shortening in many genes as seen in HeLa cells and caused shortening in over 600 genes in the samples (113). This large number of genes that are regulated can make uncovering the smoking gun for changes seen due to this APA difficult, thus I first looked at the pathways that were enriched in those genes that were shortened by NUDT21 depletion. In my RNA-seq dataset I saw modulation of several pathways that are linked to the phenotypic changes in PASMCs I observed in

patient samples. These include pathways involved in proliferation and migration and ECM. In fact, I showed that NUDT21 depletion in PASMCs in cell culture was sufficient to cause an increase in Col1A and Fn depositions. This suggests that NUDT21 reduction also induces a synthetic phenotype in these cells. As studying each APA event discovered to describe the change it induces in PASMC is not feasible I selected a gene which as described in the next chapter, is an important driver in PH; this gene is HAS2.

RNA-seq data can have many factors that cause anomalies in the data including hard to sequence regions with repetitive sequences or other sequence features. This makes it important to verify this data with other techniques. Here I verified the data with additional RT-PCR experiments. This also allowed me to measure gene level changes as a result of shortening. This was very exciting, as it revealed that NUDT21 depletion leads to shortening of the HAS2 mRNA in cell culture as well as patient tissue. This change appears to lead to increased transcript level of HAS2. The following chapters will discuss the consequences of increased HAS2 in PASMC of patients with PH.

The results shown here indicate that NUDT21 levels are reduced in patient samples of PH. This reduction is also recapitulated in the hypoxia-sugen mouse model. When mice in this model have additionally reduced levels of NUDT21 the PH symptoms are severely worsened, pointing to a role of NUDT21 in the progression of this disease. To determine the mechanism that leads to this worsened PH, I described the phenotypic changes seen in PASMCs with depleted NUDT21. These phenotypic changes resemble differences seen between healthy and PASMC isolated from PH patients. I then determined that NUDT21 reduction leads to widespread APA events in PASMCs

and that the shortening events are enriched for pathways such as metabolism, proliferation and ECM. I verified the shortening and increased expression of one target, HAS2 by RT-PCR. Together these results describe an important role for NUDT21 mediated APA in the development and progression of PH. Understanding the role other CFIm members play in these cells as well as more completely describing the APA landscape changes seen in patients with PH will allow for targeted research and therapy discovery in this newly discovered mechanism of PH development.

Chapter 4: Uncovering the role of Hyaluronan in the pathogenesis of PH

This chapter is based upon research originally published in the *British Journal of Pharmacology*. Collum SD, Chen NY, Hernandez AM, Hanmandlu A, Sweeney H, Mertens TCJ, Weng T, Luo F, Molina JG, Davies J, Horan IP, Morrell NW, Amione-Guerra J, Al-Jabbari O, Youker K, Sun W, Rajadas J, Bollyky PL, Akkanti BH, Jyothula S, Sinha N, Guha A, Karmouty-Quintana H. Inhibition of hyaluronan synthesis attenuates pulmonary hypertension associated with lung fibrosis. *Br J Pharmacol* 2017.

Introduction

As discussed previously, the ECM is an integral compartment of all tissues and plays a large role in the development of a healthy lung as well as the progression of chronic lung diseases (177, 178). To understand the progression of diseases such as PH, I must identify the important components of this matrix and dissect the influence these molecules have on the cells involved in disease progression (65). The glycosaminoglycan, HA, is a key structural component of the lung surrounding large vessels and airways but where this molecule plays its most crucial role is signaling through multiple pathways to induce cellular changes (160).

Increased levels of hyaluronan have been observed in patients with IPF and PAH (150, 155, 179, 180). Furthermore, overexpression of hyaluronan synthase 2 (HAS2), an enzyme responsible for the synthesis of hyaluronan, has been implicated in fibrosis (153). Taken together, these observations suggest a role for hyaluronan in the pathophysiology of PAH as well as IPF + PH. However, hyaluronan-mediated vascular

remodeling and the mechanisms promoting increased hyaluronan synthesis in Group 1 and Group 3 PH is not fully understood. These observations prompted me to evaluate the role of HA in the vasculature in Group 1 PH. I was also prompted to evaluate the presence of elevated hyaluronan in patients with IPF and IPF + PH and to assess the therapeutic potential of a hyaluronan synthase inhibitor in a murine model of Group 1 PH as well as PH associated with lung fibrosis.

4-Methylumbelliferone (4MU), also known as hymecromone, is a FDA approved drug for bile therapy and it is also able to inhibit hyaluronan synthesis by depleting the cell of uridine diphosphate-glucuronic acid, an essential substrate for all HAS isoforms and by down-regulation of HAS2 and 3 mRNA expression (181-183). Increased levels of HA have been measured in PAH both in the plasma of patients as well as in cultured PASMCs from these patients (180). Additionally, the monocrotaline rat model shows increased HAS2 expression as well as increased HA deposition and aberrant degradation of HA (157).

My results show that therapy with 4MU and conditional genetic deletion of smooth muscle HAS2 prevent the development of hallmarks of PH induced by chronic exposure to hypoxia and sugen. I also have found that increased hyaluronan was associated with remodeled vessels and correlated with increased disease severity in PH associated with IPF, as defined by elevated mPAP values. In addition, I report improvements in PH but not fibrosis following therapy with 4MU in the bleomycin mouse model, which models PH associated with lung fibrosis (184). These observations provide evidence for an independent hyaluronan-mediated mechanism in the pathogenesis of PH associated with IPF. Furthermore, my results reveal that hyaluronan

leads to increased proliferation and stiffness of PASMCs and also affects the ability of these cells to migrate in a RhoA-dependent manner. Taken together, these results show evidence of a unique mechanism contributing to PH.

Results

4-Methylumbelliferone (4MU) prevents pulmonary hypertension in the hypoxia-sugen model

To investigate PH without lung parenchyma damage such as seen in Group 1 PH, the hypoxia-sugen mouse model has been used (155, 185). This model recapitulates many of the symptoms of this disease including vascular remodeling more resembling the pathology seen in PAH patients with heavily exacerbated increases in pulmonary blood pressure and eventual loss of cardiac output (55, 185). This model involves subjecting the mice to 10% O_2 for 28 days with four injections of SU5416 a vascular endothelial growth factor receptor (VEGFR) inhibitor. These mice were treated with 4MU starting at day 14 and measurements and tissues were collected on day 33. In this model, I see deposition of HA around the pulmonary vasculature that is reduced by 4MU treatment (Figure 10A). There is an increase in RVSP at day 28 in hypoxia-sugen groups vs controls, this increase was removed by 4MU treatment (Figure 10B). LVSP remained unchanged indicating no change to systemic pressures, while a hypoxia-sugen induced right ventricle hypertrophy as measured by Fulton index was reduced by 4MU treatment (Figure 10C –D).

PASMC deletion of HAS2 prevent PH in the hypoxia-sugen model

As stated earlier the HA producing enzyme HAS2 is upregulated in the monocrotaline rat model of PH (157). To further dissect the role of HAS2, which has been associated with multiple disease states (153, 186), in these experiments I also utilized the $Has2^{f/f}$-TaglnCre mouse line. This line is a knockout of the expression of HAS2 in vascular smooth muscle cells with no phenotype in nomoxic mice. At day 28 I see that RVSP which is increased in control $HAS2^{f/f}$ hypoxia-sugen mice was reduce towards normal with LVSP showing no changes (Figure 11A-B). Interestingly there is no effect of HAS2 KO on RVH (Figure 11C).

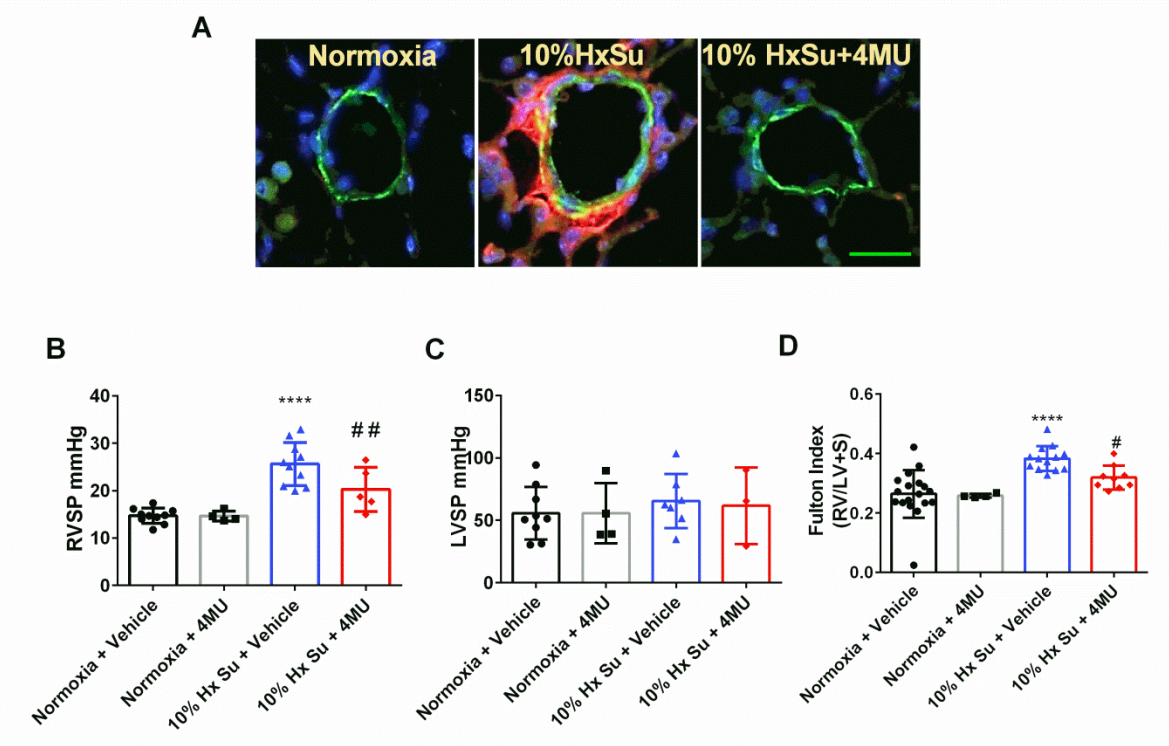

Figure 10 4MU prevents pulmonary hypertension in the hypoxia-sugen model.

IF-stained lung sections (A) for αSMA (green) and HA (red) from mice treated with Normoxia + vehicle, Hypoxia-sugen + vehicle, or Hypoxia-sugen + 4MU. RVSP (B); LVSP(C); Fulton index determined from measuring dry weights of RV and LV + septum (D). Data are shown as scatter plot showing the mean ± SD. **** $P \leq 0.05$, significant difference between PBS + vehicle and bleomycin (BLM) + vehicle treatment; ANOVA. # $P < 0.05$, significant difference between BLM + vehicle and BLM + 4MU treatment; ANOVA. The N used for these studies are 10 (Normoxia + vehicle); 4 (Normoxia + 4MU); 10 (Hx Su + Vehicle); 5 (Hx Su + 4MU) for panel B. Variations in N are due to violation of a predetermined criteria: heart rate below 250 BPM at the time of LVSP. The scale bar represents 50 μm.

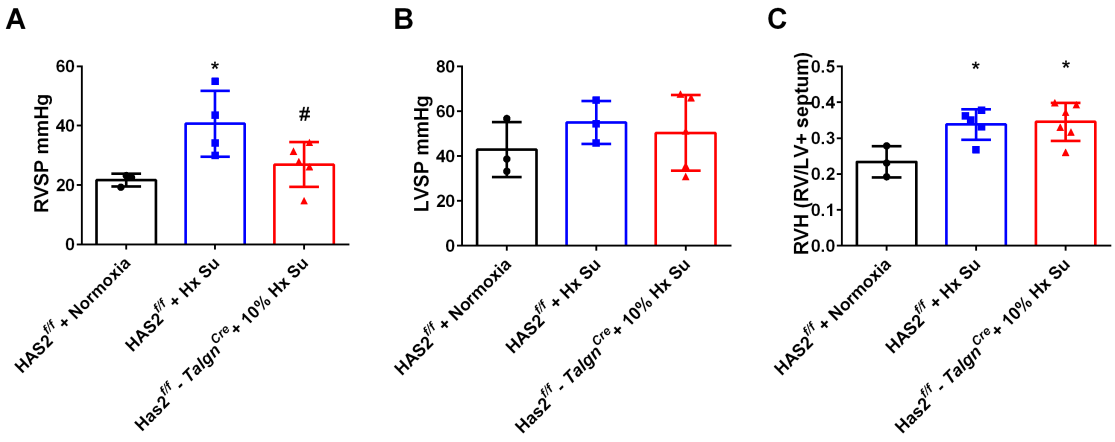

Figure 11 PASMC KO of HAS2 prevents pulmonary hypertension.

$HAS2^{f/f}$ Normoxia, $HAS2^{f/f}$ hypoxia-sugen, $HAS2^{f/f}Tagln^{Cre}$. RVSP (A); LVSP(B); Fulton index determined from measuring dry weights of RV and LV + septum (C). Data are shown as scatter plot showing the mean ± SD. * P ≤ 0.05, significant difference between $HAS2^{f/f}$ + Normoxia and $HAS2^{f/f}$ + Hx Su; ANOVA. # P < 0.05, significant difference between $HAS2^{f/f}$ + Hu Su and $HAS2^{f/f}$ – $Tagln^{Cre}$ + Hu Su; ANOVA. The scale bar represents 50 µm. The *N* used for A is 3 ($HAS2^{f/f}$ + Normoxia); 4 ($HAS2^{f/f}$ + Hx Su); 5 ($HAS2^{f/f}$ – $Tagln^{Cre}$ + Hu Su). Variations in *N* are due to violation of a predetermined criteria: heart rate below 250 BPM at the time of RVSP or LVSP.

Hyaluronan is elevated in patients with Group 3 pulmonary hypertension

HA deposition is increased in IPF and HA levels are associated with PH secondary to COPD (153, 158). No study has shown a link between HA and IPF + PH. I stained lung sections from patients diagnosed with IPF and those with IPF + PH. I found increased hyaluronan levels, observed histologically, in IPF patients compared to controls. This increase appeared to be enhanced further in patients with IPF + PH in areas adjacent to the smooth muscle but not in the endothelial layer (Figure 12A). Interestingly, increased hyaluronan deposition was observed in areas rich in vascular remodeling (Figure 12A). Transcript levels of HAS1, HAS2 and HAS3 (Figure 12B–D) from isolated lung sections revealed a significant correlation between elevated HAS2 and HAS3 expression but not HAS1 expression levels and increased mPAP values for patients with IPF (Figure 12B–D). Similarly, immunofluorescence for HAS2 and HAS3 revealed increased signals for HAS2 and HAS3 in remodeled vessels of patients with IPF + PH but not in IPF or normal (Figure 13A). Immunoblots for HAS1, HAS2 and HAS3 revealed increased expression of HAS1 and HAS2 in IPF + PH samples compared with normal and in IPF + PH compared with IPF groups (Figure 13B). Taken together these results suggest that hyaluronan accumulation is present in fibrotic lung diseases and is increased in patients with an additional diagnosis of PH.

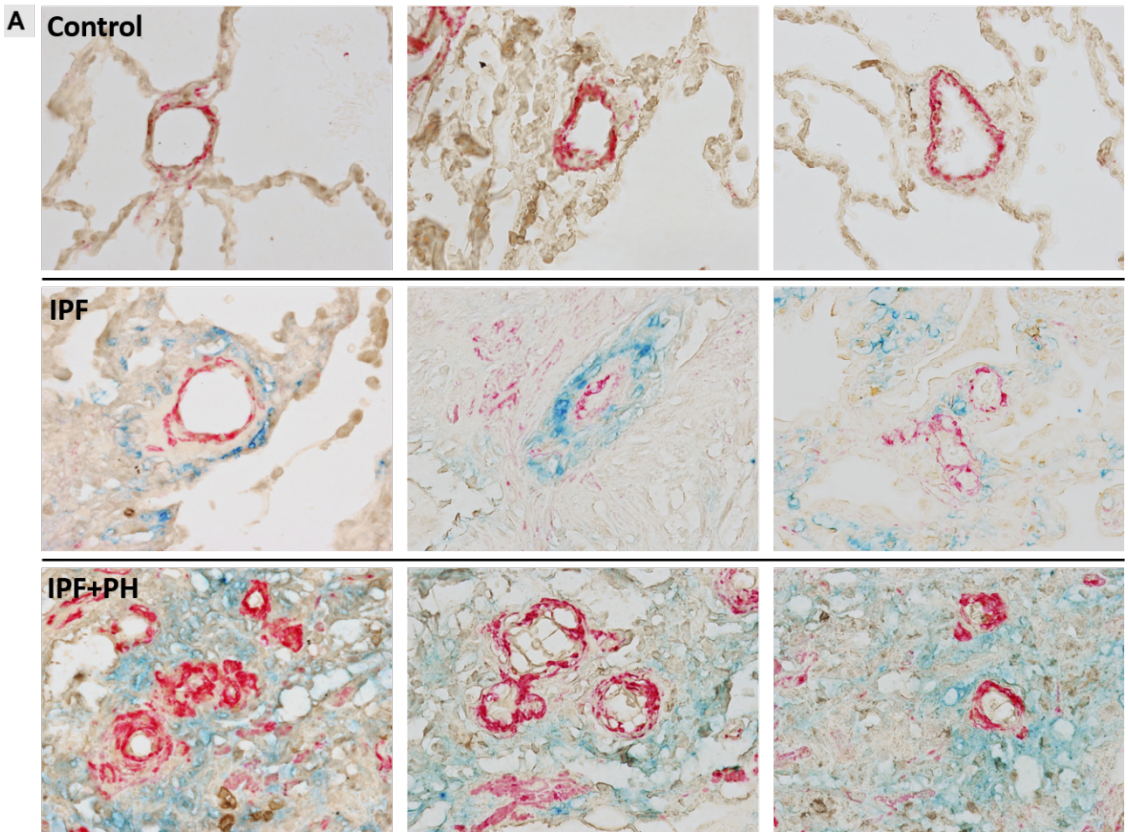
A
Control
IPF
IPF+PH

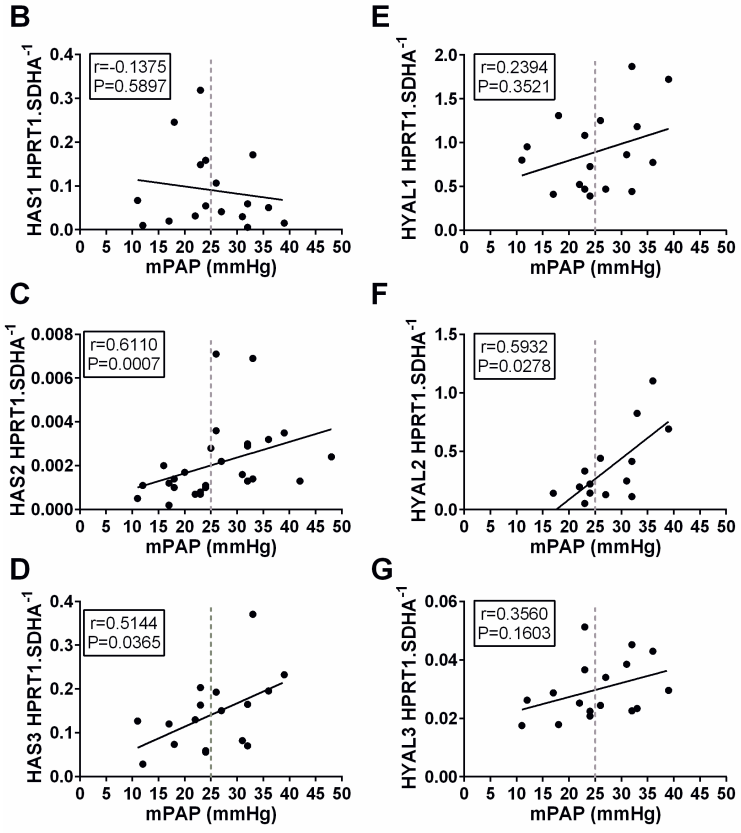
B
HAS1 HPRT1.SDHA-1
r=-0.1375
P=0.5897
mPAP (mmHg)
C
HAS2 HPRT1.SDHA-1
r=0.6110
P=0.0007
mPAP (mmHg)
D
HAS3 HPRT1.SDHA-1
r=0.5144
P=0.0365
mPAP (mmHg)
E
HYAL1 HPRT1.SDHA-1
r=0.2394
P=0.3521
mPAP (mmHg)
F
HYAL2 HPRT1.SDHA-1
r=0.5932
P=0.0278
mPAP (mmHg)
G
HYAL3 HPRT1.SDHA-1
r=0.3560
P=0.1603
mPAP (mmHg)

Figure 12 Increased hyaluronan levels and degradation in Group III PH.

Lung sections double stained for α-smooth muscle actin (α-SMA; red signals) and hyaluronan (blue signals) from representative normal lungs (top panel) or patients with IPF (middle panel) or IPF + PH (bottom panel) (A). Linear regression and Spearman correlation analysis for mRNA levels for HAS1 (B; r = 0.1375, P>0.05), HAS2 (C; r = 0.6110, P<0.05), HAS3 (D; r = 0.5144, P<0.05), HYAL1 (E; r = 0.2394, P>0.05), HYAL2 (F; r = 0.5932, P<0.05) and HYAL3 (G; r = 0.3560, P>0.05) ratio to geometric mean of control genes HPRT1 and SDHA against mPAP from patients with IPF. The scale bar represents 100 μm. n = 6 (Control); 10 (IPF); 9 (IPF + PH). PH is defined as mPAP ≥25 mmHg.

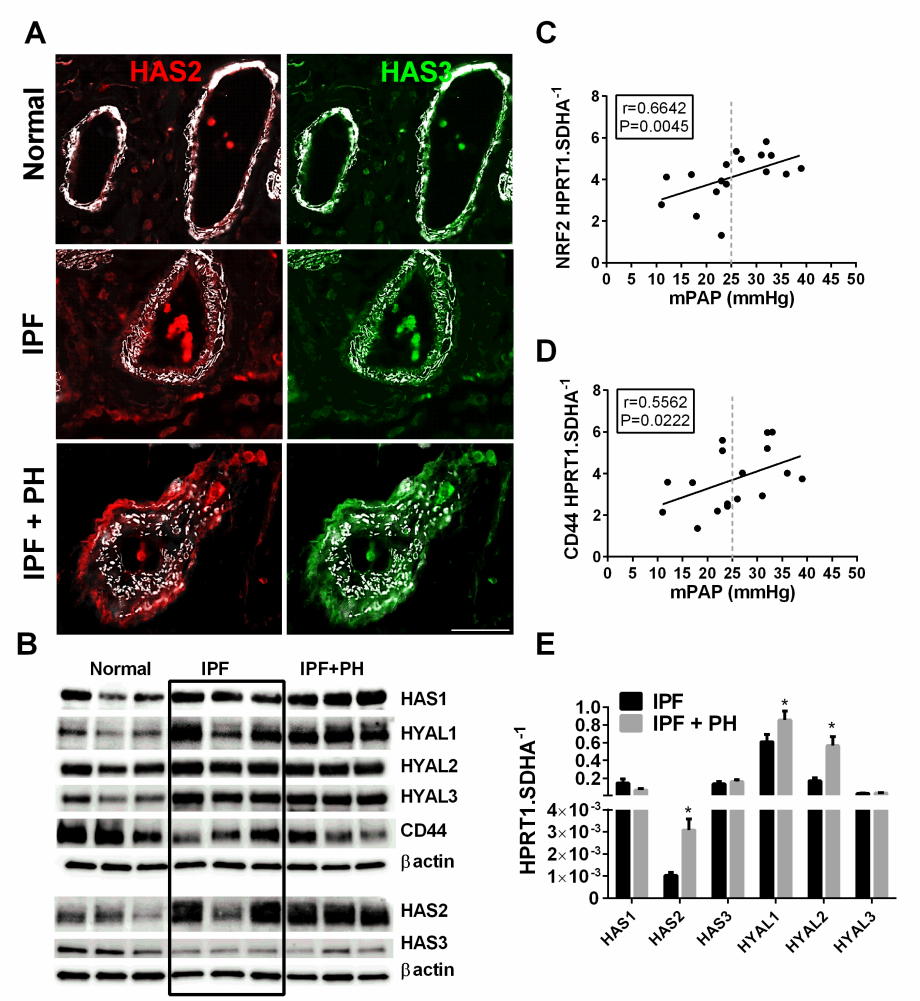

Figure 13 HAS2, HAS3, NRF2 and CD44 levels in human samples.

Immunofluorescence (IF) for HAS2 (red signals), or HAS3 (green signals) and αSMA (white signals) for normal IPF and IPF + PH vessels (A); scale bar represents 50 μm. (B) Immunoblots for HAS1–3, HYAL1–3, CD44 and βactin from 3 normal, 3 IPF and 3 IPF + PH lung tissue samples. Linear regression and Spearman correlation between NRF2 expression levels and mPAP values for patients with IPF with or without a diagnosis of PH (C). Linear regression and Spearman correlation with CD44 expression levels (D). Expression levels for HAS1–3 and HYAL1–3 showing direct comparisons between IPF and IPF + PH samples (E). Significance levels * $P \leq 0.05$ refers to comparisons between IPF and IPF + PH values.

Increased hyaluronan degradation in Group 3 pulmonary hypertension

Hyaluronan can be degraded into low molecular weight fragments by hyaluronidases and increased ROS (187, 188). Interestingly I report a significant correlation between enhanced expression of hyaluronidase 2 (HYAL2) and mPAP (Figure 12F) and elevated HYAL2 signals by immunoblots between IPF and normal but not between IPF and IPF + PH. I also show increased protein levels for HYAL3 between IPF and normal lung but no increases between IPF + PH and IPF but similar results were not seen for HYAL1 or HYAL3. (Figure 12E–G) Immunoblots for HYALs revealed an overall increase in IPF compared with normal groups and a further increase in IPF + PH groups compared with IPF (Figure 13B). Finally, I report a significant correlation between increased expression of Nrf2, a marker of increased oxidative stress, and elevated mPAP (Figure 13C). Small MW hyaluronan fragments have been reported to interact with CD44 to mediate pathogenic effects and I therefore measured CD44 levels (177, 189). However, my data appears to show a reduction in CD44 protein levels despite a correlation between increased CD44 and mPAP levels (Figure 13D, E). Expression levels of all HAS and HYALs (IPF vs. IPF + PH) are shown in Figure 13. Taken together, these observations show increased hyaluronan deposition in IPF and IPF + PH and suggest that degradation of hyaluronan to smaller MW fragments is mediated by enhanced expression of HYALs and the presence of ROS.

4-Methylumbelliferone (4MU) reduces hyaluronan levels in a model of lung fibrosis and PH

In this experiment, I treated mice exposed to bleomycin or vehicle, with 4MU starting on day 15, consistent with previous studies from the lab where changes in the lung parenchyma are apparent at this time point (190). On day 33, physiological readouts and tissues were collected (Figure 14A). This is the intraperitoneal bleomycin model that creates a more chronic fibrosis compared to the more commonly utilized intratracheal bleomycin model. This model produces fibrosis progression from the distal portion of the lung more in line with that seen in patients. Eight twice weekly injections are performed and then the model progresses until day 33. BLM induces lung fibrosis due to the relative lack of bleomycin hydrolase in the lung (191).

Hyaluronan levels observed by immunohistochemistry (IHC) show increased hyaluronan deposition in bleomycin-exposed mice that were treated with 4MU therapy (Figure 14B). In line with this, bronchoalveolar lavage fluid (BALF) revealed a significant elevation of HA in bleomycin-exposed mice that was attenuated by 4MU treatment (Figure 14C). These observations were consistent with increased levels of Has1, Has2 and Has3 expression in bleomycin-exposed mice (Figure 14D-F) 4MU attenuated Has2 and Has3 but not Has1 expression (Figure 14D–F). Analysis of hyaluronidases demonstrated increased protein levels of Hyal1 and Hyal2 in bleomycin and bleomycin + 4MU treatment groups compared to PBS consistent with increased Hyal2 but not Hyal1 or Hyal3 mRNA expression levels (Figure 15B–D). Transcript levels for Nrf2 were elevated in bleomycin, compared to PBS, groups (Figure 15E). These observations echo my studies with human lung, showing evidence for increased hyaluronan fragment

degradation in experimental lung fibrosis. Here I also measured CD44 levels and I report increased both protein and mRNA levels in bleomycin-exposed mice (Figure 15A, F).

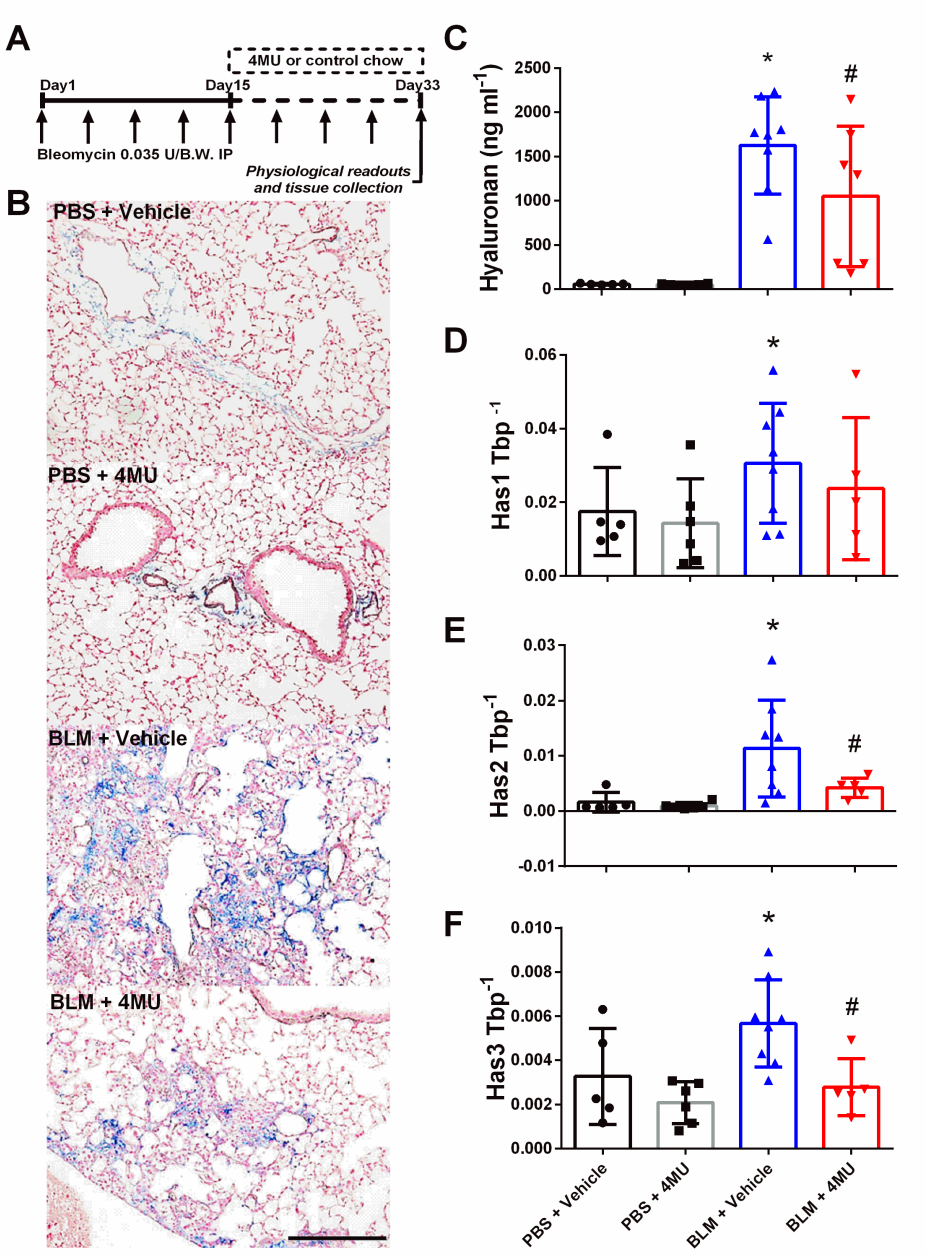

Figure 14 Reduction of hyaluronan levels with 4MU in lung fibrosis and PH.

Experimental mice are treated biweekly for 4 weeks with bleomycin (BLM; 0.035 U/g, i.p.) or PBS; 20 mg/kg/day 4MU or normal chow was administered beginning on day 15 until the end of the experiment (A). IHC (B) for hyaluronan from PBS + vehicle, PBS + 4MU, BLM + vehicle and BLM + 4MU treatment groups. Hyaluronan levels determined from BALF (C); mRNA levels from lung lysates for Has1 (D); Has2 (E) and Has3 (F) using

TATA-box binding protein (TBP). Data are shown as scatter plots showing the mean ± SD. * $P \leq 0.05$, significant difference between PBS + vehicle and BLM + vehicle treatment; ANOVA. # $P < 0.05$, significant difference between BLM + vehicle and BLM + 4MU treatment; ANOVA. The scale bar represents 50 μm. The N used for these studies are 5 (PBS + vehicle); 6 (PBS + 4MU); 8 (BLM + vehicle); 7 (BLM + 4MU) for panel C and 5 (PBS + vehicle); 6 (PBS + 4MU); 8 (BLM + vehicle); 5 (BLM + 4MU) for panels D–F. Variations in N are due to violation of a predetermined criteria: presence of blood in BALF (C) or repeatedly poor RNA quality and loss of sample (D–F).

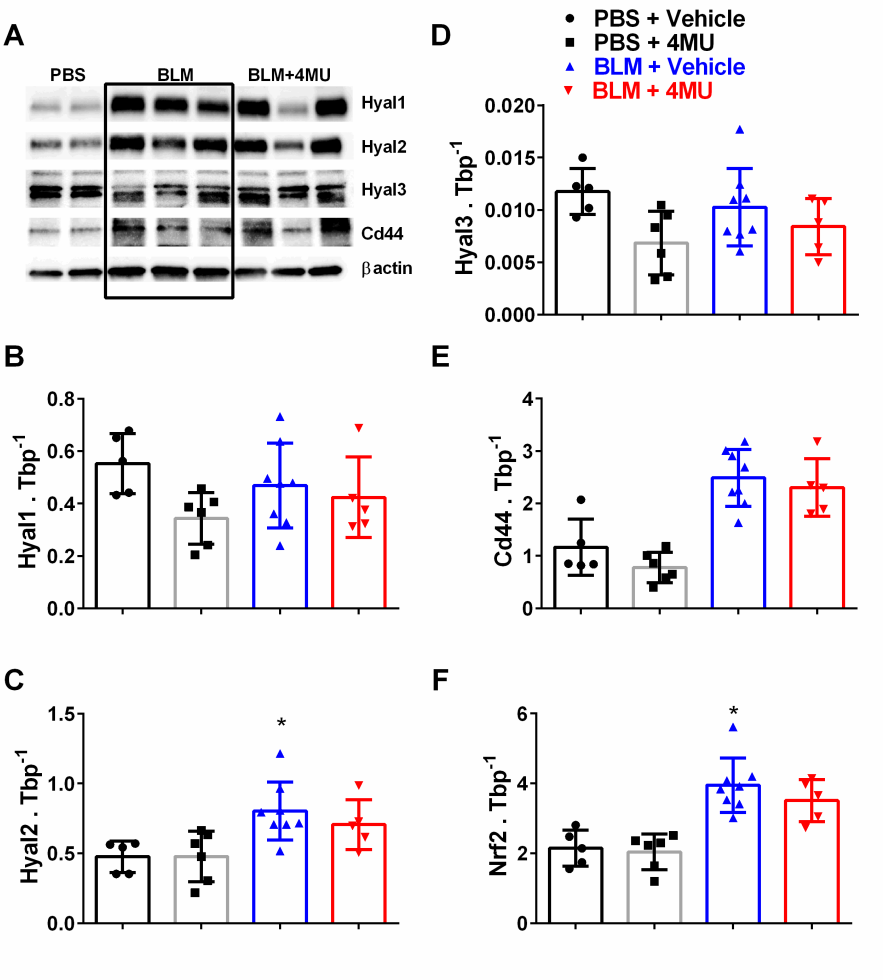

Figure 15 Hyaluronidases in mouse samples.

Immunoblots of 2 PBS [+vehicle], 3 BLM [+vehicle] and 3 BLM + 4MU for Hyal1, Hyal2, Hyal3, Cd44 and βactin (A). Transcript levels for Hyal1 (B), Hyal2 (C), Hyal3 (D), Cd44 (E) and Nrf2 (F). The N number used for these studies are 5 (PBS + Vehicle); 6 (PBS + 4MU); 8 (BLM + Vehicle); and 5 (BLM + 4MU). Significance level * $P \leq 0.05$ refers to ANOVA comparisons between PBS + Vehicle and BLM + Vehicle treatment groups. Variations in the N number are due to violation of a predetermined criteria: repeatedly poor RNA quality and loss of sample (B-D).

4-Methylumbelliferone (4MU) prevents vascular remodeling and PH

Using a mouse model of lung fibrosis and PH, I show increased vascular α-smooth muscle actin (αSMA) deposition in addition to Has1, Has2 or Has3 expression consistent with vascular remodeling in bleomycin-exposed mice compared to controls (Figure 16A) (190). Treatment with 4MU in bleomycin-exposed mice led to a reduction in αSMA deposition and Has1, Has2 or Has3 expression levels observed by immunofluorescence (Figure 16A) and assessed morphometrically (Figure 16B). These changes are in-line with physiological readouts of pulmonary hypertension such as RVSP where I report increased pressures in bleomycin-exposed mice that were significantly attenuated in the bleomycin + 4MU group (Figure 16C). Similarly, the Fulton index, a measure of RVH revealed increased values in bleomycin-exposed mice that were significantly inhibited in 4MU-treated bleomycin-exposed mice (Figure 16D). I also report a significant improvement in arterial oxygenation (SpO_2) in bleomycin+ 4MU treated mice compared with bleomycin-exposed mice where reduced oxygenation is apparent compared to controls (Figure 16E). No changes in LVSP or heart rate were observed between treatment groups (Figure 17A, B). Taken together my data show that 4MU can prevent vascular remodeling and the subsequent development of PH in the model. In addition, I performed bioanalysis by LC–MS/MS to determine the levels of 4MU and its metabolite 4-methylumbelliferyl-β-D-glucuronide (4MUG) from plasma samples. Interestingly I report increased levels of 4MU in bleomycin-exposed 4MU-treated mice compared with PBS-exposed 4MU groups (Figure 17C). 4MUG levels were elevated in both bleomycin and PBS exposed mice that received 4MU in the diet (Figure 17D).

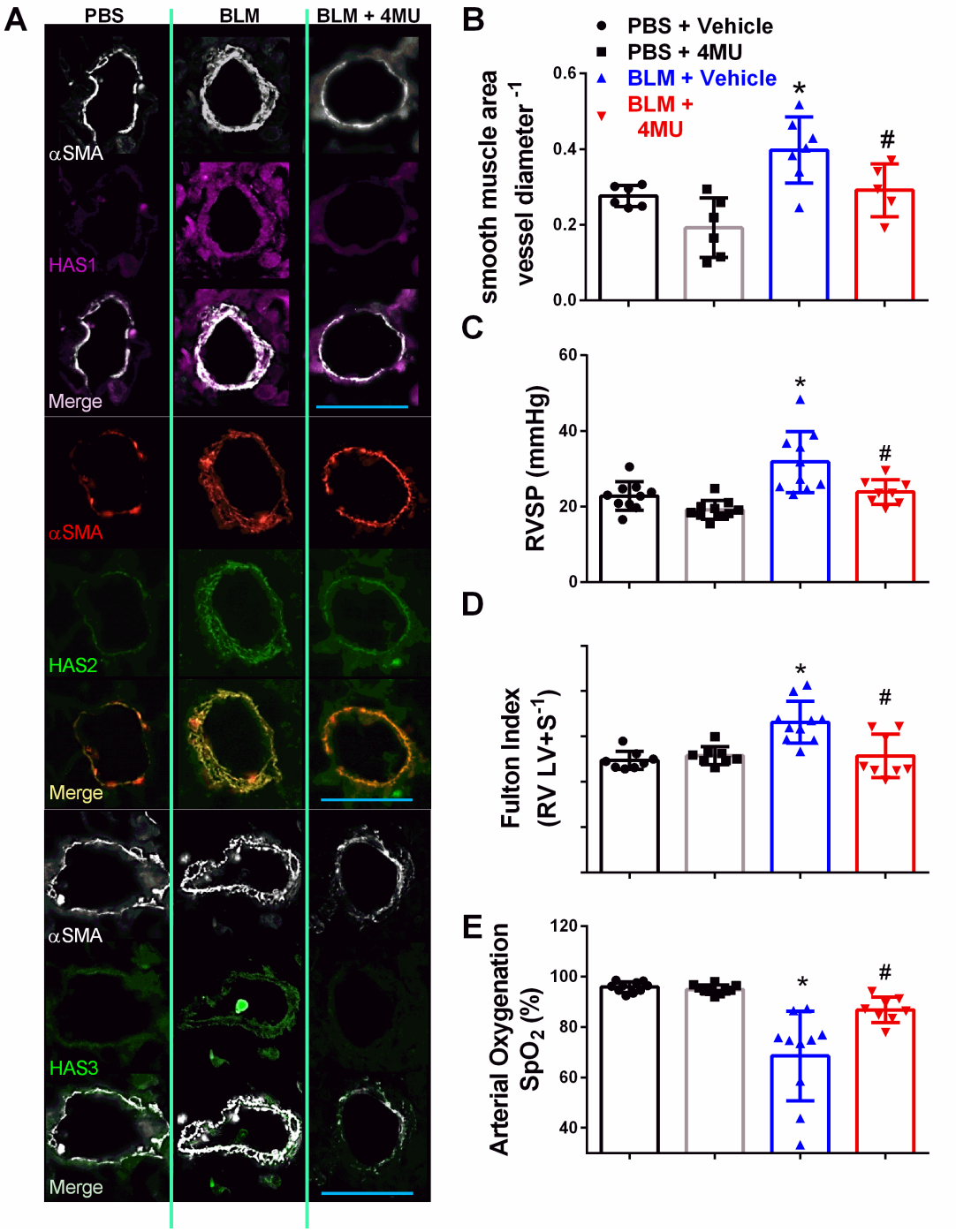

Figure 16 4MU prevents vascular remodeling and pulmonary hypertension.

IF-stained lung sections (A) for αSMA (white or red signals) and Has1 (violet/purple signals); Has2 (green signals); or Has3 (green signals) from mice treated with PBS + vehicle, bleomycin (BLM) + vehicle, or BLM + 4MU. Vascular remodeling determined

morphometrically (B); RVSP (C); Fulton index determined from measuring dry weights of RV and LV + septum (D); arterial oxygen (SPO_2) determined by pulse oximetry (E) from PBS + vehicle, PBS + 4MU, BLM + vehicle and BLM + 4MU treatment groups. Data are shown as scatter plot showing the mean ± SD. * $P \leq 0.05$, significant difference between PBS + vehicle and BLM + vehicle treatment; ANOVA. # $P < 0.05$, significant difference between BLM + vehicle and BLM + 4MU treatment; ANOVA. The scale bar represents 50 μm. The N used for these studies are 6 (PBS + vehicle); 6 (PBS + 4MU); 7 (BLM + vehicle); 5 (BLM + 4MU) for panel B; and 10 (PBS + vehicle) for panel B and 10 (PBS + 4MU); 10 (BLM + vehicle); and 8 (BLM + 4MU) for panels C, D and E. Variations in the N are due to violation of a predetermined criteria: inadequate inflation of the lung (C) or heart rate below 250 BPM at the time of RVSP or inability to perform pulse oximetry determination (C–E).

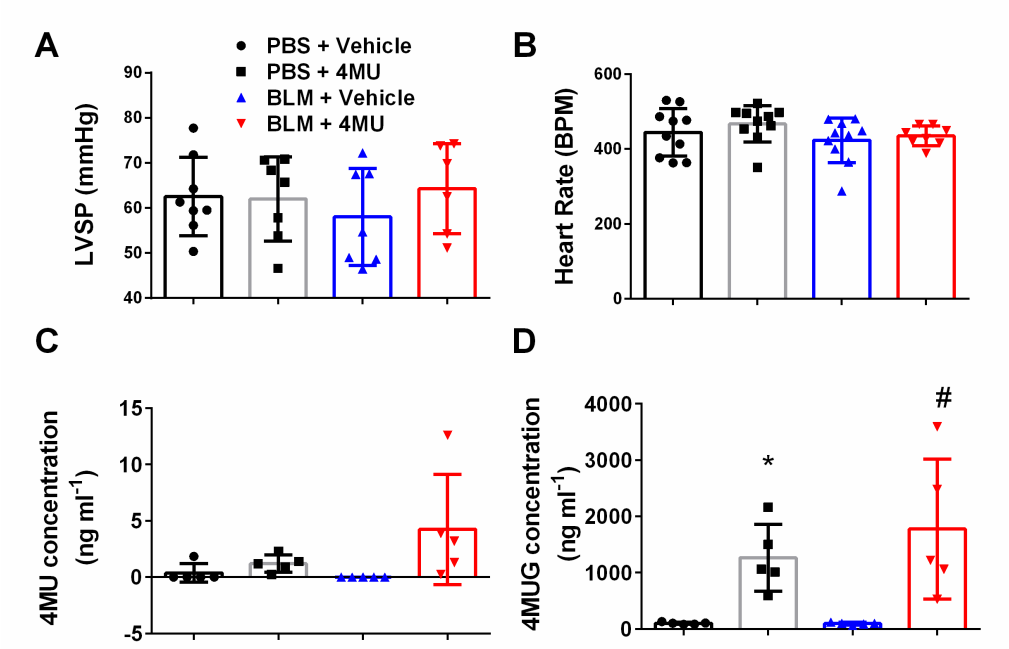

Figure 17 Additional hemodynamic data and 4MU / 4MUG levels in plasma.

Left ventricle systolic pressure (LVSP) (A) and heart rate (B) from PBS (PBS) + vehicle, PBS + 4MU, bleomycin (BLM) + vehicle, and BLM + 4MU treatment groups. Data is shown as a scatter plot showing the mean ± SD. The N number used for these studies are 8 (PBS + Vehicle); 7 (PBS + 4MU); 7 (BLM + Vehicle); and 6 (BLM + 4MU) for panel A and 10 (PBS + Vehicle); 10 (PBS + 4MU); 10 (BLM + Vehicle); and 8 (BLM + 4MU) for panel B. Plasma levels for 4-methylumbelliferone (4MU) and its metabolite: 4-methylumbelliferyl-β-D-glucuronide (4MUG) from PBS + Vehicle; PBS + 4MU; BLM + Vehicle; and BLM + 4MU treatment groups. n = 5 for all groups. Significance level * P ≤ 0.05 refers to ANOVA comparisons between PBS + Vehicle and BLM + Vehicle treatment groups. # P ≤ 0.05 refers to ANOVA comparisons between PBS + 4MU and BLM + 4MU treatment groups. Variations in the N number are due a violation of a predetermined criteria: heart rates below 250 BPM at the time LVSP determination (A) or below 250 BPM at the time of RVSP determination (B).

Fibrotic deposition is not altered in 4MU-treated mice

Numerous studies have shown a role for hyaluronan in the pathophysiology of lung fibrosis (152, 153, 180). Based on these observations, I anticipated that 4MU treatment would diminish the extent of fibrotic deposition in bleomycin-exposed mice. Interestingly, I report that treatment with 4MU did not reduce the extent of fibrotic scarring in the lungs as shown histologically (Figure 18A) or following Ashcroft score grading (Figure 18B). These observations are consistent with Col1a1 and Fn1 transcript levels showing elevated expression in bleomycin-exposed mice that were not inhibited in bleomycin + 4MU mice (Figure 18C, D). Consistent with these observations, an immunoblot for fibronectin (FN) shows increased FN signals in bleomycin-exposed mice compared with controls, that were not altered in bleomycin + 4MU mice (Figure 18E) and staining for SMA shows no difference in myofibroblast deposition between bleomycin-exposed mice following vehicle or 4MU treatment (Figure 18F). Collectively, these results suggest that 4MU, although able to inhibit vascular remodeling, may not influence fibrotic deposition at the dose and regimen used in this study.

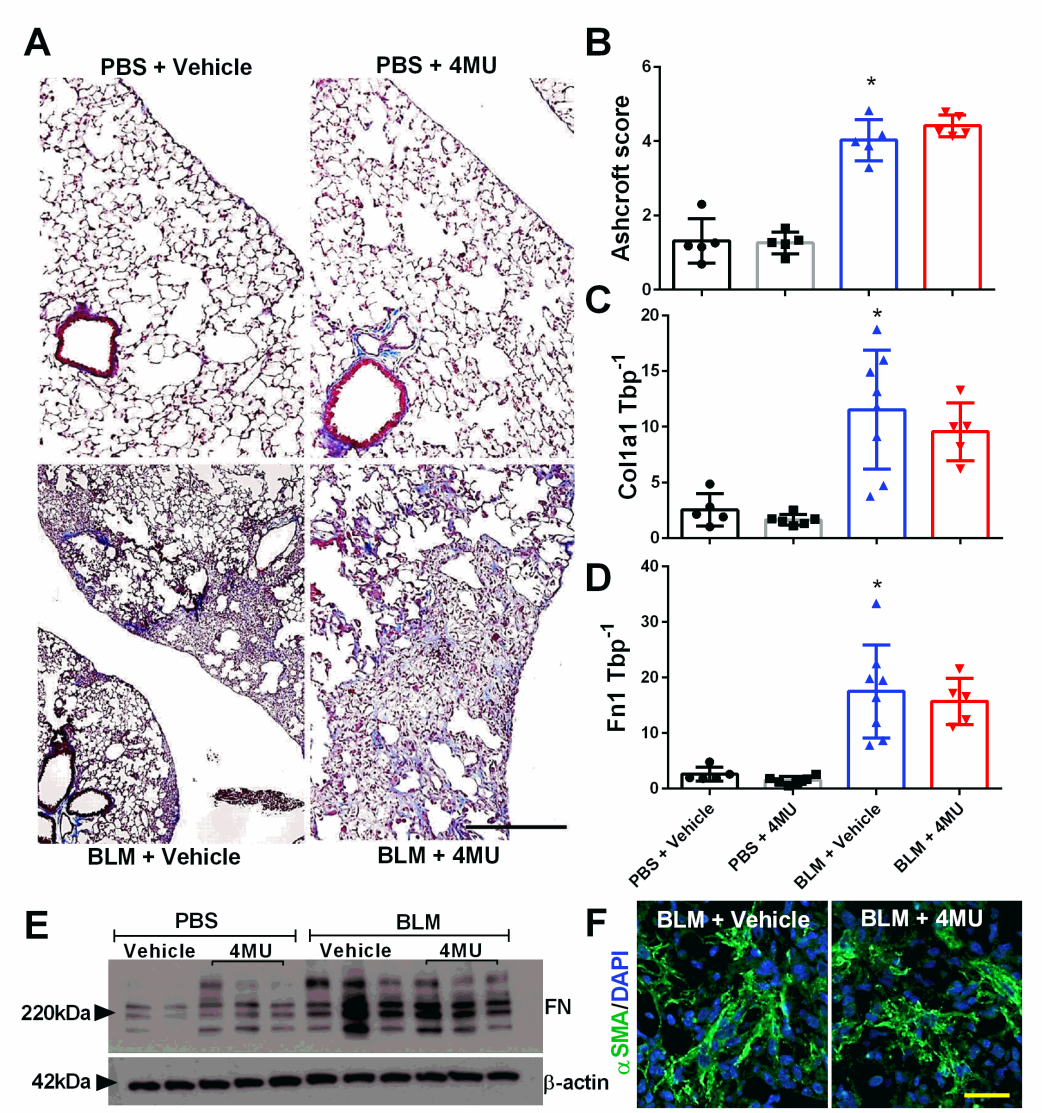

Figure 18 Fibrotic deposition is maintained in 4MU-treated mice.

Masson's trichome (A); Ashcroft scores (B); transcript levels for Col1a1 (C) and Fn1 (D); and immunoblots for FN and β-actin (E) from PBS + vehicle, PBS + 4MU, bleomycin (BLM) + vehicle and BLM + 4MU treatment groups. Lung sections IF stained for αSMA (green signals) and counterstained with DAPI (blue signals) (F) from BLM + vehicle or BLM + 4MU treatment groups. Data are shown as scatter plot showing the mean ± SD. * P ≤ 0.05, significant difference between PBS + vehicle and BLM + vehicle treatment; ANOVA. The scale bar represents 50 μm. The N used for these studies are 5

(PBS + vehicle); 5 (PBS + 4MU); 5 (BLM + vehicle); and 5 (BLM + 4MU) for panel B and 5 (PBS + vehicle); 6 (PBS + 4MU); 8 (BLM + vehicle); and 5 (BLM + 4MU) for panels C and D. Variations in the N are due to violation of a predetermined criteria: repeatedly poor RNA quality and loss of sample (B–D).

4MU treats established PH

I next examined the capability of 4MU to treat established PH. In this experiment, mice received 4MU or vehicle (control chow) starting on day 33 (Figure 19A), a time point where PH is present in the model (Figure 19A), for 14 days. Consistent with my previous experiment, 4MU resulted in reduced mRNA expression of Has1, Has2 and Has3 observed from flash-frozen lung samples and vascular protein levels shown by immunofluorescence (IF) (Figure 19B–D). Remarkably, I report higher RVSP levels on day 47 in mice treated with control chow compared with mice on day 33, that are drastically attenuated following treatment with 4MU (Figure 19E). Interestingly, 4MU did not appear to affect RVH when therapy started on day 33 (Figure 19F). No changes in LVSP were observed in these mice (Figure 19G). Consistent with my previous results, 4MU did not affect fibrotic deposition as observed histologically and through Ashcroft scores (Figure 6A, B). RT-PCR for Col1a1, Col1a2 and Col3a1 did not reveal differences between bleomycin + 4MU and bleomycin + vehicle treatment groups (Figure 20C–E). Interestingly, no significance differences between Hyal1, Hyal2, Hyal3 and CD44 at the mRNA or protein level were detected between bleomycin + vehicle and bleomycin + 4MU groups (Figure 20F–I). However, reduced levels for RhoA guanine nucleotide exchange factor 25 (GEFT), a signaling protein seen to act downstream of CD44 (192), were found in bleomycin-exposed 4MU-treated mice compared to bleomycin-exposure and vehicle treatment (Figure 20I). Determination of hyaluronan fragment size in isolated lung tissue revealed increased LMW hyaluronan fragments in bleomycin-exposed mice compared to controls; 4MU treatment reduced total hyaluronan fragment size, particularly LMW-HA (Figure 20J). Taken together, these results highlight the

properties of 4MU in reversing PH associated with lung fibrosis, despite not inhibiting FN and Col1a1 levels. These results also show that 4MU does not appear to have an effect on Hyal expression levels but that it may also alter GEFT levels that may be important for PH.

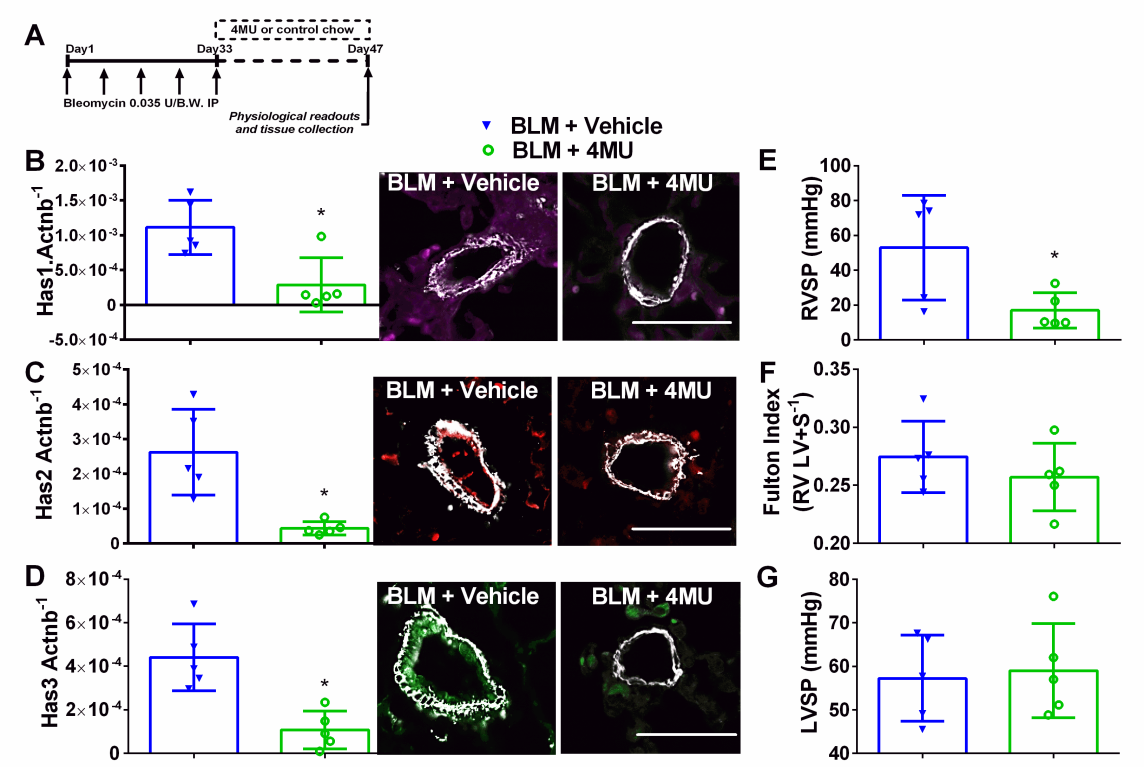

Figure 19 4MU attenuates established pulmonary hypertension.

Here mice are treated biweekly for 4 weeks i.p. with bleomycin (BLM; 0.035 U·g–1, i.p.) or PBS; 20 mg·kg–1·day–1 4MU or normal chow was administered beginning on day 33; once PH was established for 2 weeks, measurements were performed on day 47 (A). mRNA expression levels and IF staining for Has1 (violet/purple signals) and αSMA (white signals) (B); Has2 (red signals) and αSMA (white signals) (C) and Has3 (green signals) and αSMA (white signals) (D) normalized to β-actin (Actnb). RVSP (E), RVH determined from measuring dry RV and LV + septum masses (F); and LVSP (G); BLM + vehicle and BLM + 4MU treatment groups. Data are shown as scatter plot showing the mean ± SD. * P ≤ 0.05, significant difference between BLM + vehicle and BLM + 4MU treatment; unpaired Student's t-test. The N used for these studies are 5 (BLM + vehicle); and 5 (BLM + 4MU).

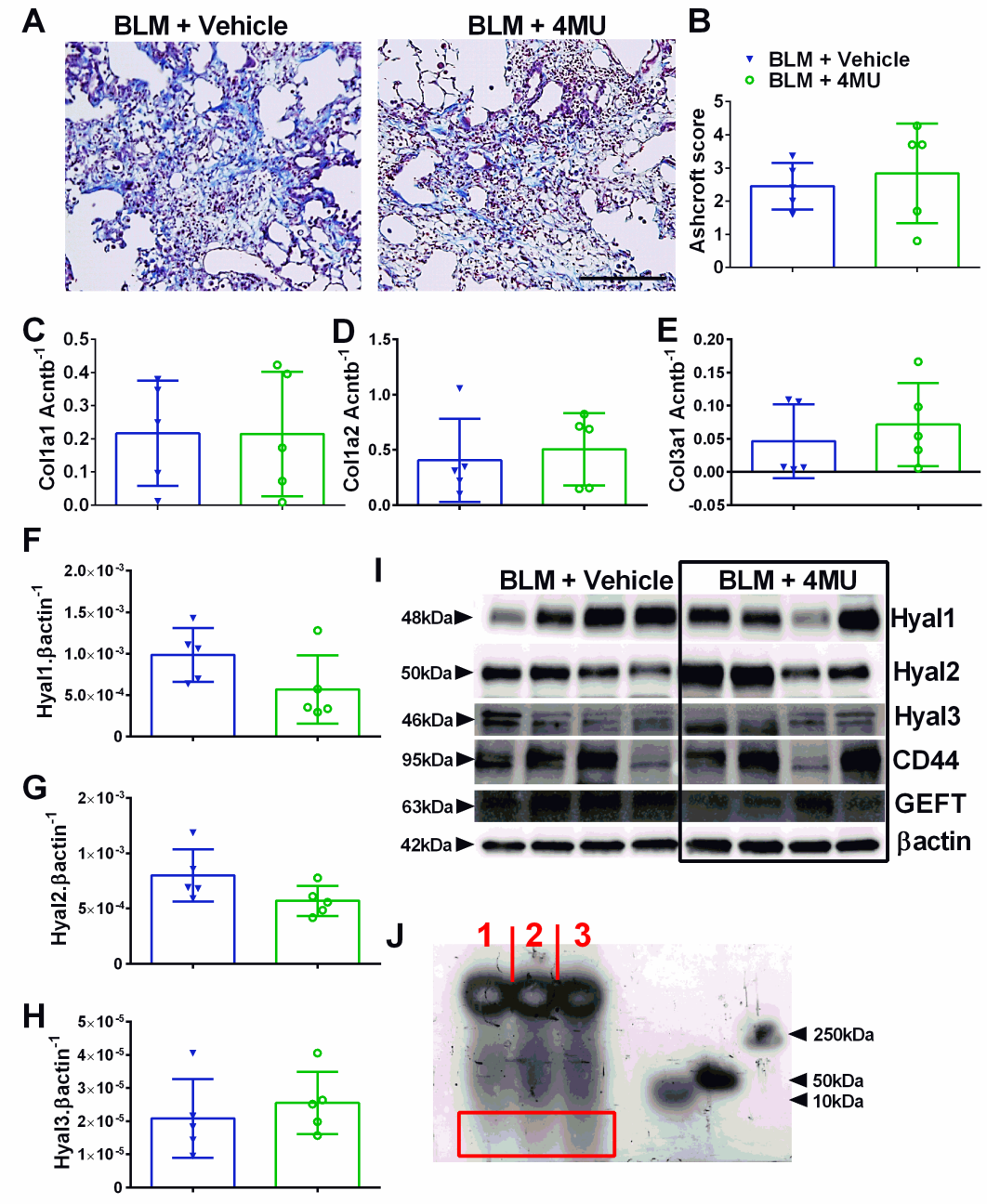

Figure 20 4MU does not affect fibrotic deposition in established PH.

Masson's trichrome-stained lung sections (A) and Ashcroft scores (B) from bleomycin (BLM) or BLM + 4MU-treated mice. Expression levels of Col1a1 (C), Col1a2 (D), Col3a1 (E), Hyal1 (F), Hyal2 (G) and Hyal3 (H) normalized to β-actin (Actnb). immunoblots (I) for Hyal1, Hyal2, Hyal3 Cd44, GEFT and β-actin for four representative mice from

BLM + vehicle and BLM + 4MU treatment groups. Hyaluronan fragment size (J) from a PBS (lane 1), BLM + 4MU (lane 2) or a BLM-exposed (lane 3) lung. The red rectangle highlights an area with LMWHA fragments showing a greater density in lane 3. Data are shown as scatter plot showing the mean ± SD (Panels B–H). The N used for these studies are 5 (BLM + vehicle); and 5 (BLM + 4MU).

Increased vascular hyaluronan-binding protein 2 (HABP2) is observed

Studies have shown that HABP2, an extracellular serine protease that binds hyaluronan and has been implicated in mediating endothelial dysfunction (193). Interestingly, in my study, I show increased levels of HABP2 in remodeled vessels from mice exposed to bleomycin compared with controls, that are subsequently reduced in bleomycin-exposed mice treated with 4MU (Figure 21). In line with these observations, I report increased HABP2 in and adjacent to remodeled vessels in the lung from patients with IPF + PH compared to IPF and normal lungs (Figure 22A). In support of these data, an immunoblot for HABP2 revealed increased levels in IPF + PH patient samples compared to IPF or normal lungs (Figure 22B, C). Studies have implicated increased signaling of HABP2 and hyaluronan complexes through a RhoA mechanism (193). As such, I examined whether increased signals for GEFT, a protein that interacts with Rho GTPases and is involved in the activation of RhoA and subsequent contraction of vascular smooth muscle (194). Indeed, I report increased GEFT in lung lysates from patients with IPF + PH compared to normal or IPF alone (Figure 22D, E). Remarkably, increased HABP2 was only observed in remodeled vessels and not in fibrotic lesions of the lung as observed in mice lungs exposed to bleomycin and treated with vehicle or 4MU or in fibrotic lesions of patients with IPF + PH (Figure 23). These observations suggest that the interaction between HABP2 and hyaluronan and subsequent RhoA activation may be a unique mechanism contributing to PH associated with lung fibrosis.

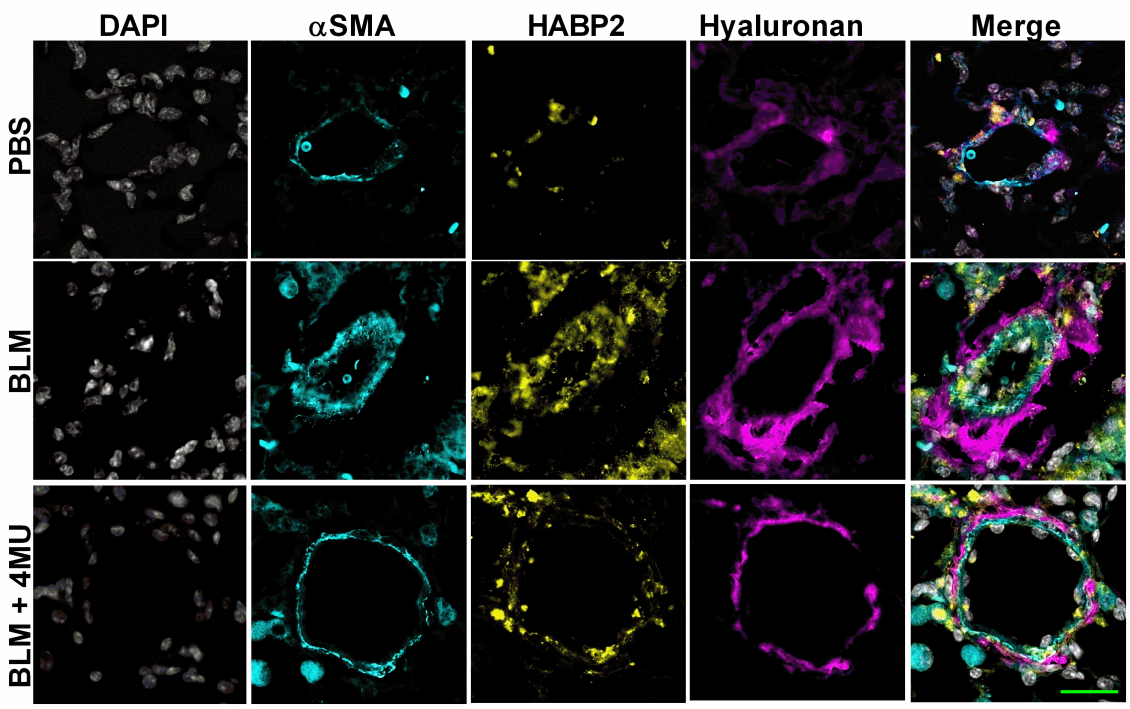

Figure 21 4MU reduces vascular HABP2 levels.

Lung sections triple immunofluroescently stained for αSMA (turquoise signals), HABP2 (yellow signals) and hyaluronan (violet/purple signals) and counterstained with DAPI (white/grey signals) from PBS, bleomycin (BLM) or BLM + 4MU-exposed mice. The scale bar represents 50 μm.

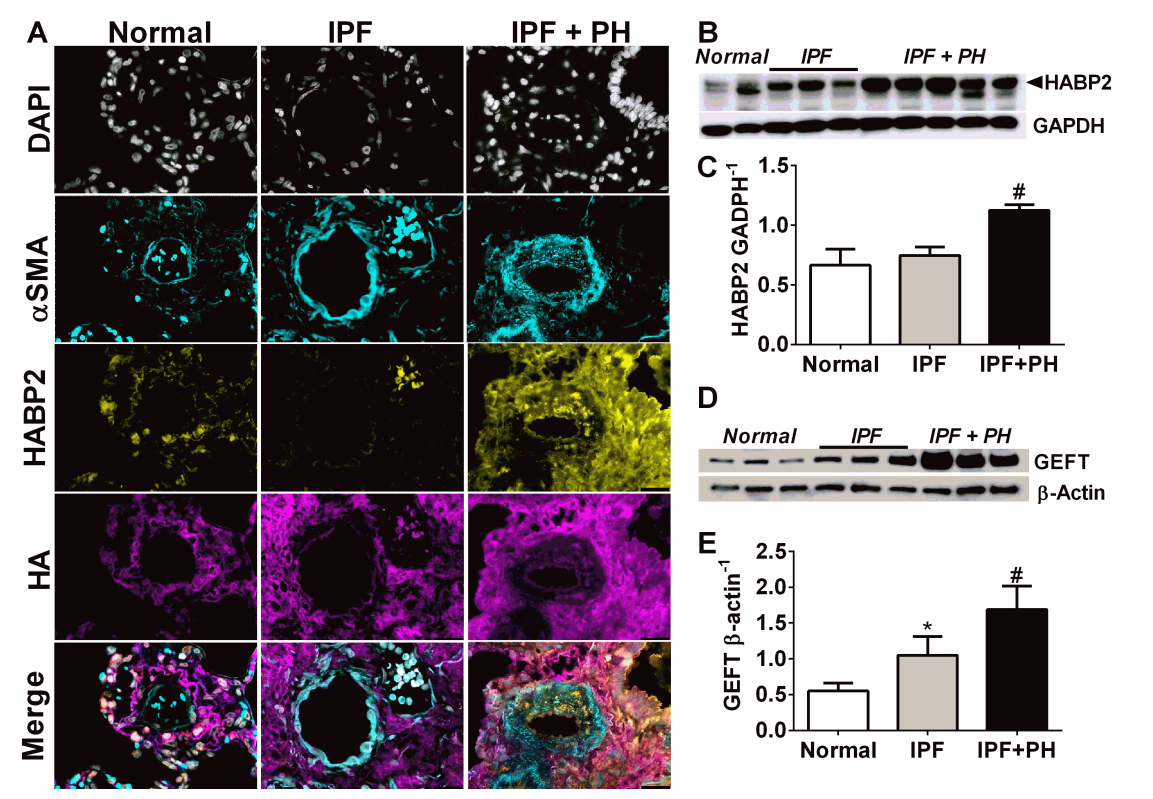

Figure 22 Increased vascular HABP2 in patients with IPF and IPF + PH.

Lung sections from a pulmonary vessel showing triple immunofluroescent staining for αSMA (turquoise signals), HABP2 (yellow signals) and HA (violet/purple signals) and counterstained with DAPI (white/grey signals) (A); immunoblots for HABP2 and GADPH (B); densitometry for HABP2 normalized to GADPH (C); immunoblots for GEFT and β-actin (D); and densitometry for GEFT normalized to β-actin (E) from normal lung tissue and from lung explants from patients with IPF and IPF + PH. The scale bar represents 50 μm. * $P \leq 0.05$, significant difference between normal and IPF + PH values.

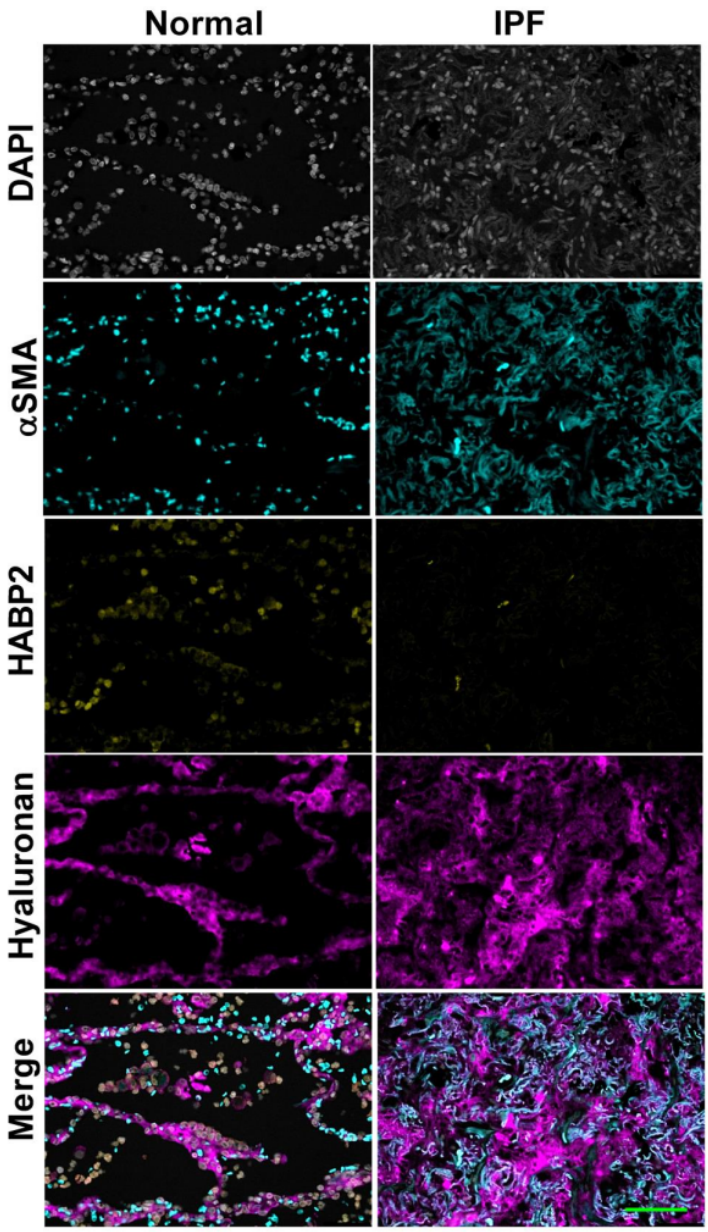

Figure 23 HABP2 is not expressed in the lung parenchyma.

Lung sections triple immunofluroescently (IF) stained for αsmooth muscle actin (α-SMA/ turquoise signals), HABP2 (yellow signals), and hyaluronan (HA; violet/purple signals) and counterstained with DAPI (white/grey signals). No HABP2 signals are observed in the lung parenchyma from patients with IPF.

Hyaluronan fragments affect PASMC properties

Using human PASMC from normal areas of resected cancer tissue, I demonstrate that MMW and LMW hyaluronan fragments lead to increased proliferation of PASMC that is inhibited by fasudil, a Rho kinase inhibitor (Figure 24A); no significant differences were seen in cytotoxicity between treatment groups (Figure 24B). I next examined the capacity of these cells to migrate using a 3D cell culture protocol (195). In these experiments, I report reduced cell migration in PASMC following treatment with LMW-HA and ULMW-HA that was reversed following treatment with fasudil (Figure 24C). Surprisingly, atomic force microscopy (AFM) experiments revealed that MMW and ULMW-HA fragments were both able to increase PASMC stiffness that was reversed using fasudil (Figure 24E). AFM measurements were performed in the center of the cell (Figure 24F). Taken together, these results demonstrate that hyaluronan fragments are able to cause stiffening of PASMC and that LMW-HA induced increased proliferation but reduced motility of these cells in a Rho-dependent manner that contribute to the pathophysiology of PH associated with lung fibrosis.

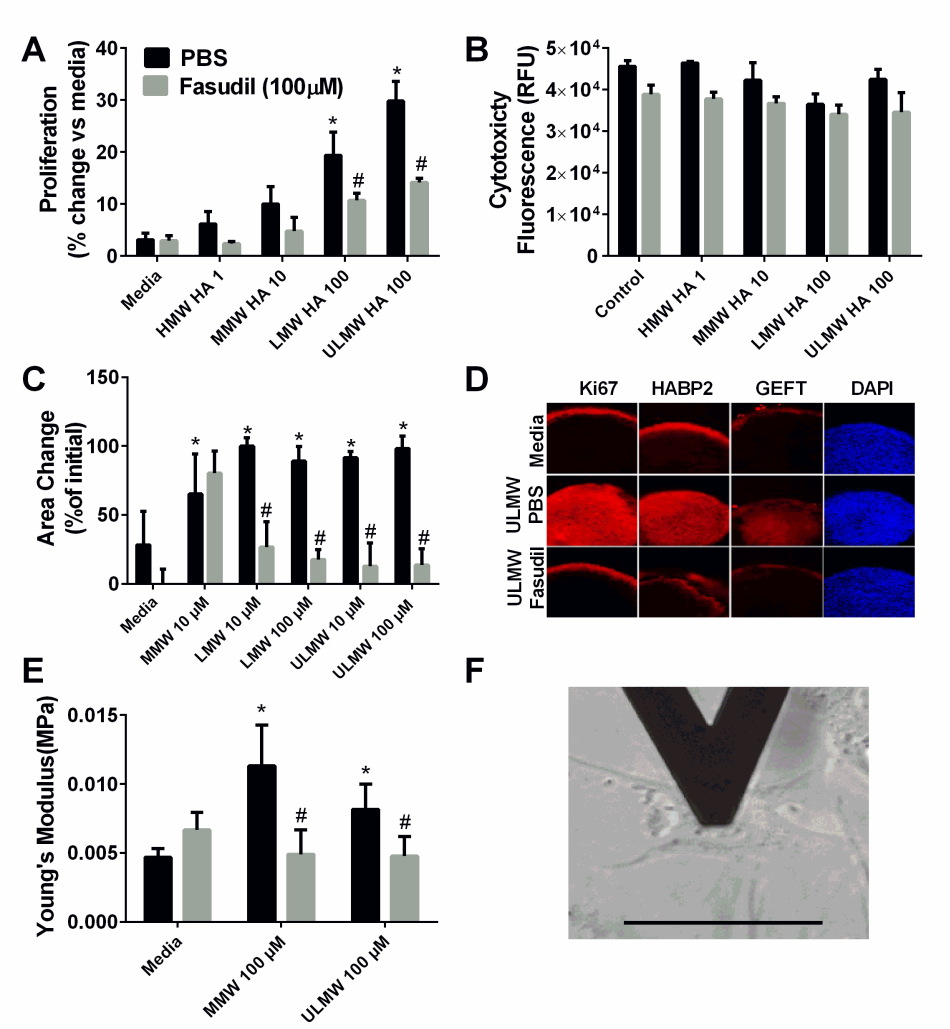

Figure 24 Hyaluronan affects PASMC properties.

Cellular proliferation (A) and cytotoxicity (B) from cells exposed to HMW, MMW, LMW or ULMW hyaluronan treated with PBS or fasudil (100 μM). Migration assay for MMW, LMW and ULMW (C). Staining for Ki67, HABP2 and GEFT in cell culture after treatment with ULMW HA and Fasudil (D). Atomic force microscopy experiments showing increased cells stiffness using Young's modulus for PASMC treated with media only, MMW or ULMW HA (E). Detail of the positioning of the AFM tip on the centre of a PASMC (F). * $P \leq 0.05$, significant difference between media and MWM + PBS, LMW + PBS or ULMW + PBS experimental, ANOVA. # $P \leq 0.05$, significant difference between PBS and fasudil treatment groups; unpaired Student's t-test.

Discussion

A major finding of this study was that HAS2 expression is associated with increased PH in patients with IPF. Additionally, we see increases in HAS3 and Hyal2 expression. Furthermore, these expression changes are associated with staining for HA in patients with IPF, including those with secondary PH, near the pulmonary vasculature. These findings are confirmed in the bleomycin model of lung fibrosis and PH. Provocative results from this study demonstrate that treatment with 4MU, a hyaluronan synthesis inhibitor that also targets HAS mRNA expression, prevented the development of PH and treated established PH associated with lung fibrosis. My results are remarkable as they show that 4MU is able to attenuate RVSP and vascular remodeling, but it does not appear to affect fibrotic deposition in the lungs. In a second model of PH, initial studies indicate 4MU also reduced RVSP and RVH while deletion of the HAS2 gene from vascular smooth muscle cells was able to reduce RVSP without changes to RVH. These results point at a unique mechanism for hyaluronan in the pathogenesis of PH. Novel findings from my study demonstrate increased expression of HABP2 and GEFT in remodeled vessels from patients with Group 3 PH and in experimental models of PH and lung fibrosis. I also show that hyaluronan fragments induce increased PASMC proliferation and stiffness of the cell and also affect cellular migration in a RhoA-dependent fashion. Taken together, my results demonstrate that elevated hyaluronan is modulating PH associated with lung fibrosis that can be treated by inhibiting hyaluronan synthesis or RhoA activation. These results are significant given the poor prognosis of patients with chronic lung diseases with an additional diagnosis of PH, where no treatment options are available(196).

Elevated hyaluronan has been reported in lung diseases including IPF and PH and in PH associated with chronic obstructive pulmonary disease as well as PAH (153, 155, 158, 180, 189, 197). Consistent with these findings, I report increased hyaluronan levels in IPF compared with normal lungs that are elevated further in patients with a diagnosis of PH. Interestingly, my data show evidence for elevated HAS enzymes in disease. These findings are significant as HAS2 has been shown to promote senescence in fibroblasts in pulmonary fibrosis suggesting a similar pathogenic role for HAS2 in PASMC (198). HMW hyaluronan fragments are typically associated with beneficial properties with smaller fragments inducing pathogenic effects through its interaction with cell membrane receptors such as CD44 (189, 199). Hyaluronidases and ROS have been shown to degrade HMW hyaluronan to lower molecular weight fragments. In line with this, I report increased levels of several hyaluronidases in IPF in addition to a correlation between NRF2 transcripts and elevated mPAP levels in patients in IPF. Taken together, these studies demonstrate that hyaluronan synthesis is up-regulated, perhaps as a protective response, but that the higher levels of hyaluronidases and oxidative stress lead to degradation of hyaluronan to pathogenic factors. Although the mechanisms that lead to elevated expression of HAS and HYALs are not the focus of this study, I anticipate that activation of the adenosine A2B receptor modulates this process, consistent with the notion of elevated adenosinergic-hypoxic axis in PH associated with IPF and the role of adenosine in modulating hyaluronan synthesis associated with chronic obstructive pulmonary disease (158). It is well known that higher molecular fragments of hyaluronan are beneficial (180). In addition, hyaluronan has been shown to promote progenitor cell renewal and prevent severe fibrosis in mice

(200). Therefore, an alternative approach to inhibiting hyaluronan synthases would be to prevent the degradation of hyaluronan to the more pathogenic smaller fragments by developing selective inhibitors of hyaluronidases. Interestingly, two patients from the study cohort were treated with N-acetylcysteine, a compound known to inhibit hyaluronidases (201). It is worth noting that these patients did not have a diagnosis of PH and one had the lowest levels of mPAP in the cohort.

The mechanisms that lead to the development of PH associated with chronic lung diseases are not fully understood (17, 202). Traditional views suggest that eliminating the underlying chronic lung disease such as fibrosis will result in the improvement of PH outcomes. Although studies have shown that inhibition of fibrotic deposition or airspace enlargement in the lungs improves PH, the identification of a unique mechanism leading to PH associated with lung fibrosis has been elusive (158, 190). Surprisingly, my results show that inhibiting hyaluronan synthesis by 4MU prevents the development of PH and reduces established PH without affecting fibrotic deposition in the lungs. An explanation for these results may reside in the fact that although hyaluronan levels were reduced, the levels may still be high enough to maintain fibroproliferative lesions. Alternatively, findings demonstrating a protective role for hyaluronan in severe fibrosis could also help explain my findings (200).

These effects are consistent with reduced Has transcripts and vascular Has levels seen by IF. Consistent with previous publications showing a beneficial effect for 4MU my results demonstrate that 4MU treatment attenuated bleomycin-induced vascular remodeling, elevated RVSP and RVH and led to an increased arterial oxygenation (203-205). It is important to note that in experiments where 4MU was administered in

established PH (on day 33 vs. 15), RVSP but not RVH was attenuated. In this model, I believe that lung vascular remodeling precedes RVH; thus, I anticipate that in already established PH, a longer treatment time may be necessary to have an effect on RVH. Despite this, these results point at a potential use for 4MU in patients with IPF with the aim of preventing the development of PH. Lowering elevated mPAP levels in patients with Group 3 PH and preventing the development of PH in patients with IPF would be a valuable clinical outcome, as PH in IPF is strongly associated with mortality (17). However, it is important to note that despite these observations, there is still controversy over whether treating PH in the setting of IPF improves survival, despite early improvements in functional status and quality of life (206). However, in those studies, the effects of a vasodilator were evaluated, and it remains possible that therapies that are aimed to alter the process of vascular remodeling would have greater beneficial effects (206). It is also important to mention that patients with IPF + PH who have a lung transplant, have worse outcomes than those without PH, suggesting that treating PH might lead to similar outcomes to those patients with IPF and no PH. Moreover, reducing elevated mPAP levels in patients with chronic lung diseases and out-of-proportion PH would enable these patients to become eligible for lung transplantation, a procedure that is often unavailable for them. The doses of 4MU I have used here, while lower than some studies, especially those that characterized the pharmacokinetics of this drug, were able to produce a physiological response and detectable levels in the plasma of the treated animals (207). This dose is similar to the dose used in a human clinical study in motor disorders of the bile ducts (208). These results may indicate that inhibition of HA production in the lung is possible with

comparatively lower doses of 4MU, leading to the potential to use less drug and consequently produce fewer side effects.

In my effort to identify how elevated hyaluronan may play a role in the development of PH, I identified increased expression of HABP2 in remodeled vessels of patients with Group 3 PH and in experimental models of PH and lung fibrosis. Interestingly, increased HABP2 appeared to be localized in remodeled vessels and was not observed in areas rich in fibroproliferative injury. Increased HABP2 has been shown to down-regulate vascular integrity through a RhoA-dependent mechanism (193). In line with this, I report increased expression of GEFT, an essential component of the RhoA pathway activation that has been linked to hyperplasia of vascular smooth muscle cells (209). In subsequent experiments, I demonstrated that LMW and ULMW hyaluronan fragments induced increased proliferation of isolated human PASMC that were inhibited by the RhoA inhibitor fasudil. These studies are consistent with the capacity of hyaluronan to induce cellular proliferation and demonstrate a novel role for fasudil in hyaluronan-induced PASMC proliferation (189, 197, 210). Furthermore, in contrast to published experiments showing increased cellular migration by hyaluronan, my studies show that cellular migration PASMC is drastically inhibited by LMW and ULMW hyaluronan fragments in a RhoA-dependent manner (189, 197, 199). These differences may derive from the fact that most cells where hyaluronan-induced cellular migration has been reported are in cancer cells that are prone to migration. However, my results showing reduced cellular migration are in line with increased PASMC stiffness observed by AFM following exposure to hyaluronan (189, 197, 210). These observations are consistent with increased vascular stiffness induced by hyaluronan

accumulation in the aorta (177). Interestingly, in this study, increased proliferation of vascular smooth muscle cells was also associated with increased hyaluronan accumulation. This is consistent with experiments showing increased PASMC proliferation when grown in substrates with similar stiffness as that seen in distal vessels in PH (162). Taken together, my results show that increased HABP2 and GEFT are present in remodeled vessels of patients with Group 3 PH. My data show evidence that hyaluronan fragments are able to induce both cellular proliferation and increased stiffness of PASMC while attenuating migration of these cells that contribute to the development of PH. These findings would support the use of fasudil for the treatment of Group 3 PH. Indeed, fasudil has been used in Group 1 PH where it has shown promising results and is effective in models of lung fibrosis , although it's potential as a treatment for Group 3 PH has not yet been fully evaluated (179, 211, 212). Another promising approach is the development of inhibitors of HABP2, a protein that is strongly associated with the development of Group 3 PH and has recently been linked with cancer (213).

Chapter 5: Identifying the role of hyaluronan in Combined Pulmonary Fibrosis and Emphysema

This chapter is based upon research originally published in *Disease Models and Mechanisms*. Collum SD, Molina JG, Hanmandlu A, Bi W, Pedroza M, Mertens TCJ, Wareing N, Wei W, Wilson C, Sun W, Rajadas J, Bollyky PL, Philip KM, Ren D, Thandavarayan RA, Bruckner BA, Xia Y, Blackburn MR, Karmouty-Quintana H. Adenosine and hyaluronan modulate lung fibrosis and pulmonary hypertension in combined pulmonary fibrosis and emphysema (CPFE). *Dis Model Mech* 2019.

Introduction

In the previous chapter I have demonstrated the important role that HA plays in the development of PH. I also indicate that though HA is associated with pulmonary pressure increases, patients with IPF have increased HA over healthy individuals. This is in line with previous studies indicating that HA signaling is important for invasive fibroblast during the progression to severe lung fibrosis (153). In fact HA depositions has long been a hallmark of lung fibrosis (214).

Continued research has shown that HA deposition and degradation play an important role in COPD as well. Patients with severe COPD have increased levels of HA and HYAL2 compared to control subjects (149). HA and HYAL activity have strong correlations with survival time in patients with COPD (215). Additionally, a previous publication from the Karmouty lab has shown increased levels of HA associated with PH secondary to COPD in patient samples (158).

However, whether abnormal HA synthesis and destruction are present in CPFE is not known. CPFE is a complex disease where both fibrotic matrix deposition, similar to IPF, is present and airspace enlargement, a hallmark of COPD, is also present in the same lungs. Up to 90% of patients with CPFE also develop PH, a sever complication for this disease. My results in the previous chapter, showing a mechanistic role of HA in PH, and previous data showing strong correlation for HA with IPF and COPD indicate that it may be a common mechanism that plays a role in CPFE. This motivated me to investigate the role of HA in CPFE to investigate the shared role in fibrotic deposition and emphysematic alveoli destruction.

Traditionally, COPD (specifically emphysema) and IPF are regarded as separate disease entities. Nonetheless, hallmarks of both COPD and IPF were first described in autopsies of lungs in 1974 (216); however, it was not until 2005 that this condition was classified as a well-defined syndrome termed CPFE (217). Male smokers or ex-smokers most often present with CPFE (217-219) and it has a dismal prognosis with only a 55% survival rate at 5 years (217). CPFE is a distinct under-recognized syndrome where no specific diagnostic guidelines are present, yet studies show that its presentation is much more frequent than previously believed (159). An important and highly fatal co-morbidity in CPFE is the development of PH (220). The prevalence of PH in CPFE ranges between 47-90% and is much higher than in patients with IPF or emphysema alone (19, 26, 28, 159). Confirmation of PH by right-heart catheterization data plummets 1-year survival rates to only 60% (26). Despite this dismal prognosis, no therapy options exist for patients with CPFE outside of smoking cessation, oxygen therapy and lung transplantation (27, 219). Specifically, for PH in CPFE, endothelin receptor antagonists,

prostanoids and phosphodiesterase type 5 inhibitors have been used. However, these agents are not recommended for PH in CPFE due to the vasodilation profile of these agents resulting in ventilation/perfusion mismatch (28), highlighting the need to develop novel treatment approaches for CPFE.

Although several gene mutations have been associated with CPFE, including telomerase genes (hTERT or hTR), surfactant protein C (SFTPC) and ATP binding cassette subfamily A member 3 (ABCA3), these have been performed in very small familial cohorts (hTERT/hTR) or in case studies (SFTPC/ABCA3) (27). As such no single gene defect is known be associated with CPFE and the mechanisms leading to the development of CPFE remains vastly unknown (219). Despite this, studies in COPD and IPF patients with PH have revealed increased activation of the adenosinergic axis and enhanced levels of the glycosaminoglycan hyaluronan (158, 190, 221). In these studies, increased activation of the adenosine A2B receptor (ADORA2B) was shown to enhance expression of the hyaluronan synthases, contributing to the pathophysiology of chronic lung disease (158, 190, 221, 222). Furthermore, several studies from our group, have implicated macrophages in the pathophysiology of lung fibrosis and PH. In these studies, deletion of myeloid ADORA2B was able to prevent BLM-induced PH and lung fibrosis (222). Further studies from our group have also demonstrated an important link between macrophage activation and ADORA2B expression promoting fibrotic lung injury (223). These results point at macrophages as a potential mechanism promoting lung fibrosis and PH, however whether they play a role in CPFE is not known.

Using a unique model of experimental lung injury that replicates features of CPFE, namely airspace enlargement, PH and fibrotic deposition (158, 224), I investigated

the capacity of a hyaluronan synthase inhibitor to attenuate features of chronic lung injury and determined a link between hyaluronan expression and macrophages.

Results

Characterization of an experimental model of CPFE.

I used *Ada*$^{-/-}$ mice to model features of CPFE. *Ada*$^{-/-}$ mice received supplemental PEG-ADA, allowing them to live normally, from birth up to week 24. Starting on week 24, PEG-ADA was gradually reduced over 9 weeks and starting on week 34 mice were provided with control chow or medicated with 4MU for 4 weeks. The gradual reduction of PEG-ADA results in accumulation of extracellular adenosine that is associated with chronic injury (225).

A hallmark of CPFE is the presence of fibrotic deposition and airspace enlargement. I determined the extent of fibrotic deposition first by staining lung sections with Masson's Trichrome and performing Ashcroft scores to determine the extent of fibrosis. These experiments revealed a marked increase in fibrotic deposition in *Ada*$^{-/-}$ mice compared to *Ada*$^{+}$ mice that was significantly attenuated in *Ada*-deficient mice treated with the hyaluronan inhibitor: 4-Methylumbelliferone (4MU) (Figure 25 A, B). These histological changes were consistent with expression levels of fibronectin that were elevated in *Ada*$^{-/-}$ mice compared to *Ada*-competent mice. Therapy with 4MU reduced *Fn* expression levels in *Ada*$^{-/-}$ mice (Figure 25 C). I next examined the extent of airspace enlargement, a key feature of CPFE, in the mouse model using black and white images of the lung parenchyma. *Ada*$^{-/-}$ mice presented with evidence of airspace enlargement as observed histologically and by mean chord length measurements

determined morphometrically in comparison to *Ada*$^{+}$ mice (Figure 25 D, E). Treatment with 4MU did not alter the emphysematous development in *Ada*-deficient mice (Figure 25 D, E), despite improved arterial oxygenation (SpO_2) compared to *Ada*$^{-/-}$ mice exposed to control chow (Figure 25F). The development of PH is a serious and common complication of CPFE (26). A feature of PH associated with chronic lung disease is vascular remodeling and hyaluronan deposition (158, 190, 226). In order to assess the extent of vascular remodeling, I performed dual-IHC for SMA and hyaluronan. These experiments revealed extensive muscularization of arterioles in *Ada*$^{-/-}$ compared to *Ada*$^{+}$ mice that was significantly attenuated in 4MU-treated *Ada*$^{-/-}$ mice (Figure 25G). Widespread hyaluronan deposition was observed surrounding remodeled vessels in *Ada*$^{-/-}$ mice whereas no hyaluronan was present in parenchymal vessels of *Ada*-competent animals; 4MU treatment drastically reduced the levels of peri-vascular hyaluronan in mice lacking ADA (Figure 25G). These observations were backed by morphometric evaluation of vascular wall remodeling and hyaluronan levels in BALF (Figure 25 H, I). These analyses demonstrated increased SMA signals in the remodeled vessels of *Ada*$^{-/-}$ mice compared to *Ada*$^{+}$ mice that were attenuated in *Ada*$^{-/-}$ mice exposed to 4MU (Figure 25 H). BALF hyaluronan levels revealed patently increased hyaluronan levels in *Ada*$^{-/-}$ compared to control mice that were markedly reduced in *Ada*$^{-/-}$ + 4MU exposed mice (Figure 25 I). Taken together, my results show that my model of *Ada*$^{-/-}$ mice presents with cardinal features of CPFE: fibrotic deposition, airspace enlargement and vascular remodeling, a key component of PH. Furthermore, I demonstrate that treatment of these mice with 4MU is able to attenuate both the fibrotic deposition and vascular remodeling in *Ada*$^{-/-}$ mice.

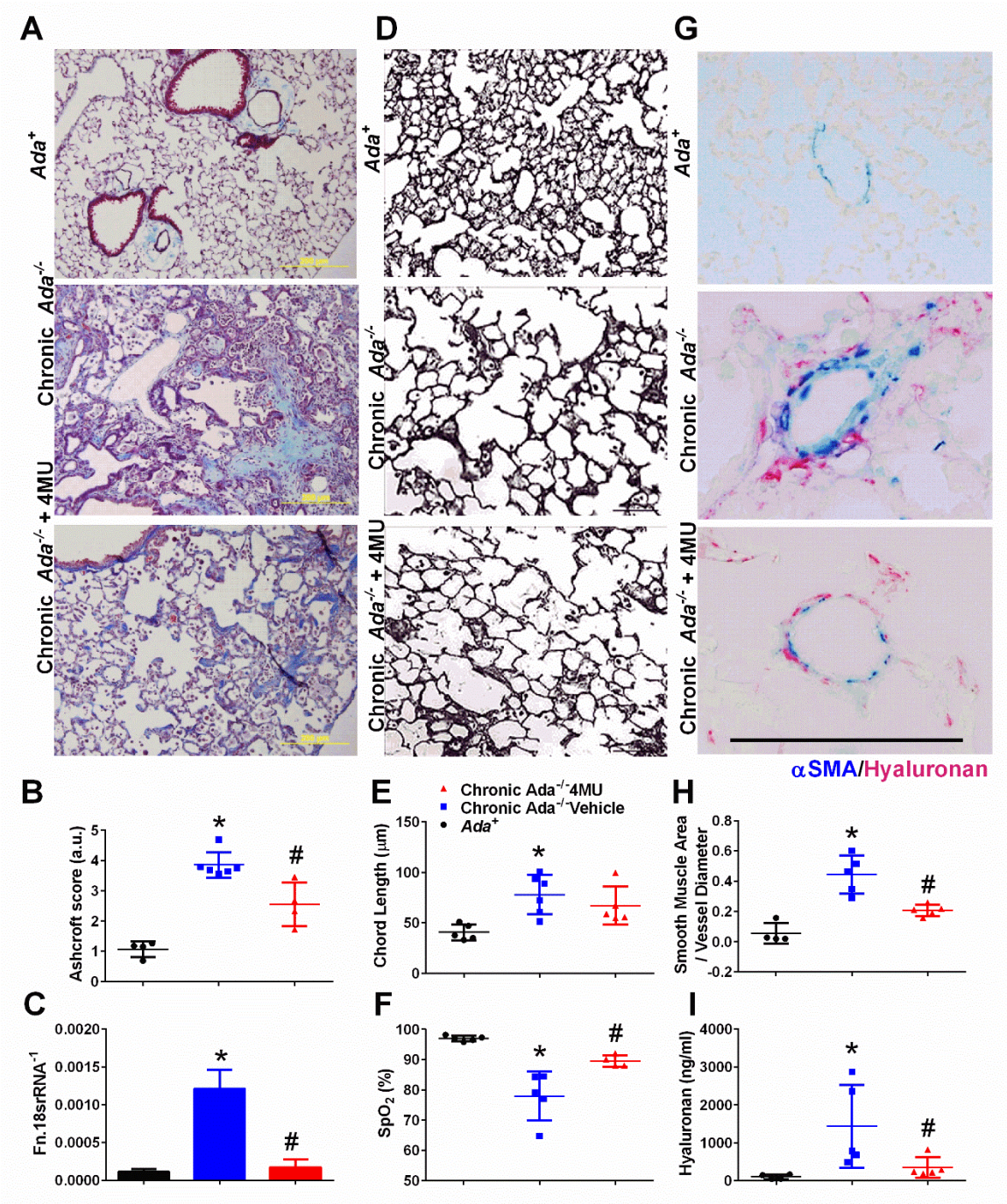

Figure 25 Features of chronic lung injury in Ada-/- mice and the effect of (4-methylumbelliferone [4-MU]) or control chow.

(A) Representative Masson's Trichome images showing fibrotic deposition in the in *Ada*$^{-/-}$ mice (middle panel) compared to *Ada*$^{+}$ mice (upper panel). The effect of 4-MU in

Ada$^{-/-}$ mice is shown in the bottom panel. Aschroft scores from Masson's Trichome images (B) and mRNA expression levels of Fibronectin (FN, C) from *Ada*$^{+}$(white bars), *Ada*$^{-/-}$ (grey bars) and *Ada*$^{-/-}$ + 4MU treated mice (black bars). (D) Black and white images of the lung parenchyma from *Ada*$^{+}$ mice (upper panel), *Ada*$^{-/-}$ (middle panel) and *Ada*$^{-/-}$ + 4MU treated mice (lower panel). Mean chord length determined histologically (E) and arterial oxygen saturation (F) from *Ada*$^{+}$ (white bars), *Ada*$^{-/-}$ (grey bars) and *Ada*$^{-/-}$ + 4MU treated mice (black bars). (G) Representative dual-immunohistochemistry staining for alpha smooth muscle actin (SMA, blue signals) and hyaluronan (magenta signals) showcasing arterioles from *Ada*+ (upper panel) *Ada*$^{-/-}$ (middle panel) and *Ada*$^{-/-}$ + 4MU (lower panel). Morphometric evaluation of SMA deposition from 5 to 7 vessels for each mouse (H) and broncho-alveolar lavage fluid (BALF) levels of hylauronan (I) from *Ada*$^{+}$ (white bars), *Ada*$^{-/-}$ (grey bars) and *Ada*$^{-/-}$ +4MU treated mice (black bars). For panels B, C, E, F, H, I data is presented as mean + SEM. *P< 0.05 refers to comparisons between *Ada*$^{+}$ and *Ada*$^{-/-}$ treatment groups. #< 0.05 refers to comparisons between *Ada*$^{-/-}$ and *Ada*$^{-/-}$ + 4MU treatment groups. Scale bars represent 200 μm

Vascular physiology, metabolism and hyaluronan levels in $Ada^{-/-}$ mice.

Although vascular remodeling is a key feature of PH, right-heart catheterization and determination of RVSP in mice is necessary to adequately evaluate the extent of PH. As such, RVSP measurements were determined in my experimental model. I report increased RVSP in $Ada^{-/-}$ mice compared to Ada^{+} mice that were attenuated in $Ada^{-/-}$ + 4MU mice (Figure 26A). Consistent with the phenomenon of PH, no differences in LVSP were observed between treatment groups (Figure 26B). The RVSP data was accompanied by evidence of right ventricle hypertrophy (RVH) in $Ada^{-/-}$ mice compared to Ada^{+} littermates that did not appear to be significantly attenuated following 4MU therapy (Figure 26C). In order to probe the mechanisms associated with the development of PH, I next evaluated the expression levels of the Adora2b and evidence of metabolic alterations. Enhanced adenosinergic axis and metabolic alterations have been reported in Group 3 PH (158, 190, 221, 222). These experiments revealed heightened *Adora2b* expression in $Ada^{-/-}$ mice but no expression in Ada^{+} or $Ada^{-/-}$ + 4MU mice (Figure 26D). Consistent with dysregulated metabolism, I report reduced levels of Pparg and Sdha that were not rescued following 4MU therapy (Figure 26 E, F). I next evaluated the expression levels of hyaluronan synthases, which are known to be up-regulated by ADORA2b activation. These experiments revealed elevated expression of *Has3* but not *Has1* or *Has2* in $Ada^{-/-}$ mice compared to controls that was significantly reduced following 4MU treatment in Ada-deficient mice (Figure 26 G-I). Dual IHC for hyaluronan and αSMA revealed increased hyaluronan deposition in fibrotic areas in $Ada^{-/-}$ mice that was significantly attenuated following 4MU therapy (Figure 26J). These results demonstrate that $Ada^{-/-}$ mice present with physiological features of PH including

elevated RVSP and RVH in addition with increased *Adora2b* and *Has3* expression, concomitant with elevated hyaluronic acid deposition observed histologically. 4MU therapy was able to attenuate the increased RVSP and hyaluronic acid deposition associated with reduced *Adora2b* and *Has3* expression levels, but did not affect the dysregulated metabolic profile or reverse RVH.

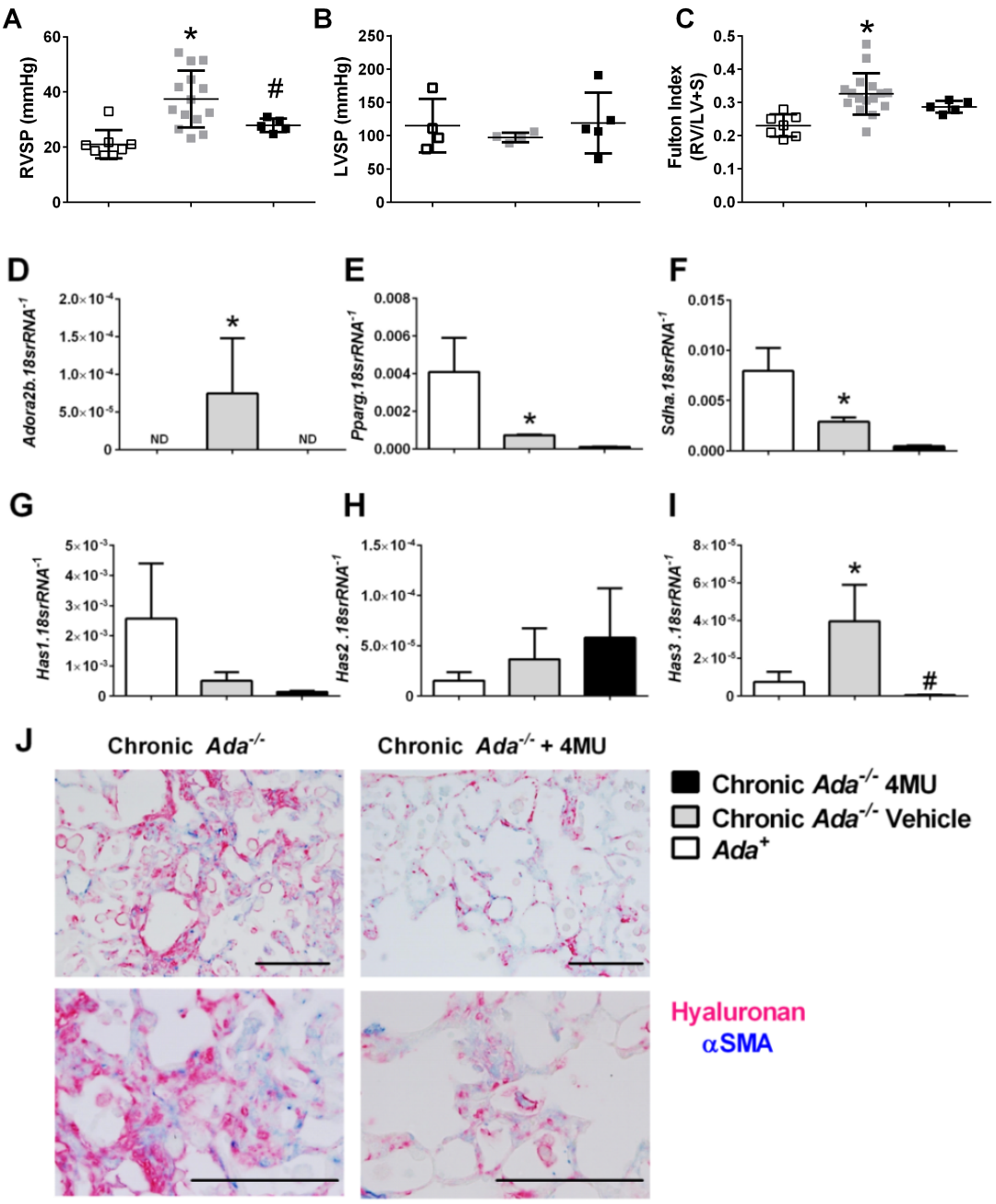

Figure 26 Cardiovascular physiology, metabolic profile and hyaluronan synthesis and deposition in *Ada*$^{-/-}$.

Right ventricular systolic pressure (RVSP, A), left ventricular systolic pressure (LVSP, B) and Fulton Index ratio (C) determined by the measure of right ventricle and left ventricle with septum from *Ada*$^{+}$ (white bars), *Ada*$^{-/-}$ (grey bars) and *Ada*$^{-/-}$ +4MU treated

mice (black bars). Transcript expression levels from lung tissue for Adora2b (D), Pparg (E), Sdha (F), Has1 (G), Has 2 (H), Has 3 (I) by RT-PCR from *Ada*$^{+}$ (white bars), *Ada*$^{-/-}$ (grey bars) and *Ada*$^{-/-}$ +4MU treated mice (black bars). (J) Representative dual-immunohistochemistry staining in fibrotic areas of *Ada*$^{-/-}$ or *Ada*$^{-/-}$ + 4MU treatment groups for alpha smooth muscle actin (SMA, blue signals) and hyaluronan (magenta signals). Scale bars represent 200 μm. For panels A-I data is presented as mean + SEM. *P< 0.05 refers to comparisons between *Ada*$^{+}$ and *Ada*$^{-/-}$ treatment groups. #< 0.05 refers to comparisons between *Ada*$^{-/-}$ and *Ada*$^{-/-}$ + 4-MU treatment groups. The N used for these studies are 8 (Ada+); 13 (Ada-/-); 5 (Ada-/- +4MU). Variations in N are due to violation of a predetermined criteria: heart rate below 250 BPM at the time of RVSP or LVSP.

Macrophages in Ada$^{-/-}$ mice.

An interesting feature of the *Ada*$^{-/-}$ mice was the presence of F4/80 *positive* cells in the lung (Figure 27A), while treatment with 4MU resulted in an attenuation of F4/80+ cells in *Ada*$^{-/-}$ mice (Figure 27A, B). I next evaluated whether these cells were positive for HAS3. Indeed, double-IHC for HAS3 and F4/80 revealed signals for HAS3 and F4/80 in *Ada*$^{-/-}$ mice that appeared reduced following treatment with 4MU (Figure 27 C, D). Interestingly, increased HAS3 signals were observed in vascular and epithelial cells. Further IHC demonstrated that these HAS3-positive cells also expressed hyaluronan and were observed close to vessels in *Ada*$^{-/-}$ mice (Figure 28 A). Treatment with 4MU resulted in an attenuation of HAS3/hyaluronan positive cells and a marked reduction of hyaluronan (Figure 28 A, B). These HAS3+ cells were also observed in areas rich in myofibroblasts (observed using αSMA IF) that were reduced following 4MU treatment (Figure 28 C, D). Our group has previously demonstrated that activation of hypoxic adenosinergic axis in macrophages is important for the development of lung fibrosis (222, 223). In these studies, reduced hyaluronan deposition was observed in mice lacking Adora2b in myeloid cells (222). Thus, using MH-S cells, a murine macrophage cell line, I next examined whether increased expression of the hyaluronan synthase isozymes was Adora2b-dependent. These experiments revealed that Has2 and Has3, but not Has1, was increased following treatment with the ADORA2b agonist Bay60-6583, and that this response was inhibited by the presence of the ADORA2b antagonist GS-6201 (Figure 29 A-C). This response was consistent with elevated BAY60-6583-induced interleukin-6 that was inhibited by GS-6201 (Figure 29 D). IL-6 is a known pro-fibrotic mediator downstream of macrophage ADORA2b stimulation (222, 223, 227). Taken

together, these results point at an ADORA2b-mediated increase of HAS3-expressing macrophages (F4/80 positive cells) that lead to increased hyaluronan deposition.

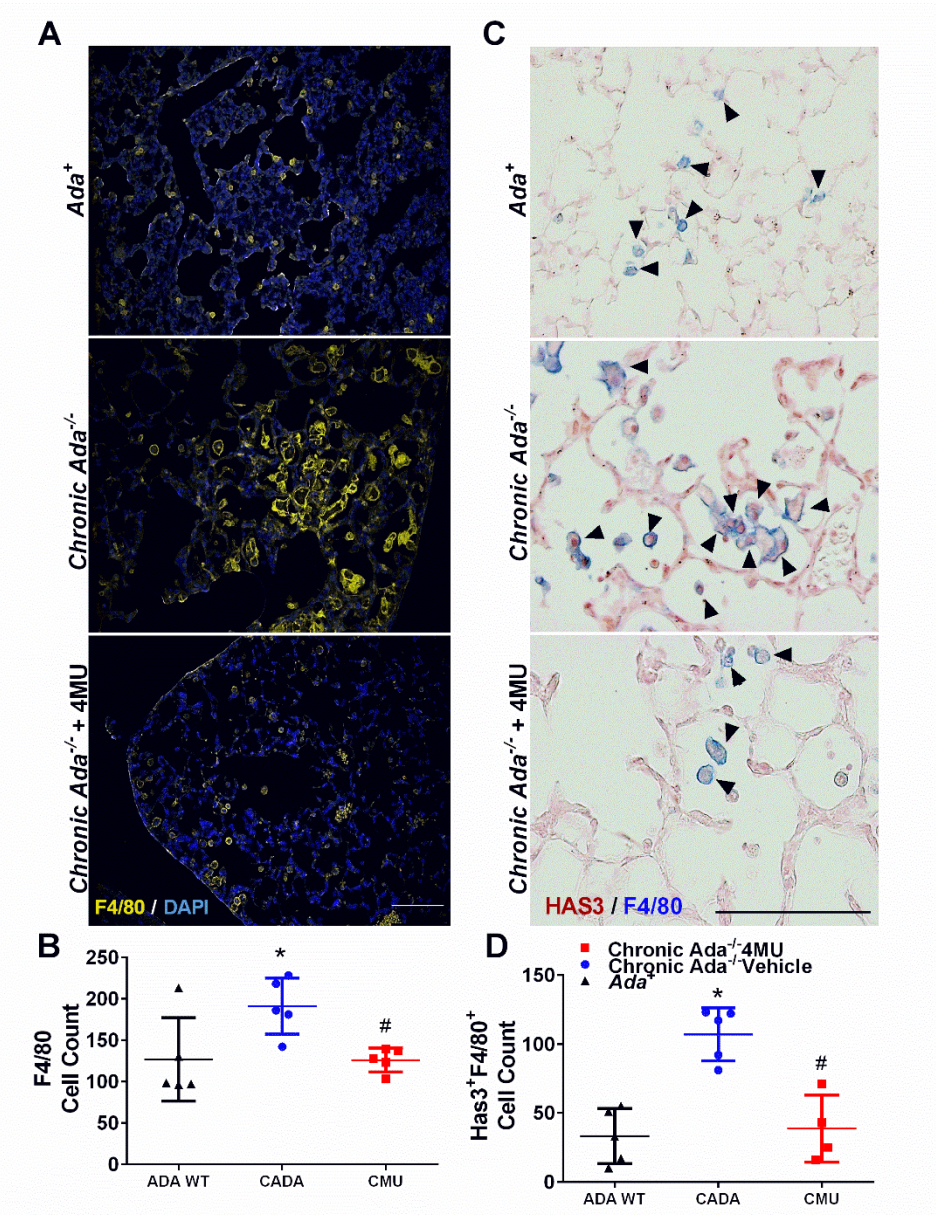

Figure 27 Macrophages in *Ada*$^{-/-}$ mice.

(A) Immunohistochemistry for F4/80 (yellow signals) and nuclear DAPI stain showing F4/80 positive cells in *Ada*$^{+}$ (upper panel) *Ada*$^{-/-}$ (middle panel) and *Ada*$^{-/-}$ + 4MU (lower panel). Scale bar represents 75 µm. (B) F4/80 positive cells from 10 micropictographs from the lung parenchyma from Ada+ (white bars), *Ada*$^{-/-}$ (grey bars) and *Ada*$^{-/-}$ + 4MU treated mice (black bars). *P< 0.05 refers to comparisons between *Ada*$^{+}$ and *Ada*$^{-/-}$

treatment groups. #< 0.05 refers to comparisons between *Ada*$^{-/-}$ and *Ada*$^{-/-}$ + 4MU treatment groups. (C) Dual immunohistochemistry for hyaluronan synthase 3 (Has3, red/brown signals) and F4/80 (blue signals) in *Ada*+ (upper panel) *Ada*$^{-/-}$ (middle panel) and Ada$^{-/-}$ + 4MU (lower panel). Scale bar represents 200 μm. (D) Double F4/80 and HAS3 positive cells from 10 micropictographs from the lung parenchyma from Ada+ (white bars), *Ada*$^{-/-}$ (grey bars) and *Ada*$^{-/-}$ + 4MU treated mice (black bars). *P< 0.05 refers to comparisons between *Ada*$^{+}$ and *Ada*$^{-/-}$ treatment groups. #< 0.05 refers to comparisons between *Ada*$^{-/-}$ and *Ada*$^{-/-}$ + 4-MU treatment groups

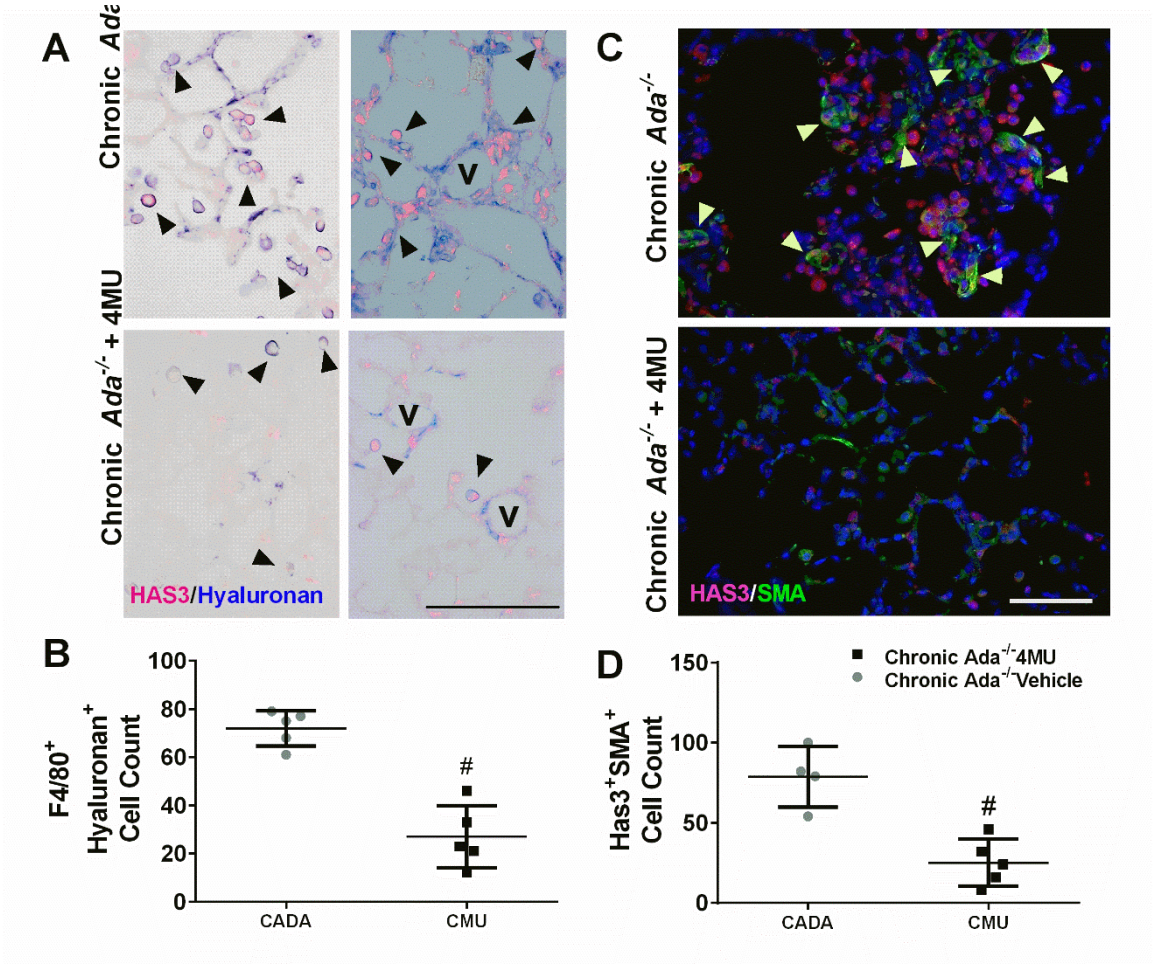

Figure 28 Macrophages in *Ada*$^{-/-}$ mice express HAS3.

(A) Dual immunohistochemistry for hyaluronan synthase 3 (Has3, magenta signals) and hyaluronan (blue signals) in *Ada*$^{-/-}$ (upper panels) and *Ada*$^{-/-}$ + 4MU (lower panels). Scale bar represents 100 µm. (B) Double HAS3 and hyaluronan positive cells from 10 micropictographs from the lung parenchyma from *Ada*$^{-/-}$ (grey bars) and *Ada*$^{-/-}$ + 4MU treated mice (black bars). (C) Dual immunohistochemistry for hyaluronan synthase 3 (Has3, magenta signals) and alpha-smooth muscle actin (SMA green signals) in *Ada*$^{-/-}$ (upper panels) and *Ada*$^{-/-}$ + 4MU (lower panels). Scale bar represents 75 µm. (D) Double HAS3 and SMA positive cells from 10 micropictographs from the lung parenchyma from *Ada*$^{-/-}$ (grey bars) and *Ada*$^{-/-}$ + 4MU treated mice (black bars). #< 0.05 refers to comparisons between *Ada*$^{-/-}$ and *Ada*$^{-/-}$ + 4-MU treatment groups

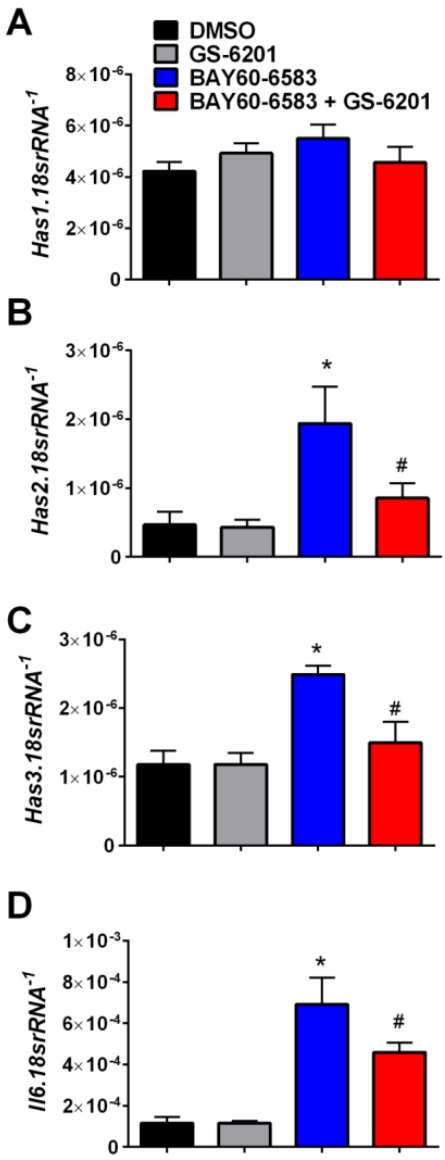

Figure 29 Response to macrophages to an ADORA2B agonist.

Experimental Design Mertens TCJ, Collum SD, Karmouty-Quintana H. Experiment performed by and experimental data compliments of Mertens TCJ.

Transcript levels of (A)Has1, (B) Has2, (C) Has3, (D) IL6 of MH-S cells exposed to DMSO (black bars); the Adora2b antagonist: GS-2601 (grey bars), the Adora2b agonist: BAY60-6583 (blue bars), or under the presence of both GS-2601 and BAY60-6583 (red bars). *P<

0.05 refers to comparisons between DMSO and BAY60-6583 treatment groups. #< 0.05 refers to comparisons between BAY60-6583 and BAY60-6583 + GS-2601 treatment groups.

The adenosinergic response in CPFE.

Using explanted lung tissue derived from upper or lower lung lobes from CPFE patients or from normal lungs that were discarded for transplantation, I evaluated mediators involved in the generation and degradation of adenosine, in addition to adenosine receptors. In CPFE, upper lobes often present with emphysema while fibrotic deposition is more prevalent in lower lobes. Quantitative RT-PCR for the ectonucleotidases CD39 and CD73 (Figure 30 A, B) demonstrated increased expression of the rate limiting enzyme CD73 but not CD39 in lower lobes but not upper lobes of CPFE compared to normal lung tissue (Figure 30 A, B). No differences were seen in *ADA* expression levels from lung tissue derived from upper or lower lobes (Figure 30 C). Equilibrative nucleoside transporters (ENT) also regulate extracellular adenosine levels whereby reduced expression is associated with increased adenosine accumulation and the development of lung injury (228). However, I report no difference in ENT expression in CPFE despite a downward trend for *ENT-2* in lower lobes of CPFE lungs (Figure 30D). Expression levels of adenosine receptors did not show significant alterations in ADORA1 or ADORA2A between normal and CPFE lung tissue (Figure 30 E, F). However, increased expression levels of ADORA2B were detected in lower lobes of CPFE compared to normal lungs but not in tissue derived from upper lobes (Figure 30 G). Similarly, to ADORA1 and ADORA2A, no significant differences in expression of ADORA3 were observed between normal and CPFE-derived lung tissue (Figure 30 H). Taken together, these results suggest that in CPFE, like in other chronic lung diseases(225), increased adenosine synthesis is enhanced in concert with expression of its low-affinity receptor, ADORA2B.

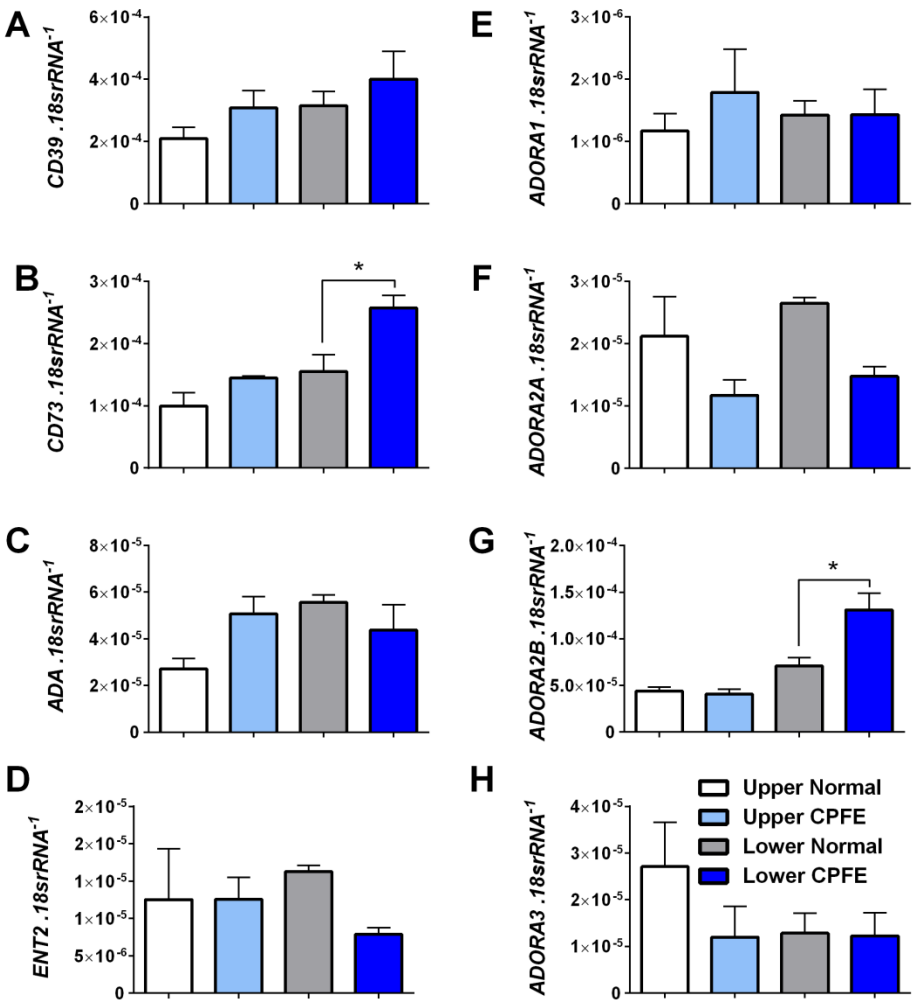

Figure 30 The adenosinergic response in CPFE.

Lung transcript levels for (A) CD39, (B) CD73, (C) ADA, (D) ENT2, (E) ADORA1, (F) ADORA2A, (G) ADORA2B, (H) ADORA3; from upper lobes from normal lungs (white bars), upper lobes from CPFE lungs (light blue bars), lower lobes from normal lungs (grey bars), and lower lobes from CPFE lungs (dark blue bars). *P< 0.05 refers to comparisons between normal and CPFE groups within upper or lower lung lobes.

The extra-cellular matrix in CPFE.

Next, I evaluated the protein levels of ADORA2B and HAS3 in CPFE. Protein expression levels for ADORA2B revealed increased expression in lower lobes from CPFE lung tissue vs normal controls, concomitant with increased signals for HAS3 (Figure 31 A-C). These observations were in-line with IHC for αSMA, revealing hyaluronan signals in highly remodeled areas of lung characterized by dense myofibroblast presence and prominent vascular remodeling in CPFE lungs compared to normal tissue (Figure 31 D). Similarly, staining for HAS3 and CD68 (a human monocytic phagocyte marker) revealed positive signals for CD68 and HAS3 in lower lobes of CPFE lungs (Figure 31 E, F). These results did not show alterations in *HAS1* or *HAS2* between normal and CPFE lung tissue derived from upper or lower lobes (Figure 32 A, B). Gene expression for fibrotic genes revealed increased expression of *FN1* in upper lobes of CPFE vs normal lungs but not in lower lobes (Figure 32 C). Expression levels of *COL1A1* revealed significantly increased expression levels in lung tissue derived from lower lobes from CPFE vs normal lung tissue (Figure 32 D). *COL1A2* was significantly elevated in both upper and lower lobes in CPFE vs normal lung tissue, whereas *COL2A1* was elevated only in the lower lobes from CPFE lungs (Figure 32 E, F). These collagens have previously been shown to express in the lung and be associated with lung disease (73, 158, 229). Interestingly, these results demonstrate that purinergic remodeling and increased ADORA2B levels in CPFE are observed in the lower lobes were fibrotic deposition is most evident and in areas of vascular remodeling, in line with the role of adenosine in promoting fibrotic deposition and vascular remodeling in chronic lung injury (225).

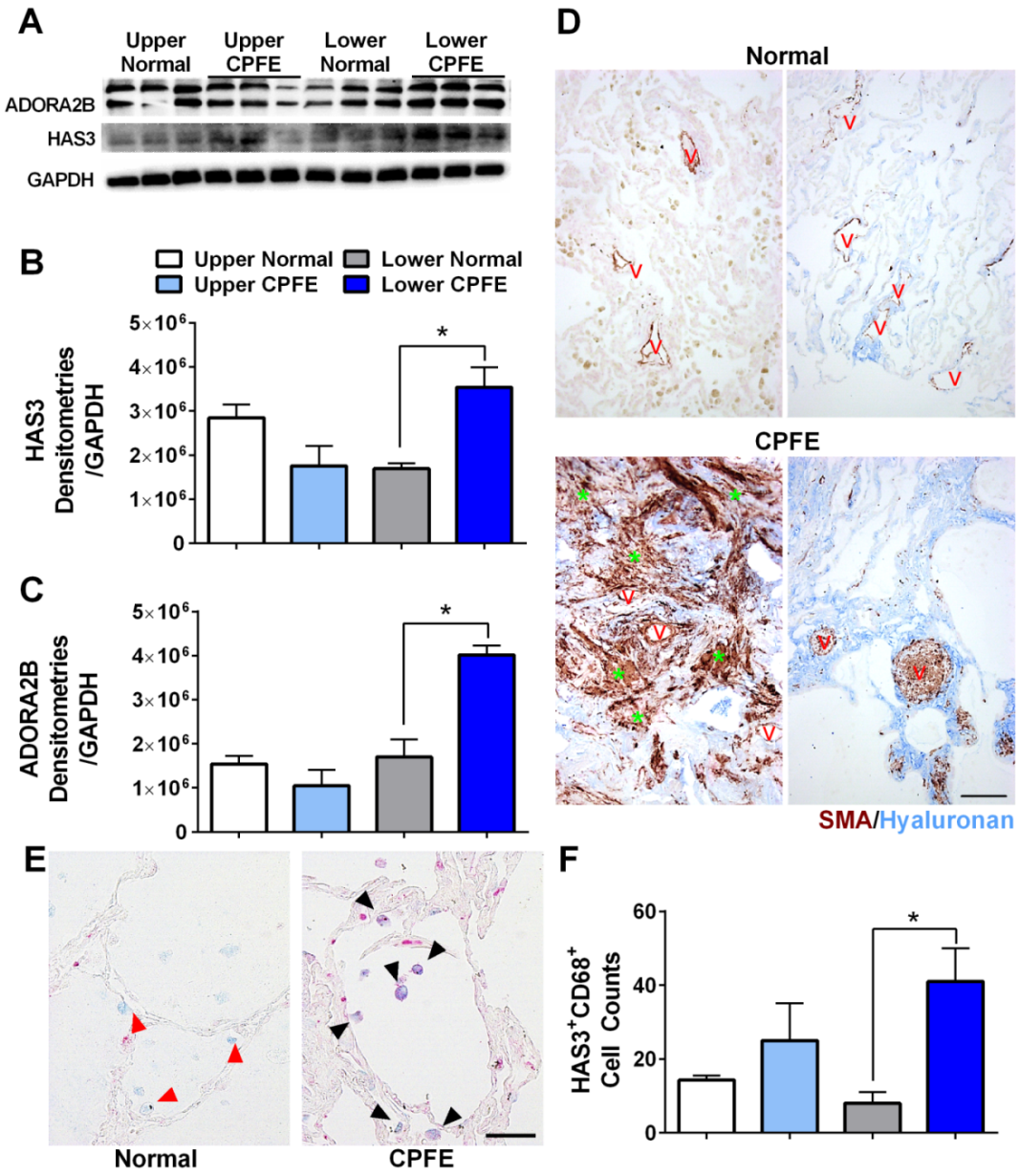

Figure 31 ADORA2B and HAS3 are elevated in CPFE.

Western blot for ADORA2B, HAS3 and GAPDH from upper and lower lobes from normal or CPFE lungs (A). Densitometries for ADORA2B (B) and HAS3 (C) from upper lobes from normal lungs (white bars), upper lobes from CPFE lungs (light blue bars), lower lobes from normal lungs (grey bars), and lower lobes from CPFE lungs (dark blue bars). (D) Dual immunohistochemistry for alpha smooth muscle actin (SMA, red/brown

signals) and hyaluronan (blue signals) in normal (upper panels) or CPFE (lower panels) lungs. The red V denotes vessels and the green asterisks point at myofibroblasts. (E) Immunohistochemistry for CD68 (blue signals) and HAS3 (red signals) from lower lobes from normal and CPFE lungs. Red arrows represent CD68 positive (HAS3 negative) signals. Black arrows point at dual HAS3 and CD68 signals, scale bar represents 50 μm. (F) Double HAS3 and CD68 positive cells from 10 micropictographs from the upper lobes from normal lungs (white bars), upper lobes from CPFE lungs (light blue bars), lower lobes from normal lungs (grey bars), and lower lobes from CPFE lungs (dark blue bars). *P< 0.05 refers to comparisons between normal and CPFE groups within upper or lower lung lobes.

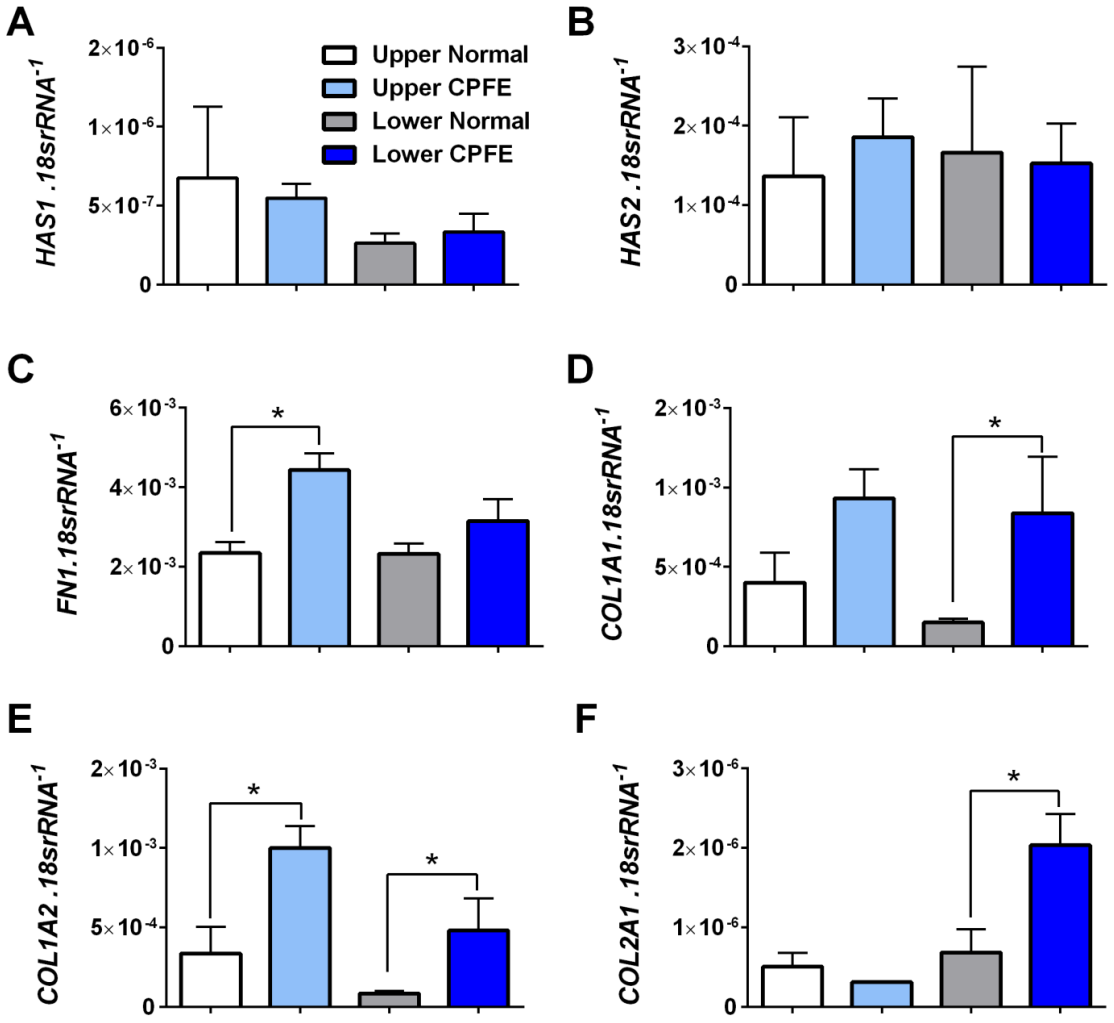

Figure 32 Extracellular matrix signals in CPFE.

Transcript levels for (A) HAS1, (B) HAS2, (C) FN1, (D) COL1A1, (E) COL1A2, (F) COL2A from upper lobes from normal lungs (white bars), upper lobes from CPFE lungs (light blue bars), lower lobes from normal lungs (grey bars), and lower lobes from CPFE lungs (dark blue bars). *P< 0.05 refers to comparisons between normal and CPFE groups within upper or lower lung lobes.

Discussion

Despite reductions in mortality in cancer and cardiovascular disease, mortality rates for chronic lung diseases including interstitial lung disease have remained unaffected over the last decade(230). This is a direct result of disparate funding allocated towards research in chronic lung disease that in no way reflects the heavy societal burden of the disease (230). This translates to an overwhelming lack of effective therapies for chronic lung diseases. CPFE represents a chronic lung disease syndrome that has higher mortality and morbidity rates than diseases such as COPD or IPF. Like other chronic lung diseases, limited therapeutic options exist outside lung transplantation (27, 218, 219). Thus, there is a need to identify novel treatments that can attenuate features of CPFE and improve the morbidity and mortality rates. In this study, I have characterized an experimental model of CPFE using male 6-month-old *Ada*$^{-/-}$ mice and demonstrated that they present with features of CPFE, namely fibrotic deposition, airspace enlargement and PH. I have also generated preliminary results that show that 4MU, also known as hymecromone, an FDA-approved drug, is capable of attenuating fibrotic deposition and PH in a murine experimental model of chronic lung injury that recapitulates features of CPFE. Furthermore, my studies utilizing lung tissues derived from upper or lower lobes from explanted lungs from patients with CPFE or from normal lungs that were discarded for transplantation, reveal an upregulated adenosinergic response and evidence of increased hyaluronic acid deposition. Evaluation of the potential mechanisms leading to increased hyaluronan in the experimental model point at Adora2b-mediated Has3 expression in macrophages that is supported by dual F4/80 and Has3 *positive* cells observed histologically.

There is a lack of experimental models of lung disease that can accurately recapitulate the pathophysiology of chronic lung diseases (231). This is particularly the case for CPFE, where limited animal models that recapitulate its cardinal features (fibrotic deposition, airspace enlargement and PH) have been described. Features of CPFE have been modeled by treating mice with both the fibrotic agent bleomycin and elastase to induce airspace enlargement (232, 233). Experiments have also been performed treating cigarette-smoke exposed mice with the pro-fibrotic agents bleomycin or herpesvirus leading to airspace enlargement and fibrotic matrix deposition (234). Additionally, exposure to the halogen gas bromine (Br_2) has also been shown to induce combined airway fibrosis and emphysema (235). Although these models are able to recapitulate features of CPFE, they rely on chemical-induced lung injury, which does not accurately represent the etiology of CPFE (219). Furthermore, these models have not characterized the presence of PH, an important feature of CPFE (19, 26, 28, 159).

The *Ada*$^{-/-}$ mouse model of lung injury was first reported by Blackburn et al.(236, 237) and has demonstrated to recapitulate important features of chronic lung injury such as fibrotic deposition, airspace enlargement and PH (158, 238, 239). In these studies both male and female littermate *Ada*$^{-/-}$ and *Ada*$^{+}$ mice were utilized and PEG-ADA therapy was maintained typically up to post-natal day 21 whereupon it was discontinued, leading to a rapid increase in extracellular adenosine levels resulting in lung injury observed typically 15 to 20 days after cessation of PEG-ADA therapy (158, 238, 239). To adequately model CPFE, a disease that primarily affects males (217-219), I utilized male 6-month old *Ada*$^{-/-}$ mice that were subjected to a progressive reduction in

PEG-ADA therapy leading to a gradual increase in extracellular adenosine. Using this approach, I aimed to mimic the repeated subclinical injury that is associated with chronic lung diseases. Using this approach, mice presented with extensive remodeling of the lung parenchyma including airspace enlargement, fibrotic deposition and vascular remodeling and PH consistent with previous publications(158, 238, 239). However, the extent of fibrotic injury and features of PH, such as RVSP, appeared enhanced in the model of gradual reduction of PEG-ADA therapy using male mice.

An important therapeutic finding from my study was that 4MU was capable of inhibiting PH in the *Ada*$^{-/-}$ mice, consistent with previous studies using bleomycin-exposed mice that presented with fibrotic deposition and PH (226). However, contrary to the study of Collum et al (226), this study demonstrates that 4MU is capable of attenuating the fibrotic deposition in *Ada*$^{-/-}$ mice. This discrepancy could be explained by the different treatment regimen of 4MU. In the present study, 4MU was administered for 4 weeks whereas in the previous study it was only given for 2 weeks (226). Thus the longer treatment regimen may explain the effect of 4MU at inhibiting both PH and fibrotic deposition; this effect is supported by a greater reduction of hyaluronan levels, observed by ELISA in BALF, in the present study using *Ada*$^{-/-}$ mice compared to previous studies in the bleomycin model of lung fibrosis (226). These are important pre-clinical results demonstrating that an FDA-approved drug has the capacity of attenuating cardinal features of CPFE, a disease that currently lacks any effective therapy outside lung transplantation (27, 219).

Consistent with previous publications from our group(158, 190), I demonstrate that both elevated Adora2b expression and hyaluronan accumulation are present in the

experimental model of lung injury. A novel finding of this study was that Has3, but not Has1 or Has2 as in previously reported in models of lung injury (158, 190, 226), was the main hyaluronan synthase that was upregulated in the experimental model. My results are consistent with cigarette-exposed mice where increased lung hyaluronan and Has3 expression was observed (240). Interestingly, elevated Has3 signals were primarily observed in macrophages in *Ada*$^{-/-}$ mice. In addition, increased Has3 expression in macrophages was Adora2b-dependent, consistent with previous publications utilizing mice lacking Adora2b-expression in the monocyte lineage (222) and from studies demonstrating an Adora2b-dependent Has expression in pulmonary artery smooth muscle cells (190, 226). Treatment with 4MU was able to attenuate Has3 expression levels consistent with reduced hyaluronan accumulation and macrophages. These results point at macrophages as an important contributor to the development of lung fibrosis and PH, consistent with prior studies (222, 223, 241, 242) where alternatively-activated macrophages were shown to promote the development of features of chronic lung injury. It is important to mention that increased Has3 signals were also observed in epithelial and vascular cells in *Ada*$^{-/-}$ mice that could also contribute to increased hyaluronan accumulation. Increased vascular or peri-vascular expression of Has3 and subsequent hyaluronan deposition could also contribute directly to vascular remodeling and PH by promoting vascular stiffness and proliferation as demonstrated previously by our group (226). Pulmonary artery smooth muscle cell expression of hyaluronan synthases has been shown to be modulated by activation of Adora2b (55, 190). This is in line with studies showing Adora2b-mediated macrophage Has3 expression.

A novel finding of this study was that Has3-expessing macrophages appeared to contribute to chronic lung injury. This is significant, as typically Has3 is associated with the generation of low-molecular-weight (LMW) hyaluronan fragments (243). These LMW hyaluronan fragments are associated with pathogenic effects (189, 240). Importantly, results from the experimental model were consistent with the presence of HAS3-expressing CD68 cells in CPFE that was consistent with massive hyaluronan deposition surrounding fibrotic areas and remodeled vessels from CPFE explanted lungs. These results are highly significant since little is known regarding the pathogenic mediators involved in the pathophysiology of CPFE.

It is important to mention that adenosine is a danger-associated molecular pattern that is generated following cell injury and subsequent extracellular release of ATP that is converted to adenosine by CD39 and CD73, with the latter being the rate-limiting enzyme (244). Adenosine can then activate any of its four receptors: ADORA1, ADORA2A, ADORA2B and ADORA3 (245). Adenosine is known to have many protective effects acutely, however chronically elevated levels of adenosine and subsequent activation of its low-affinity receptor, ADORA2B, has been extensively associated with chronic lung injury (225). An important phenomenon that promotes adenosine accumulation is purinergic remodeling, a phenomenon characterized by increased expression of the ectonucleotidase CD73 and reduced ADA and ENTs that collectively promote extracellular adenosine accumulation and subsequent ADORA2B activation (246). This phenomenon has been shown to be present in chronic lung diseases such as COPD and IPF (247), and my data from CPFE explanted lung tissue reveals evidence of purinergic remodeling consistent with increased ADORA2B

expression. Taken together, these observations advocate the use of an ADORA2B antagonist to treat chronic lung diseases. Indeed, preclinical studies using both *Ada*$^{-/-}$ and bleomycin-treated mice have demonstrated that genetic or pharmacological abrogation of Adora2b signaling is capable of attenuating features of chronic lung injury (158, 190, 239, 248).

Unexpectedly, treatment with 4MU was not able to attenuate airspace enlargement, RVH or metabolic changes in *Ada*$^{-/-}$ mice. RVH is typically a response to increased RVSP, as such it is conceivable for changes to be observed over time following normalization of blood pressure. Airspace enlargement may however be due to other adenosinergic mechanisms promoting alveolar cell destruction. These potential mechanisms may include elevations in deoxy-adenosine a molecule that is also metabolized by ADA and accumulates in *Ada*$^{-/-}$ mice (249). Increased phosphorylation of deoxy-adenosine by deoxy-cytosine kinase has been shown to contribute to airspace enlargement in *Ada*$^{-/-}$ mice and increased deoxy-cytosine kinase signals have been detected in stage 4 COPD (249). Taken together, these studies suggest that treatment of 4MU may not alter deoxy-cytosine kinase or deoxy-adenosine levels to alter airspace enlargement. Similarly, alterations in metabolism have also been reported in *Ada*$^{-/-}$ mice (237) that may not be affected by 4MU, but this compound may be effective at treating lung fibrosis and PH in CPFE.

In conclusion, my study has demonstrated that a gradual reduction of PEG-ADA to male 6-month-old *Ada*$^{-/-}$ mice results in the development of hallmarks of CPFE: airspace enlargement, fibrotic deposition and PH. In addition, I demonstrate using a therapeutic approach that the FDA-approved drug, 4MU, is capable of reducing the

extent of fibrotic injury and features of PH. My study also proposes a novel mechanism whereby Has3-*positive* macrophages contribute to chronic lung injury in *Ada*$^{-/-}$ mice. Importantly, observations in the experimental model of CPFE were recapitulated in lung explants from patients with CPFE, where increased hyaluronan was detected in remodeled areas of the lung consistent with HAS3 expressing CD68-*positive* cells. These results are significant since very little is known regarding the mechanisms that promote injury in CPFE and as a result limited therapies exist for this deadly condition. My study proposes that inhibition of hyaluronan accumulation is as a novel potential therapy for CPFE.

Chapter 6: Conclusions and Future Directions

Conclusions

The work presented here contributes to our understanding of the molecular changes involved in vascular remodeling and PH. My work has identified a role for NUDT21 in the pathogenesis of PH. Specifically, I demonstrate that NUDT21 depletion is present in remodeled vessels of patients with either Group 1 or Group 3 PH and that NUDT21 depleted PASMCs undergo a phenotypic switch that promotes vascular remodeling. There were also large gaps in the knowledge about the role of HA in contributing to vascular remodeling in Group 1 or Group 3 PH. While HA and HA related enzymes had been shown to be associated with PH, the mechanism had not been fully explored. I describe two pathways through which changes in HA deposition in the lung contribute to disease.

The results in Chapter 3 describe a novel mechanism for changes in PASMCs during PH development through regulation of RNA maturation. While NUDT21 mediated APA has been described in several disease states to this point, it has not been shown in PASMCs or in PH. These changes observed in the PASMCs are consistent with changes seen in the literature in PH. Interestingly, NUDT21 deletion in PASMCs leads to increased RVSP in the absence of hypoxia-sugen model. This finding together with the fact that over-expression of NUDT21 in PASMCs from patients restores them to a proliferative phenotype similar to cells from healthy donors indicates that NUDT21 is a key regulator of vascular remodeling and PH. This new mechanism adds to our current knowledge of the pathways that drive vascular remodeling and PH.

The results in Chapter 4 describe the role and mechanism of HAS2 in PASMCs. Here I describe the role of HA in the development of PH, showing that, 4MU, an inhibitor of HA production, inhibited RVSP in two models of PH. I additionally showed that deletion of HAS2 from the PASMCs of mice is also protective from PH. While previous studies have shown an association between increased HA and chronic lung disease, my research was the first to identify a causative role of HA. This research is also the first to use pharmacological inhibition of HA production to treat PH. This finding is exciting in that it identifies a potential therapy for this disease. Not only did I describe the role of HA in PH, I also identified one of the pathways through which these cellular changes are produced. Using the Rho-kinase inhibitor fasudil allowed me to describe the RhoA/ROCK signaling pathway as the signaling pathway through which HA signals in these cells.

The results in Chapter 5 describe the role of HA in CPFE, a relatively recently defined disease. As a recently classified disease, few mechanistic studies have been performed to understand the initiation and development of CPFE. Previous work in the lab has described the role of ADORA2B in regulating HA production in chronic lung diseases but did not describe mechanism or look at CPFE. In this work I first studied the ADA deficient mouse and discovered a novel model for CPFE, including the combined fibrotic deposition and destruction of the alveoli and associate PH. As ADORA2B expression and HA were upregulated in this model I then were able to describe the use of 4MU in treatment of the fibrotic deposition and PH symptoms in this mouse model. This also revealed that the emphysematic portion of this disease may be caused by adenosinergic signaling but it is not associated with HA. I also describe a

group of HAS3 expressing macrophages that is found in association with both the mouse model of CPFE and patient samples of CPFE.

Given the complex cellular interaction in the lung and equally complex intracellular regulation of pulmonary cells it is difficult to discover the mechanisms that contribute to chronic lung diseases. Here I describe two mechanisms involved in the progression of PH and one of the first mechanisms described for the progression of CPFE. This advance in knowledge is important in the continued struggle to understand these chronic and progressive diseases, and will provide novel opportunities for continued research and therapeutic research.

Future Directions

NUDT21 in other chronic lung diseases

The most direct next step that is indicated by the research here as well and previously published studies is to identify the role of NUDT21 depletion in other chronic lung diseases. One of the first to be investigated should be CPFE. The role of NUDT21 mediated APA has been shown in fibroblast in IPF and this thesis has shown this process is important in PH. Additionally, preliminary data here shows NUDT21 depletion in COPD lung tissue (Figure 33). Taken together, these data strongly support a role for this mechanism in the pathogenesis of CPFE as it is important in key malignant processes, fibrosis and emphysema, as well as the often-associated PH.

To characterize the role of NUDT21 mediated APA in CPFE a two-pronged approach should be taken. Human CPFE tissue should be analyzed for NUDT21 changes by western blot, and then RT-PCR should be utilized to test for APA events in the genes

most well characterized to shorten such as VMA21. At the same time tissue from the ADA deficient mouse model of CPFE should be analyzed in the same manner.

To identify the APA targets important to this disease, it is likely that analysis of whole tissue will be confounded by APA events that differ between cell types. To mitigate this, cells should be isolated from either patients or the mouse model and then analyzed for APA changes against healthy controls. The cell types to be analyzed should be fibroblasts, PASMCs, and alveolar epithelial type 2 cells which undergo apoptosis in COPD (250). Identifying this mechanism as important in CPFE would add additional knowledge to this poorly understood and complex disease.

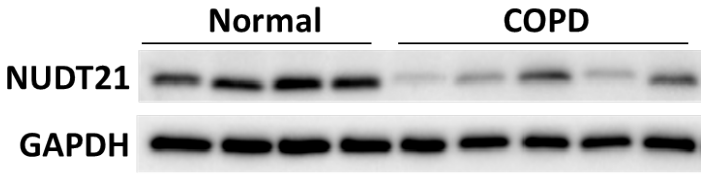

Figure 33 Reduced NUDT21 Levels in COPD

Western blot for NUDT21 and GAPDH in Normal and COPD patient lung samples.

What other genes are shortened by NUDT21 depletion in PH.

As discussed in Chapter 1 several key changes happen to PASMCs during vascular remodeling. My results show that NUDT21 depletion plays a role in modulating the proliferative and migratory capacity of PASMCs. While shortening and increased expression of HAS2 mRNA plays a role in this change, other genes are also involved. The DaPars algorithm identified 664 shortened genes in the NUDT21 knock down in

PASMCs. The data from this algorithm identified RUNX1 as one of the most shortened targets of NUDT21 depletion. This shortening was also associated with increased reads indicating increased mRNA levels. RUNX1 is a poorly described transcription factor known to be expressed in hematopoietic stems cells and plays an important role in controlling proliferation and self-renewal (251). Additionally mutations in this gene contribute to a wide variety of leukemia types (252). RUNX2 along with a common cofactor with RUNX1, CBFβ, has been implicated in proliferation of PASMCs and remodeling in PH (253). As shortening of RUNX1 lead to aberrant expression in the NUDT21 knock down, and RUNX1 is a strong driver of disease states, investigating the role of this shortening in PH is encouraging.

To identify if RUNX1 3'UTR shortening is an important downstream effect of NUDT21 depletion several studies need to be performed. First RUNX1 shortening in PAH patient samples should be confirmed by DaPars analysis of RNA-seq data. This should also be determined by RT-PCR experiments to show dPAS usage. After this APA event has been confirmed in human samples of disease, a mechanistic link should be determined. *In vitro* it should be shown that RUNX1 is necessary for NUDT21 mediated changes in PASMCs phenotype by knocking down NUDT21 with siRNA and then treating the cells with 2-pyridyl benzimidazole AI-4-57, a RUNX1-CFBβ inhibitor. If the phenotype of these cells differs from controls with only NUDT21 a mechanistic link will be confirmed. In the event that inhibitor is toxic to these cells I can use siRNA to knockdown RUNX1 as well. It will also be confirmed that RUNX1 is shortened in the PASMCs of C57B/6 mice and NUDT21$^{f/+}$TaglnCre mice in the hypoxia-sugen model. The same inhibitor can be used to treat these mice to determine if blocking RUNX1 induced by NUDT21

mediated APA is a therapeutic option in PH. Continued studies could identify aberrantly expressed genes activated by RUNX1 binding. Identifying the pathways that lead to proliferation in NUDT21 downregulation will likely identify pathways key for PH development.

Targeting NUDT21 depletion mediated APA therapeutically.

While NUDT21 depletion appears to be sufficient to induce phenotypic changes in PASMCs, it is not evident what mechanisms control these levels during the initiation of PH. In order to target this mechanism therapeutically it is important to know what regulated NUDT21 levels. It is known that several miRNAs including miRNA-181a target NUDT21. In fact miRNA181a appears to drive a NUDT21 depletion dependent increase in proliferation in osteosarcoma (116). To determine if miRNAs control the level of NUDT21 in PASMCs during PH the transcript sequence of NUDT21 should be analyzed by a tool such as TargetScanHuman 7.2. The miRNA hits that this tool predicts should then be cross-referenced against miRNAs known to be induced during PH (254). The miRNAs in both sets should then be investigated using a dual luciferase vector with the NUDT21 3'UTR as the target sequence. Identification of one or more miRNAs that are upregulated in PH and that strongly downregulate NUDT21 in this assay would provide strong evidence that this is the mechanism of control. It is also possible that other pathways contribute to changes in NUDT21 levels. Investigating the transcription factors and enhancers that activate NUDT21 expression would require more in-depth studies but could provide interesting insights.

An additional area of potential therapeutics is the CFIm complex as a whole. My research focused on the role of NUDT21 on PH but I did show reduced levels of CFIm59 and CFIm68 in several disease states. These decreases were not as consistent as with NUDT21 but could be as important for some roles of CFIm. As discussed previously NUDT21 likely acts in concert with its partners by binding two of the same protein in quaternary complex (255). If these other partners provide some specificity in controlling cleavage and polyadenylation, it is possible that targeting only one of CFIm59 or CFIm68 would provide more targeted changes in PASMCs without effecting APA in such a global scale, which may have unintended effects. To investigate this, PASMCs in culture should be depleted of either CFIm59 or CFIm68 and then proliferative and migratory outcomes can be observed. If these changes are similar to that seen in NUDT21 depletion, then a study of the APA landscape can begin, first with RT-PCR of known regulators seen in the NUDT21 studies and eventually with RNA-seq to understand how the APA landscape differs. The eventual goal would be to identify a target interaction key to PH associated APA but not necessary for steady state cleavage and polyadenylation that could be used as a target to screen compounds that would simply interrupt that one interaction.

4MU as a therapy for PH in patients

Undoubtedly the most significant and daunting next steps implicated by the findings here is that of testing 4MU in patients with PH. 4MU is an approved therapy for biliary dyskinesia in some countries under the name hymecromone. In the clinical trials for this use no severe side effects were seen and treatment by oral delivery is effective.

Unfortunately the pharmacology is not ideal for treatments, as 4MU is quickly metabolized and excreted from the body (256). This drug has also not been tested in a chronic treatment scenario with on label usage only for acute biliary spasms and a single trial showing relative safety for three months of treatment (257). Despite this, my findings support using this drug for patients with PH. This drug is also a potential target for cancer research as *in vitro* studies have shown that 4-MU treatment reduces cancer metastasis (258). In a mouse model with implanted cancer cells, 4MU treatment reduced tumor size (259). As there is no curative treatment and PH is progressive any treatment that could provide distinct benefits should be investigated, especially one with few side effects that has been used to treat other disease.

Appendix: Materials and Methods

Scientific Rigor

All analyses were blinded to the experimenter. A two-way analysis of variance (ANOVA) with the Bonferroni correction was performed for all experiments with more than 2 groups. For experiments that consisted of two groups, an un-paired two-tailed Students t-test. The Grubbs' test was used to detect outliers. GraphPad Prism 7.0 or higher was used to analyze the data. All software used in this study is available commercially.

Sex as a biological variable

In experiments using IP BLM, male mice were utilized, as IPF is more prevalent in males than in females (260-262). Male mice also have a greater response to BLM than female mice irrespective of age (263). In the hypoxia-sugen model both male and female mice are used and no difference in symptoms or histology is observed. As CPFE is ~20 times more prevalent in males than females, the chronic ADA deficient mouse model utilizes only males of six months of age (264).

As IPF is much more prevalent in males, male patients dominated the samples of this diagnosis though a more even sex distribution is available for patients with IPF+PH. PAH is 2-4 times more prevalent is females and this is evident in the available samples (5). CPFE patient samples were only collected from males as the disease is almost exclusively male and the disease was only recently described. As healthy lungs are typically only explanted for potential transplantation, it is uncommon to receive healthy tissue from age matched controls.

Human subjects

The use of human material for this study was reviewed by the University of Texas Health Science Center at Houston Committee for the Protection of Human Subjects (Institutional Review Board no. HSC-MS-08-0354). The demographic details of the study population are summarized in Table 1. De-identified lung explant tissue from patients with IPF and corresponding de-identified clinical parameters were obtained from the Methodist Hospital (Houston, TX). IPF was diagnosed by board-certified pulmonologists upon admittance for lung transplantation at the Houston Methodist Hospital. Pulmonary hypertension was defined as a mean pulmonary pressure ≥ 25 mmHg and a pulmonary capillary wedge pressure ≤ 15 mmHg; the hemodynamic measurements were obtained from the right heart catheterization performed as part of the transplant evaluation. Control lung tissue was obtained from lungs that were declined for transplantation but had no pulmonary chronic disease or contusion. Healthy control lung tissue was obtained from the International Institute for the Advancement of Medicine (Edison, NJ).

Tissue was collected at the time of lung explantation and processed on site within 20 min. The lobes were identified from each lung explant, and for each lobe, the center was identified, taking the airway as a reference point. A 1 cm transverse center cut was performed to obtain a section from the center of each lobe. Consequently, this tissue was divided into three sections to separate external (closest to pleura), center and internal (closest to bronchi) portion according to the airway. A piece from each portion was then cut for histology, and an adjacent section was flash frozen in liquid nitrogen.

	IPF (n=10)	IPF + PH(n=9)	PAH(n=6)	CPFE(n=4)	Healthy(n=8)
Female	2/10	4/9	5/6	0/4	5/10
Males	8/10	5/9	1/6	4/4	5/10
Age	63.4±2.9	57.3±4.6	47.5±13.1	60.4±7.0	41.1±14.3
mPAP	20.0±1.7	31.3±1.5	48±9.6	24±4.5	Not Measured
BMI	27.9±1.7	30.0±1.8	25.5±5.5	28.0±1.0	31.3±3.8

Table 1 Human Subjects

Animal subjects

All animal care and experimental studies were reviewed and approved by the University of Texas Health Science Center at Houston Animal Welfare Committee Animal studies are reported in compliance with the ARRIVE (Kilkenny et al., 2010; McGrath and Lilley, 2015), institutional and NIH guidelines. Male C57/BL6 mice 4–5 weeks old weighing 20–22 g were purchased from Envigo Industries (Indianapolis, IN, USA). All mice were housed in ventilated cages equipped with microisolator lids and maintained under strict containment protocols. Mice were housed 5 per cage and were provided with variable free paper bedding (Pure-o'Cel The Andersons, Inc. Maumee, OH, USA) and Nestlets™ provided by Ancare (Bellmore, NY, USA). Mice were kept at an ambient temperature of 22°C and in a 12 h dark/light cycle.

Hypoxia-sugen

Mice were kept in a naturally ventilated cage inside a chamber with positive pressure (A-Chamber, Biospherix, Lacona, NY) and exposes to 10% oxygen by addition of displacing nitrogen for 28 days. Oxygen levels were monitored and controlled by an oxygen regulator from OKO Labs (Pozzuoli, NA, Italy). Once weekly 20mg/kg of SUGEN (SU5416; Tocirs, Bristol, United Kingdom) was injected intra-peritoneal after dissolving in 10% Kolliphor HS 15(Sigma Aldrich, St Louis, MO). Control mice were

maintained in room air in the same room. Hemodynamic measures of the mice were made at day 28 and samples harvested after they were euthanized.

Bleomycin

Mice were treated with 0.035 Ug–1 of bleomycin (TEVA Pharmaceuticals, Sellersville, PA, USA) or vehicle (PBS; Life Technologies, Grand Island, NY) twice a week for 4 weeks i.p On day 15, mice were provided with chow containing 4-MU (Sigma Aldrich, Saint Louis, MO, USA), at a dose of 20 mg·kg–1 per day or normal chow (vehicle, Teklad, Industries, Indianapolis, IN, USA) for the remainder of the experiment. To deliver 20 mg·kg–1 per day 4MU was added to the diet at a concentration of 125 mg·kg–1 diet (assuming mean body weight ~25 g and intake ~4 g·per day). This was calculated by a Nutritionist at Harlan Laboratories (now Envigo). On day 33, physiological readouts were performed and the animals were then sacrificed for the collection of tissues and fluids for analysis. Mice were assessed bi-weekly for changes in body weight, lack of grooming or hunched posture by lab personnel and once-weekly by veterinarians at our facility. In a separate cohort of experiments, 4MU therapy (or control chow) began on day 33 of BLM exposure and lasted for 14 days. Physiological readouts and tissue collection were performed on day 47.

NUDT21 KO Mice

NUDT21$^{F/F}$ mice were crossed with TaglnCreKI (Tagln$^{tm2(cre)Yec}$/J Jackson Laboratory) mice. These NUDT21$^{F/-}$ were used as the experimental group with TaglnCreKI as the control group. Mice were age matched.

ADA mice

To generate *Ada*$^{-/-}$ postnatal mice, an ADA minigene that targeted expression specifically to the trophoblast lineage was introduced onto the *Ada*$^{-/-}$ background. This was accomplished by intercrossing mice carrying the trophoblast-specific ADA minigene (Tg) with mice heterozygous for the null Ada allele (m1/+). Subsequent intercrosses yielded litters that contained mice harboring the ADA minigene (Tg) that were also homozygous for the nullAda allele (m1/m1). Given that the regulatory elements used targeted Ada expression only to trophoblasts, once born, and with the loss of the placenta, Tg-m1/m1 mice lacked ADA enzymatic activity. Mice homozygous for the Ada-null allele were designated *Ada*$^{-/-}$, while control mice, designated Ada+, were heterozygous for the Ada-null allele. *Ada*$^{-/-}$ and Ada+ mice were congenic on a C57BLk/6J background. Male 24-week-old *Ada*$^{-/-}$ mice or littermate Ada+ controls were used for all experiments.

Ada$^{-/-}$ mice were identified at birth and maintained on ADA enzyme therapy from postnatal day (PD) 2 until postnatal day 25 as follows: PD5: 1.25 UI IM, PD9-PD17: 2.5 UI IM, PD21: 2.5 UI IP, PD25: 5 UI IP. Starting on PD25 mice received weekly doses of PEG-ADA (5UI IP) until PD168 (week 24). Mice were randomized to group treatment using a random number generator using www.graphpad.com/quickcalcs. Starting on week 24, PEG-ADA was gradually reduced over the course of 9 weeks to 0.125 UI IP as follows: week 1: 5UI IP, week 2: 2.5UI IP, week 3 and 4: 1.25UI IP, week 5 and 6: 0.625UI IP, week 7 and 8: 0.312 UI IP, week 9: 0.125UI IP. On week 34 mice were provided with medicated chow containing 4-Methylumbelliferone (4MU; Sigma Aldrich, Saint Louis,

MO) also known as hymecromone at a dose of 20 mg kg-1 body weight (BW) per day-1 or normal chow (vehicle, Teklad, Industries, Indianapolis, IN) for 4 weeks. During the course of these 4 weeks, mice were kept at 0.0125 UI IP of PEG-ADA. On PD 266 (week 38) physiological readouts were performed and the animals were then sacrificed for the collection of tissues and fluids for analysis (details below).

Arterial oxygen saturation

Physiological assessment measuring arterial oxygen saturation was conducted on conscious mice using the pulse MouseOx software analysis (STARR Life Sciences Corp, Oakmont, PA). The hair around the neck was removed from mice in order to use the collar clip light sensor. The MouseOx provides real-time percent oxygen saturation of functional arterial hemoglobin by utilizing pulse oximetry measurements of light absorption from the red and infrared LEDs (Light Emitting Diodes).

Hemodynamic measurements

Right ventricle systolic pressure (RVSP); heart rate and right ventricle (RV) hypertrophy. Mice are given 0.75 mg g–10f 5% Avertin (a mixture of tert-amyl alcohol and 2–2-2 tribromoethanol, Sigma Aldrich) to induce a surgical plane of anesthesia. Mice are placed on a heated surgical workstation (Molecular Imaging Products, Bend, OR) and secured with surgical tape. Mice were then tracheotomized with a 19G blunt needle (BRICO, Dayton, NJ) and attached to a small animal ventilator (MiniVent, Hugo-Sachs Elektronik, March-Hugstetten, Germany) and ventilated at a stroke volume of 250 µL at 200 strokes per minute. The surgical site was viewed using a surgical

microscope (SMZ-2B, Nikon, Tokyo, Japan). An incision of ~1 cm in length was made just below the xiphoid process. An alm retractor (ALM-112, Braintree Scientific, Braintree, MA) was used to expose the abdominal cavity to visualize the diaphragm and the liver. An incision was then made on the diaphragm to expose the heart and the pericardium then removed. The right ventricle was then identified and a puncture made with a 28G needle. A 1 French pressure catheter (SPR-1000, Millar Instruments, Houston, TX) was then inserted through the puncture. Using the same procedure, I recorded LVSP, immediately after RVSP measurements. The heart rate results were continuously recorded using a Powerlab 8-SP A/D (AD Instruments) converter, acquired at 1000 Hz. All RVSP results were recorder to a PC utilizing Chart8 software. After completion of the measurements, blood was collected and the lungs were excised and flash frozen in liquid nitrogen for RNA extraction. The heart was excised and the atria were removed. The right ventricle was then surgically removed and the dry weights of the RV were used to determine the extent of RV-hypertrophy (RV/left ventricle [LV] + septum). A heart rate below 250 beats per minute (BPM) during the determination of the RVSP or LVSP was considered as a violation of a predetermined criteria.

RT-PCR

Total RNA was isolated from frozen lung tissue using Trizol reagent (Life Technologies). RNA samples were then DNase treated (ArticZymes, Tromso, Norway) and subjected to quantitative real-time RT-PCR. Here two technical replicates were performed per sample. Prior to RT-PCR experiments RNA quality was evaluated using a Nanodrop (Thermo Fisher Scientific, Waltham, MA, USA); to evaluate 260 nm / 280 nm

absorbance values. Samples with 260/280 absorbance rations below 1.90 or above 2.10 were considered to have poor RNA quality and thus violated a predetermined criterion.

Gene	Forward	Reverse
18SrRNA	GTAACCCGTTGAACCCCATT	CCATCCAATCGGTAGTAGCG
hADA	GGGCTGCTGAACGTCATTG	AGGCATGTAGTAGTCAAACTTGG
hADORA1A	TGCACTGACTTCTACGGCTG	GGTCCCCGTGACCAAACTT
hADORA2A	CGCTCCGGTACAATGGCTT	TTGTTCCAACCTAGCATGGGA
hADORA2B	TGCACTGACTTCTACGGCTG	GGTCCCCGTGACCAAACTT
hADORA3	TCATTCTACTCTCCTTGGCTCTC	GTGGGCATTGTAGTTGCAGAT
hCD39	AGGTGCCTATGGCTGGATTAC	CCAAAGCTCCAAAGGTTTCCT
hCD44	AGAAGGTGTGGGCAGAAGAA	AAATGCACCATTTCCTGAGA
hCD73	CCAGTACCAGGGCACTATCTG	TGGCTCGATCAGTCCTTCCA
hCOL1A1	GTGCGATGACGTGATCTGTGA	CGGTGGTTTCTTGGTCGGT
hCOL1A2	GAGCGGTAACAAGGGTGAGC	CTTCCCCATTAGGGCCTCTC
hCOL2A1	TGGACGCCATGAAGGTTTTCT	TGGGAGCCAGATTGTCATCTC
hENT2	GGGGTACTTTATCACGCCCTG	GGGAATCCCGTTCTCATCAGA
hFN1	GGTGGAATAGAGCTCCCAGG	GCAGCCTGCATCTGAGTACA
hHAS1	GAGCCTCTTCGCGTACCTG	CCTCCTGGTAGGCGGAGAT
hHAS1	GAGCCTCTTCGCGTACCTG	CCTCCTGGTAGGCGGAGAT
hHAS2	TCCTGGATCTCATTCCTCAGC	TGCACTGAACACACCCAAAATA
hHAS2	TCCAAAGAGTGTGGTTCCAA	GACAGGCTGAGGACGACTTT
hHAS2Distal	CTGGCAGTGTTTTCCCAGAAC	CAGGCCACAGAACAAAACCT
hHAS2Total	TCCCGCTGAGACAGATGAGT	CAGTGCTCTGAAGGCTGTGT
hHAS3	CGCAGCAACTTCCATGAGG	AGTCGCACACCTGGATGTAGT
hHAS3	CGCAGCAACTTCCATGAGG	AGTCGCACACCTGGATGTAGT
hHPRT1	TGACCTTGATTTATTTTGCATACC	CGAGCAAGACGTTCAGTCCT
hHYAL2	CACGGGGCTTAGTGAGATG	GTCACCCCAGAGGATGACAC
hIL6	AATTCGGTACATCCTCGACGG	TTGGAAGGTTCAGGTTGTTTTCT
hNRF2	ACACGGTCCACAGCTCATC	GCCTCCAAAGTATGTCAATCAA
hSDHA	GAGGCAGGGTTTAATACAGCA	CCAGTTGTCCTCCTCCATGT
hVMA21Distal	CATCTGCACAGCACCTTACAGTTTGC	GAAATGCAGCACATCCAAATCCTCCC
hVMA21Total	GATAAGGCGGCGCTGAACGCACTGC	TGAGCCTTCATTCCAGGCCACATACACA
mADORA2b	GCGTCCCGCTCAGGTATAAAG	CGGAGTCAATCCAATGCCAAAG
mFN	ACTGGATGGGGTGGGAAT	GGAGTGGCACTGTCAACCTC
mHAS1	GCGAGCACTCACGATCATCTT	GTCCATAGCGATCTGAAGCCA
mHAS2	ACAGATGAGGCAGGGTCAAG	TGGGGTGGAAAGAGAGAAGT
mHYAL1	CCTCAACCCTGCCAGTTTCTC	CCCGCTTGTCACACCACTT
mHyal2	GCAGGACTAGGTCCCATCATC	TTCCATGCTACCACAAAGGGT
mHYAL3	TCTGTGGTATGGAATGTACCCT	TTTTGGCCGTGAAAATGTTGG

mPPARG	GGAAGACCACTCGCATTCCTT	GTAATCAGCAACCATTGGGTCA
mSDHA	GGAACACTCCAAAAACAGACCT	CCACCACTGGGTATTGAGTAGAA

Table 2 RT-PCR Primers

Mouse RT-PCR from Prime PCR plates BioRad(Hercules, CA).

Gene	**Unique Assay ID**
Actb	qMmuCED0027505
CD44	qMmuCEP0062158
COL1A1	qMmuCID0021007
COL1A2	qMmuCID0021177
COL3A1	qMmuCID0006332
FN1	qMmuCID0019534
HAS1	qMmuCIP0036412
HAS2	qMmuCID0011459
HAS3	qMmuCID0014012
HYAL1	qMmuCEP0042433
HYAL2	qMmuCEP0052809
NRF2	qMmuCIP0033901
TBP	qMmuCID0040542

Table 3 BioRad Primers

Immunoblots and ELISA

For immunoblots protein from lung tissue lysates or PASMC was extracted with RIPA buffer (Thermo Scientific, Rockford, IL) containing 1 mM of protease and phosphatase inhibitor (Sigma Aldrich). Samples (30 µg protein each) were loaded onto 4–12% Mini-Protean TGX gels (Bio-Rad, Hercules, CA) for electrophoresis and then transferred on polyvinylidene difluoride (PVDF) membranes (0.45 µm, GE Healthcare Piscataway, NJ). Membranes were then blocked in 5% milk (Bio-Rad) for 1 h at room temperature and then incubated with the appropriate primary antibody overnight. Secondary antibodies and an ECL kit from (GE Healthcare) were applied for generating chemiluminescent

signals. Blots imaged with the ChemiDoc Touch (Bio-Rad) using optimal auto exposure settings. Quantification of these blots were carried out with the Image Lab Software (Bio-Rad) to quantify densitometry as well as intensity of target bands and control bands. The expression was then calculated relative to control band and output in arbitrary units.

BALF was extracted by flushing the lungs with 0.5 mL of cold PBS twice and collecting the fluid using a 1 mL syringe. The presence of blood in BALF was considered as a violation of pre-established criteria. Hyaluronan levels in BALF were measured by ELISA using a kit from Echelon Biosciences (Salt Lake City, UT), with two technical replicates per sample.

Histology and immunohistochemistry (IHC)

Lung sections 5 microns thick, were dewaxed using histoclear (National Diagnostics, Atlanta, GA) and re-hydrated using a gradient of ethanol. Sections were then subject to high temperature antigen retrieval using a citrate buffer, endogenous peroxidase and alkaline phosphatase were inactivated using BLOXALL (Vector Labs, Burlingame, CA) and 2.5% normal horse serum (Vector Labs) was using as a blocking solution prior to incubation with the primary antibody. Following overnight incubation with the primary antibody, sections were treated with the ImmPRESS polymer detection kits for alkaline phosphatase (Vector Labs) based on the host of the primary antibody and developed using Vector red or Vector Blue (Vector Labs). For immunofluorescence chicken anti-mouse Alexa Fluor 488 (Life Technologies Carlsbad, CA) was used and counterstained DAPI (Abcam). Lungs stained with Massons's Tri-chrome were analyzed using a

modified Ashcroft scale optimized for mouse lung sections. To detect hyaluronic acid, sections were incubated with 4 μg/ml of biotinylated HA-binding protein (HABP, Calbiochem, 1:125 Darmstadt, Germany) overnight at 4°C, incubated with the ABC kit and developed with Vector Blue. For immunofluorescence, sections were incubated with SMA and incubated with Alexa Fluor 488 or Alexa Fluor 555 (1:500, Sigma-Aldrich, St Louis, MO) sections were counterstained and mounted with DAPI or PI mounting media (Sigma-Aldrich, St Louis, MO).

Antibody	**Company**	**Concentration**
αSMA	Sigma-Aldrich (clone 1a1)	1:1000
CD44	Fitzgerald 10R-2062	1:1000
CD68	Abcam ab125212	1:100
CFIm59	Proteintech	1:1000
CFIm68	Proteintech 15489-1-AP	1:1000
F4/80	Biorad MCA497	1:500
GAPDH	Thermo Fisher AM4300	1:1000
GEFT(Human)	GeneTex GTX121237	1:1000
GEFT(Mouse)	Santa Cruz sc-16137	1:200
HABP2	Thermo Fisher PA5-25573	1:100
Has1	Thermo Fisher PA550674	1:500 IB 1:100 IHC
Has2	Abbexa abx10958	1:200
Has3	Santa Cruz sc-365322	1:1000
Hyal1	Santa Cruz sc-1101340	1:200
Hyal2	Santa Cruz sc-99022	1:200
NUDT21	Proteintech 10322-1-AP	1:1000
β-actin	Sigma A5316	1:1000

Table 4 Antibodies

Morphometry

Muscularized arterioles of the lung parenchyma were observed under 40× magnification and noted as being different from both airways and non-muscularized arterioles. Muscularized arterioles were then photographed under 40× magnification. Micropictographs were then analyzed using Image Pro-Plus software (MediaCybernetics Inc, Bethesda, MD). In short, the overall area of the muscularized portion was measured for each arteriole. To correct for size, the largest diameter for each arteriole was also measured. The area of the arteriole was then divided by the largest diameter to give a relative measurement of muscularization. Poor inflation of lungs resulting in a compression of airspaces visualized histologically in normal areas of the lung by an observer blinded to group status was considered as a violation of predetermined criteria.

To quantify airspace enlargement, alveolar air-space size was determined in pressure infused lungs by measuring mean chord lengths on H&E-stained lung sections. Representative images (black and white) were digitized, and a grid consisting of 53 black lines at 10.5 μm intervals was overlaid on each image. This line grid was subtracted from the black and white lung images using Image-Pro Plus image analysis software (version 2.0; MediaCybernetics). The resultant lines were measured (in μm) and averaged to give the mean chord length of the airspace enlargement. The final mean chord lengths represent averages from 10 non-overlapping images of each lung specimen. All quantitative studies were performed blinded with regard to animal genotype and treatment. It is important to mention that for the quantification of airspace enlargement, the images taken were from the parenchyma, devoid of large airway,

vascular structures or fibrotic deposition. The exclusion of these structures is necessary to quantify airspace enlargement. However, these exclusions were not performed for the determination of Ashcroft scores.

RNA-seq

PASMCs(Lonza) were lysed using TRIzol(Life Technologies) and total RNA purified using the RNeasy Kit(QIAGEN). Total RNA-seq was performed with MiSeq(LC Sciences). RNA-seq reads were aligned to the human genome(hg19) using TopHat 2.1.1. 3'UTR APA events between control and NUDT21 siRNA treated cells were identified using the DaPars algorithm. This algorithm identifies *de novo* APA events through the use of linear regression models to identify proximal polyadenylation sites and then estimates the short and long isoform expression levels using read density upstream and downstream of this calculated polyadenylation site (169). Genes with an absolute difference of mean PDUIs of no less than 0.1 were identified as having shifted 3′-UTR events. Pathway analysis was performed using the ConsensusPathDB-human over-representation gene set analysis to identify biological networks and functional pathways enriched in the dataset.

Liquid Chromatography Tandem Mass Spectrometry

4-Methylumbelliferone-[13C4] (Toronto Research Chemicals, Ontario, Canada) and 7-hydroxy coumarin β-D-glucuronide (as sodium salt) (Toronto Research Chemicals, Ontario, Canada) were used as the internal standard (IS) for 4MU and 4MUG respectively. The stock solutions of a mixture of 4-MU and 4-MUG were diluted in 50%

methanol to prepare the spiking solutions ranging from 1 ng mL-1 to 5000 ng mL-1. For calibration standards, 25 µL of blank plasma was mixed with 25 µL of the spiking solutions. For unknown samples, 25 µL of test plasma was mixed with 25 µL of 50% methanol to make up the volume. 25 µL of a mixture of the two IS (1000 ng mL-1 in 50% methanol) was also added. After vortexing all standards and samples, 150 µL of methanol/acetonitrile 20:80 (v/v) was added to the mixture which was further vortexed vigorously for 1 min followed by centrifugation at 850 × g for 10 min. 100 µL of the supernatant was diluted with 200 µL of Milli Q water.

The LC–MS/MS system consists of an AB SCIEX QTRAP 4000 mass spectrometer coupled to a Shimadzu UFLC system. Mobile phase A is HPLC grade water. Mobile phase B is HPLC grade acetonitrile. LC separation was carried out on a Phenomenex Luna PFP(2) column (3 µm, 150 × 2 mm) with isocratic elution using 45% mobile phase B and a flow rate of 0.4 mL min-1 at room temperature. The analysis time was 2.5 min. 5 µL of the extracted sample was injected. The mass spectrometer was operated in the negative mode with multiple-reaction monitoring (MRM). The following MRM transitions were used: 4MU (m/z 174.7 → 132.9), IS for 4MU (m/z 178.7 → 134.9), 4MUG (m/z 350.8 → 174.9) and IS for 4MUG (m/z 336.9 → 160.9). Data acquisition and analysis were performed using the Analyst 1.6.1 software (AB SCIEX).

Hyaluronan fragment size assessment

Lung samples from mice were pulverized and suspended in water. Protease (Pronase Calbiochem #537088) was added to a final concentration of 200u mL-1. This was digested for 12 h at 55°C. This digestion was repeated six times. Samples were

centrifuged at 2400 × g for 10 min. The supernatant was concentrated using Corning Spin-X UF concentrators (CLS431477). Samples were mixed with 4 µL 2 M sucrose and were run in 0.5% agarose gel in TAE buffer. Hyaluronan size standards were also mixed with sucrose. Gel was stained with 0.005% Stains-All (Sigma #E-7762) and then destained in water for 48 h. Images were obtained with the BioRad ChemiDoc Touch.

Cell culture experiments and AFM

Normal control primary PASMC obtained from Dr. Morrell's group (Cambridge, UK) were cultured in DMEM with or without 100 µM fasudil (R&D Systems). For studies performed to evaluate the proliferative effect and cyotoxcity of hyaluronan and fasudil, cells were treated with high molecular weight (HMW; 1350 kDa GLR002 R&D systems, Minneapolis, MN), medium molecular weight (MMW, 289 kDa GLR004 R&D systems), low molecular weight (LMW, 20 kDa, GLR001) or ultra-low molecular weight (ULMW, 4.8 kDa GLR003) hyaluronan with or without fasudil (100 µM,). Cell proliferation and cytotoxicity was determined using the ApoTox-Glo™ Triplex Assay (Promega, Madison WI). This method relies on measuring two protease activities: one for cell viability and the other as a marker of cell cytotoxicity. The final part of the assay is the measurement of a luminogenic substrate for caspase 3/7. For AFM experiments control and fasudil were treated with no hyaluronan, 5.7 mg of medium molecular weight (MMW) hyaluronan (R&D Systems GLR004), or 5.7 mg of ULMW hyaluronan (R&D Systems GLR003). After 24 h the cells were used for AFM measurements at room temperature. The force curves measurements were performed with a Catalyst Bioscope System (Bruker Corporation, Billerica, MA). The AFM was equipped with an inverted light

microscope (Olympus IX81) so that the cells were constantly monitored. Silicon nitride cantilevers (Novascan Technologies, Inc., Ames, IA) with approximate spring constant values of 0.06 N m−1 were employed in all AFM experimentations. The AFM probe was purchased from Novascan (the probe has a silicon nitrite cantilever with a 5μm silica spherical particle on the end) with a spring constant of 0.06 N s−1. The cantilever sensitivity was calibrated with the NanoScope 9.0 software by measuring a force curve on a clean silicon wafer. Force curves were acquired at a sampling rate of 1 Hz. The Young's modulus, E, was calculated from obtained force curves based on the Hertzian fit mode using Nanoscope analysis program from the Bruker Corporation. $F = 2\pi E1-\upsilon 2 \tan\alpha \delta 2$ where F = force, E = Young's modulus, ν = Poisson's ratio (ν = 0.5, in this study), α = half-angle of the indenter (i.e. tip radius, α = 5000 nm, in this study), and δ = indentation depth.

Cell culture experiments

The mouse alveolar macrophage cell line MH-S (ATCC, Manassas, VA, USA) was maintained at 37°C and 5% CO2. MH-S cells were grown in RPMI-1640 supplemented with 10% heat-inactivated fetal bovine serum (FBS), 2 mM L-glutamine and penicillin-streptomycin. For experimental use, MH-S were serum-starved overnight in RPMI-1640 supplemented with 2% FBS, 2 mM L-glutamine and penicillin-streptomycin, followed by 24h exposure to ADORA2B agonist BAY60-6583 (10 μM, Tocris) with or without the ADORA2B antagonist GS6201 (100 nM, Tocris). PASMCs were maintained in in similar conditions with starvation occurring for 48hr coinciding with siRNA or plasmid transfection. Proliferation assay occurred with 0 or 25mM BB-PDGF while migration

occurred with no serum gradient at 1% FBS or with a gradient from 1-10% FBS in boyden chambers with 8um pore size.

PASMC isolation

The pulmonary arteries are dissected out of the tissue. The adventitia is then removed with forceps. The arteries are bisected longitudinally and then treated with 4mL of digestion mixture. Digestion mixture is a mixture of 4mL of Collagenase Type II(2mg/mL) and 75 µL of elastase(125U/µL) for about 2 hours. The cells are then grown in Smooth Muscle Growth Medium(ScienceCell). Cells are used at passage three or passage 4.

NUDT21 depletion and overexpression

For NUDT21 overexpression the coding region was cloned into the pCDNA3.1 +C plasmid. 5µg of plasmid or empty vector was transfected using jetPRIME(Polyplus New York, NY) into a 80% confluent 10cm twice 24hr separated. Depletion was performed with siRNAs purchased from Sigma-Aldrich(Human NM_007006 260 MISSION siRNA 4) with the same time points and 500pmoles of siRNA.

Bibliography

1. J. R. Sysol RFM. Classification and pathophysiology of pulmonary hypertension. *continuing cardiology education* 2018;

4.

2. Simonneau G, Gatzoulis MA, Adatia I, Celermajer D, Denton C, Ghofrani A, Gomez Sanchez MA, Kumar RK, Landzberg M, Machado RF, Olschewski H, Robbins IM, Souza R. [Updated clinical classification of pulmonary hypertension]. *Turk Kardiyol Dern Ars* 2014; 42 Suppl 1: 45-54.

3. Wijeratne DT, Lajkosz K, Brogly SB, Lougheed MD, Jiang L, Housin A, Barber D, Johnson A, Doliszny KM, Archer SL. Increasing Incidence and Prevalence of World Health Organization Groups 1 to 4 Pulmonary Hypertension: A Population-Based Cohort Study in Ontario, Canada. *Circ Cardiovasc Qual Outcomes* 2018; 11: e003973.

4. Peacock AJ, Murphy NF, McMurray JJ, Caballero L, Stewart S. An epidemiological study of pulmonary arterial hypertension. *Eur Respir J* 2007; 30: 104-109.

5. Ling Y, Johnson MK, Kiely DG, Condliffe R, Elliot CA, Gibbs JS, Howard LS, Pepke-Zaba J, Sheares KK, Corris PA, Fisher AJ, Lordan JL, Gaine S, Coghlan JG, Wort SJ, Gatzoulis MA, Peacock AJ. Changing demographics, epidemiology, and survival of incident pulmonary arterial hypertension: results from the pulmonary hypertension registry of the United Kingdom and Ireland. *Am J Respir Crit Care Med* 2012; 186: 790-796.

6. Dupuis J, Hoeper MM. Endothelin receptor antagonists in pulmonary arterial hypertension. *Eur Respir J* 2008; 31: 407-415.

7. Watanabe H. Treatment Selection in Pulmonary Arterial Hypertension: Phosphodiesterase Type 5 Inhibitors versus Soluble Guanylate Cyclase Stimulator. *Eur Cardiol* 2018; 13: 35-37.

8. Galie N, Manes A, Branzi A. Prostanoids for pulmonary arterial hypertension. *Am J Respir Med* 2003; 2: 123-137.

9. Galie N, Corris PA, Frost A, Girgis RE, Granton J, Jing ZC, Klepetko W, McGoon MD, McLaughlin VV, Preston IR, Rubin LJ, Sandoval J, Seeger W, Keogh A. [Updated treatment algorithm of pulmonary arterial hypertension]. *Turk Kardiyol Dern Ars* 2014; 42 Suppl 1: 78-94.

10. Sitbon O, Humbert M, Nunes H, Parent F, Garcia G, Herve P, Rainisio M, Simonneau G. Long-term intravenous epoprostenol infusion in primary pulmonary hypertension: prognostic factors and survival. *J Am Coll Cardiol* 2002; 40: 780-788.

11. Aldred MA, Vijayakrishnan J, James V, Soubrier F, Gomez-Sanchez MA, Martensson G, Galie N, Manes A, Corris P, Simonneau G, Humbert M, Morrell NW, Trembath RC. BMPR2 gene rearrangements account for a significant proportion of mutations in familial and idiopathic pulmonary arterial hypertension. *Hum Mutat* 2006; 27: 212-213.

12. Nasim MT, Ogo T, Ahmed M, Randall R, Chowdhury HM, Snape KM, Bradshaw TY, Southgate L, Lee GJ, Jackson I, Lord GM, Gibbs JS, Wilkins MR, Ohta-Ogo K, Nakamura K, Girerd B, Coulet F, Soubrier F, Humbert M, Morrell NW, Trembath RC, Machado RD. Molecular genetic characterization of SMAD

signaling molecules in pulmonary arterial hypertension. *Hum Mutat* 2011; 32: 1385-1389.

13. Cool CD, Stewart JS, Werahera P, Miller GJ, Williams RL, Voelkel NF, Tuder RM. Three-dimensional reconstruction of pulmonary arteries in plexiform pulmonary hypertension using cell-specific markers. Evidence for a dynamic and heterogeneous process of pulmonary endothelial cell growth. *Am J Pathol* 1999; 155: 411-419.
14. Roger VL. Epidemiology of heart failure. *Circ Res* 2013; 113: 646-659.
15. Berthelot E, Bailly MT, Hatimi SE, Robard I, Rezgui H, Bouchachi A, Montani D, Sitbon O, Chemla D, Assayag P. Pulmonary hypertension due to left heart disease. *Arch Cardiovasc Dis* 2017; 110: 420-431.
16. Delgado JF, Conde E, Sanchez V, Lopez-Rios F, Gomez-Sanchez MA, Escribano P, Sotelo T, Gomez de la Camara A, Cortina J, de la Calzada CS. Pulmonary vascular remodeling in pulmonary hypertension due to chronic heart failure. *Eur J Heart Fail* 2005; 7: 1011-1016.
17. Klinger JR. Group III Pulmonary Hypertension: Pulmonary Hypertension Associated with Lung Disease: Epidemiology, Pathophysiology, and Treatments. *Cardiol Clin* 2016; 34: 413-433.
18. Naeije R. Pulmonary hypertension and right heart failure in chronic obstructive pulmonary disease. *Proc Am Thorac Soc* 2005; 2: 20-22.
19. Caminati A, Cassandro R, Harari S. Pulmonary hypertension in chronic interstitial lung diseases. *Eur Respir Rev* 2013; 22: 292-301.

20. Nathan S, Behr J, Collard HR, Cottin V, Hoeper MM, Martinez F, Corte T, Keogh A, Leuchte H, Mogulkoc N, Ulrich S, Wuyts W, Malcolm S, Shah S, Yao M, Wells A. RISE-IIP: Riociguat for the treatment of pulmonary hypertension associated with idiopathic interstitial pneumonia. *European Respiratory Journal* 2017; 50: OA1985.

21. Raghu G, Behr J, Brown KK, Egan JJ, Kawut SM, Flaherty KR, Martinez FJ, Nathan SD, Wells AU, Collard HR, Costabel U, Richeldi L, de Andrade J, Khalil N, Morrison LD, Lederer DJ, Shao L, Li X, Pedersen PS, Montgomery AB, Chien JW, O'Riordan TG, Investigators* A-I. Treatment of idiopathic pulmonary fibrosis with ambrisentan: a parallel, randomized trial. *Ann Intern Med* 2013; 158: 641-649.

22. Raherison C, Girodet PO. Epidemiology of COPD. *Eur Respir Rev* 2009; 18: 213-221.

23. Scharf SM, Iqbal M, Keller C, Criner G, Lee S, Fessler HE, National Emphysema Treatment Trial G. Hemodynamic characterization of patients with severe emphysema. *Am J Respir Crit Care Med* 2002; 166: 314-322.

24. Oswald-Mammosser M, Weitzenblum E, Quoix E, Moser G, Chaouat A, Charpentier C, Kessler R. Prognostic factors in COPD patients receiving long-term oxygen therapy. Importance of pulmonary artery pressure. *Chest* 1995; 107: 1193-1198.

25. Cottin V, Cordier JF. Combined pulmonary fibrosis and emphysema: an experimental and clinically relevant phenotype. *Am J Respir Crit Care Med* 2005; 172: 1605; author reply 1605-1606.

26. Cottin V, Le Pavec J, Prevot G, Mal H, Humbert M, Simonneau G, Cordier JF, Germ"O"P. Pulmonary hypertension in patients with combined pulmonary fibrosis and emphysema syndrome. *Eur Respir J* 2010; 35: 105-111.

27. Lin H, Jiang S. Combined pulmonary fibrosis and emphysema (CPFE): an entity different from emphysema or pulmonary fibrosis alone. *J Thorac Dis* 2015; 7: 767-779.

28. Seeger W, Adir Y, Barbera JA, Champion H, Coghlan JG, Cottin V, De Marco T, Galie N, Ghio S, Gibbs S, Martinez FJ, Semigran MJ, Simonneau G, Wells AU, Vachiery JL. Pulmonary hypertension in chronic lung diseases. *Journal of the American College of Cardiology* 2013; 62: D109-116.

29. Xu XQ, Jing ZC. High-altitude pulmonary hypertension. *Eur Respir Rev* 2009; 18: 13-17.

30. Hackett PH, Roach RC, Hartig GS, Greene ER, Levine BD. The effect of vasodilators on pulmonary hemodynamics in high altitude pulmonary edema: a comparison. *Int J Sports Med* 1992; 13 Suppl 1: S68-71.

31. Groves BM, Reeves JT, Sutton JR, Wagner PD, Cymerman A, Malconian MK, Rock PB, Young PM, Houston CS. Operation Everest II: elevated high-altitude pulmonary resistance unresponsive to oxygen. *J Appl Physiol (1985)* 1987; 63: 521-530.

32. Hakim TS, Michel RP, Minami H, Chang HK. Site of pulmonary hypoxic vasoconstriction studied with arterial and venous occlusion. *J Appl Physiol Respir Environ Exerc Physiol* 1983; 54: 1298-1302.

33. Heath D, Williams D. Pulmonary vascular remodelling in a high-altitude Aymara Indian. *Int J Biometeorol* 1991; 35: 203-207.

34. Gamboa R, Marticorena E. The ductus arteriosus in the newborn infant at high altitude. *Vasa* 1972; 1: 192-195.

35. Kojonazarov B, Myrzaakhmatova A, Sooronbaev T, Ishizaki T, Aldashev A. Effects of fasudil in patients with high-altitude pulmonary hypertension. *Eur Respir J* 2012; 39: 496-498.

36. Richalet JP, Rivera-Ch M, Maignan M, Privat C, Pham I, Macarlupu JL, Petitjean O, Leon-Velarde F. Acetazolamide for Monge's disease: efficiency and tolerance of 6-month treatment. *Am J Respir Crit Care Med* 2008; 177: 1370-1376.

37. Pengo V, Lensing AW, Prins MH, Marchiori A, Davidson BL, Tiozzo F, Albanese P, Biasiolo A, Pegoraro C, Iliceto S, Prandoni P, Thromboembolic Pulmonary Hypertension Study G. Incidence of chronic thromboembolic pulmonary hypertension after pulmonary embolism. *N Engl J Med* 2004; 350: 2257-2264.

38. Delcroix M, Vonk Noordegraaf A, Fadel E, Lang I, Simonneau G, Naeije R. Vascular and right ventricular remodelling in chronic thromboembolic pulmonary hypertension. *Eur Respir J* 2013; 41: 224-232.

39. Kim NH, Mayer E. Chronic thromboembolic pulmonary hypertension: the evolving treatment landscape. *Eur Respir Rev* 2015; 24: 173-177.

40. Gordeuk VR, Castro OL, Machado RF. Pathophysiology and treatment of pulmonary hypertension in sickle cell disease. *Blood* 2016; 127: 820-828.

41. Asakawa H, Kobayashi T. The effect of coculture with human smooth muscle cells on the proliferation, the IL-1 beta secretion, the PDGF production and tube

formation of human aortic endothelial cells. *Cell Biochem Funct* 1999; 17: 123-130.

42. Sandoo A, van Zanten JJ, Metsios GS, Carroll D, Kitas GD. The endothelium and its role in regulating vascular tone. *Open Cardiovasc Med J* 2010; 4: 302-312.
43. Florentin J, Coppin E, Vasamsetti SB, Zhao J, Tai YY, Tang Y, Zhang Y, Watson A, Sembrat J, Rojas M, Vargas SO, Chan SY, Dutta P. Inflammatory Macrophage Expansion in Pulmonary Hypertension Depends upon Mobilization of Blood-Borne Monocytes. *J Immunol* 2018; 200: 3612-3625.
44. Tian W, Jiang X, Tamosiuniene R, Sung YK, Qian J, Dhillon G, Gera L, Farkas L, Rabinovitch M, Zamanian RT, Inayathullah M, Fridlib M, Rajadas J, Peters-Golden M, Voelkel NF, Nicolls MR. Blocking macrophage leukotriene b4 prevents endothelial injury and reverses pulmonary hypertension. *Sci Transl Med* 2013; 5: 200ra117.
45. Kojima H, Tokunou T, Takahara Y, Sunagawa K, Hirooka Y, Ichiki T, Tsutsui H. Hypoxia-inducible factor-1 alpha deletion in myeloid lineage attenuates hypoxia-induced pulmonary hypertension. *Physiol Rep* 2019; 7: e14025.
46. Frid MG, Aldashev AA, Dempsey EC, Stenmark KR. Smooth muscle cells isolated from discrete compartments of the mature vascular media exhibit unique phenotypes and distinct growth capabilities. *Circ Res* 1997; 81: 940-952.
47. Stiebellehner L, Frid MG, Reeves JT, Low RB, Gnanasekharan M, Stenmark KR. Bovine distal pulmonary arterial media is composed of a uniform population of well-differentiated smooth muscle cells with low proliferative capabilities. *Am J Physiol Lung Cell Mol Physiol* 2003; 285: L819-828.

48. Burton AC. Relation of structure to function of the tissues of the wall of blood vessels. *Physiol Rev* 1954; 34: 619-642.

49. Meyrick B, Reid L. Hypoxia and incorporation of 3H-thymidine by cells of the rat pulmonary arteries and alveolar wall. *Am J Pathol* 1979; 96: 51-70.

50. Meyrick B, Reid L. Development of pulmonary arterial changes in rats fed Crotalaria spectabilis. *Am J Pathol* 1979; 94: 37-50.

51. Wilson DW, Segall HJ, Pan LC, Dunston SK. Progressive inflammatory and structural changes in the pulmonary vasculature of monocrotaline-treated rats. *Microvasc Res* 1989; 38: 57-80.

52. Meyrick B, Reid L. The effect of continued hypoxia on rat pulmonary arterial circulation. An ultrastructural study. *Lab Invest* 1978; 38: 188-200.

53. Taraseviciene-Stewart L, Kasahara Y, Alger L, Hirth P, Mc Mahon G, Waltenberger J, Voelkel NF, Tuder RM. Inhibition of the VEGF receptor 2 combined with chronic hypoxia causes cell death-dependent pulmonary endothelial cell proliferation and severe pulmonary hypertension. *FASEB J* 2001; 15: 427-438.

54. Graham BB, Mentink-Kane MM, El-Haddad H, Purnell S, Zhang L, Zaiman A, Redente EF, Riches DW, Hassoun PM, Bandeira A, Champion HC, Butrous G, Wynn TA, Tuder RM. Schistosomiasis-induced experimental pulmonary hypertension: role of interleukin-13 signaling. *Am J Pathol* 2010; 177: 1549-1561.

55. Mertens TCJ, Hanmandlu A, Tu L, Phan C, Collum SD, Chen NY, Weng T, Davies J, Liu C, Eltzschig HK, Jyothula SSK, Rajagopal K, Xia Y, Guha A, Bruckner BA, Blackburn MR, Guignabert C, Karmouty-Quintana H. Switching-Off Adora2b in

Vascular Smooth Muscle Cells Halts the Development of Pulmonary Hypertension. *Front Physiol* 2018; 9: 555.

56. Kovacs G, Berghold A, Scheidl S, Olschewski H. Pulmonary arterial pressure during rest and exercise in healthy subjects: a systematic review. *Eur Respir J* 2009; 34: 888-894.

57. Lewis GD, Bossone E, Naeije R, Grunig E, Saggar R, Lancellotti P, Ghio S, Varga J, Rajagopalan S, Oudiz R, Rubenfire M. Pulmonary vascular hemodynamic response to exercise in cardiopulmonary diseases. *Circulation* 2013; 128: 1470-1479.

58. Morgan JP, Morgan KG. Vascular smooth muscle: the first recorded Ca2+ transients. *Pflugers Arch* 1982; 395: 75-77.

59. Somlyo AP, Somlyo AV. Ca2+ sensitivity of smooth muscle and nonmuscle myosin II: modulated by G proteins, kinases, and myosin phosphatase. *Physiol Rev* 2003; 83: 1325-1358.

60. Kimura K, Ito M, Amano M, Chihara K, Fukata Y, Nakafuku M, Yamamori B, Feng J, Nakano T, Okawa K, Iwamatsu A, Kaibuchi K. Regulation of myosin phosphatase by Rho and Rho-associated kinase (Rho-kinase). *Science* 1996; 273: 245-248.

61. Tcherkezian J, Lamarche-Vane N. Current knowledge of the large RhoGAP family of proteins. *Biol Cell* 2007; 99: 67-86.

62. Rossman KL, Der CJ, Sondek J. GEF means go: turning on RHO GTPases with guanine nucleotide-exchange factors. *Nat Rev Mol Cell Biol* 2005; 6: 167-180.

63. Galie N, Manes A, Branzi A. The endothelin system in pulmonary arterial hypertension. *Cardiovasc Res* 2004; 61: 227-237.

64. Schneider MP, Boesen EI, Pollock DM. Contrasting actions of endothelin ET(A) and ET(B) receptors in cardiovascular disease. *Annu Rev Pharmacol Toxicol* 2007; 47: 731-759.

65. Bonnans C, Chou J, Werb Z. Remodelling the extracellular matrix in development and disease. *Nat Rev Mol Cell Biol* 2014; 15: 786-801.

66. Discher DE, Mooney DJ, Zandstra PW. Growth factors, matrices, and forces combine and control stem cells. *Science* 2009; 324: 1673-1677.

67. Shi F, Long X, Hendershot A, Miano JM, Sottile J. Fibronectin matrix polymerization regulates smooth muscle cell phenotype through a Rac1 dependent mechanism. *PLoS One* 2014; 9: e94988.

68. Frantz C, Stewart KM, Weaver VM. The extracellular matrix at a glance. *J Cell Sci* 2010; 123: 4195-4200.

69. Schaefer L, Schaefer RM. Proteoglycans: from structural compounds to signaling molecules. *Cell Tissue Res* 2010; 339: 237-246.

70. Schaefer L, Iozzo RV. Biological functions of the small leucine-rich proteoglycans: from genetics to signal transduction. *J Biol Chem* 2008; 283: 21305-21309.

71. Day AJ, Prestwich GD. Hyaluronan-binding proteins: tying up the giant. *J Biol Chem* 2002; 277: 4585-4588.

72. Egeblad M, Rasch MG, Weaver VM. Dynamic interplay between the collagen scaffold and tumor evolution. *Curr Opin Cell Biol* 2010; 22: 697-706.

73. Schreier D, Hacker T, Song G, Chesler N. The role of collagen synthesis in ventricular and vascular adaptation to hypoxic pulmonary hypertension. *J Biomech Eng* 2013; 135: 021018.

74. Beagrie RA, Scialdone A, Schueler M, Kraemer DC, Chotalia M, Xie SQ, Barbieri M, de Santiago I, Lavitas LM, Branco MR, Fraser J, Dostie J, Game L, Dillon N, Edwards PA, Nicodemi M, Pombo A. Complex multi-enhancer contacts captured by genome architecture mapping. *Nature* 2017; 543: 519-524.

75. Aregger M, Kaskar A, Varshney D, Fernandez-Sanchez ME, Inesta-Vaquera FA, Weidlich S, Cowling VH. CDK1-Cyclin B1 Activates RNMT, Coordinating mRNA Cap Methylation with G1 Phase Transcription. *Mol Cell* 2016; 61: 734-746.

76. Hirose Y, Tacke R, Manley JL. Phosphorylated RNA polymerase II stimulates pre-mRNA splicing. *Genes Dev* 1999; 13: 1234-1239.

77. David CJ, Boyne AR, Millhouse SR, Manley JL. The RNA polymerase II C-terminal domain promotes splicing activation through recruitment of a U2AF65-Prp19 complex. *Genes Dev* 2011; 25: 972-983.

78. Kramer A. The structure and function of proteins involved in mammalian pre-mRNA splicing. *Annu Rev Biochem* 1996; 65: 367-409.

79. Johnson JM, Castle J, Garrett-Engele P, Kan Z, Loerch PM, Armour CD, Santos R, Schadt EE, Stoughton R, Shoemaker DD. Genome-wide survey of human alternative pre-mRNA splicing with exon junction microarrays. *Science* 2003; 302: 2141-2144.

80. Wang GS, Cooper TA. Splicing in disease: disruption of the splicing code and the decoding machinery. *Nat Rev Genet* 2007; 8: 749-761.

81. Tian B, Graber JH. Signals for pre-mRNA cleavage and polyadenylation. *Wiley Interdiscip Rev RNA* 2012; 3: 385-396.

82. Sheets MD, Ogg SC, Wickens MP. Point mutations in AAUAAA and the poly (A) addition site: effects on the accuracy and efficiency of cleavage and polyadenylation in vitro. *Nucleic Acids Res* 1990; 18: 5799-5805.

83. Levitt N, Briggs D, Gil A, Proudfoot NJ. Definition of an efficient synthetic poly(A) site. *Genes Dev* 1989; 3: 1019-1025.

84. Hu J, Lutz CS, Wilusz J, Tian B. Bioinformatic identification of candidate cis-regulatory elements involved in human mRNA polyadenylation. *RNA* 2005; 11: 1485-1493.

85. Venkataraman K, Brown KM, Gilmartin GM. Analysis of a noncanonical poly(A) site reveals a tripartite mechanism for vertebrate poly(A) site recognition. *Genes Dev* 2005; 19: 1315-1327.

86. Mandel CR, Bai Y, Tong L. Protein factors in pre-mRNA 3'-end processing. *Cell Mol Life Sci* 2008; 65: 1099-1122.

87. Schonemann L, Kuhn U, Martin G, Schafer P, Gruber AR, Keller W, Zavolan M, Wahle E. Reconstitution of CPSF active in polyadenylation: recognition of the polyadenylation signal by WDR33. *Genes Dev* 2014; 28: 2381-2393.

88. Murthy KG, Manley JL. The 160-kD subunit of human cleavage-polyadenylation specificity factor coordinates pre-mRNA 3'-end formation. *Genes Dev* 1995; 9: 2672-2683.

89. Kolev NG, Yario TA, Benson E, Steitz JA. Conserved motifs in both CPSF73 and CPSF100 are required to assemble the active endonuclease for histone mRNA 3'-end maturation. *EMBO Rep* 2008; 9: 1013-1018.

90. Gilmartin GM, Nevins JR. Molecular analyses of two poly(A) site-processing factors that determine the recognition and efficiency of cleavage of the pre-mRNA. *Mol Cell Biol* 1991; 11: 2432-2438.

91. Perez Canadillas JM, Varani G. Recognition of GU-rich polyadenylation regulatory elements by human CstF-64 protein. *EMBO J* 2003; 22: 2821-2830.

92. Kleiman FE, Manley JL. The BARD1-CstF-50 interaction links mRNA 3' end formation to DNA damage and tumor suppression. *Cell* 2001; 104: 743-753.

93. Takagaki Y, Manley JL. Complex protein interactions within the human polyadenylation machinery identify a novel component. *Mol Cell Biol* 2000; 20: 1515-1525.

94. Brown KM, Gilmartin GM. A mechanism for the regulation of pre-mRNA 3' processing by human cleavage factor Im. *Mol Cell* 2003; 12: 1467-1476.

95. Yang Q, Coseno M, Gilmartin GM, Doublie S. Crystal structure of a human cleavage factor CFI(m)25/CFI(m)68/RNA complex provides an insight into poly(A) site recognition and RNA looping. *Structure* 2011; 19: 368-377.

96. Yang Q, Gilmartin GM, Doublie S. Structural basis of UGUA recognition by the Nudix protein CFI(m)25 and implications for a regulatory role in mRNA 3' processing. *Proc Natl Acad Sci U S A* 2010; 107: 10062-10067.

97. de Vries H, Ruegsegger U, Hubner W, Friedlein A, Langen H, Keller W. Human pre-mRNA cleavage factor II(m) contains homologs of yeast proteins and bridges two other cleavage factors. *EMBO J* 2000; 19: 5895-5904.

98. West S, Proudfoot NJ. Human Pcf11 enhances degradation of RNA polymerase II-associated nascent RNA and transcriptional termination. *Nucleic Acids Res* 2008; 36: 905-914.

99. Wahle E. Purification and characterization of a mammalian polyadenylate polymerase involved in the 3' end processing of messenger RNA precursors. *J Biol Chem* 1991; 266: 3131-3139.

100. Wahle E. A novel poly(A)-binding protein acts as a specificity factor in the second phase of messenger RNA polyadenylation. *Cell* 1991; 66: 759-768.

101. Hirose Y, Manley JL. RNA polymerase II is an essential mRNA polyadenylation factor. *Nature* 1998; 395: 93-96.

102. Takagaki Y, Seipelt RL, Peterson ML, Manley JL. The polyadenylation factor CstF-64 regulates alternative processing of IgM heavy chain pre-mRNA during B cell differentiation. *Cell* 1996; 87: 941-952.

103. Setzer DR, McGrogan M, Nunberg JH, Schimke RT. Size heterogeneity in the 3' end of dihydrofolate reductase messenger RNAs in mouse cells. *Cell* 1980; 22: 361-370.

104. Derti A, Garrett-Engele P, Macisaac KD, Stevens RC, Sriram S, Chen R, Rohl CA, Johnson JM, Babak T. A quantitative atlas of polyadenylation in five mammals. *Genome Res* 2012; 22: 1173-1183.

105. Sandberg R, Neilson JR, Sarma A, Sharp PA, Burge CB. Proliferating cells express mRNAs with shortened 3' untranslated regions and fewer microRNA target sites. *Science* 2008; 320: 1643-1647.

106. Elkon R, Ugalde AP, Agami R. Alternative cleavage and polyadenylation: extent, regulation and function. *Nat Rev Genet* 2013; 14: 496-506.

107. Yonaha M, Proudfoot NJ. Specific transcriptional pausing activates polyadenylation in a coupled in vitro system. *Mol Cell* 1999; 3: 593-600.

108. Muller-McNicoll M, Botti V, de Jesus Domingues AM, Brandl H, Schwich OD, Steiner MC, Curk T, Poser I, Zarnack K, Neugebauer KM. SR proteins are NXF1 adaptors that link alternative RNA processing to mRNA export. *Genes Dev* 2016; 30: 553-566.

109. Oh JM, Di C, Venters CC, Guo J, Arai C, So BR, Pinto AM, Zhang Z, Wan L, Younis I, Dreyfuss G. U1 snRNP telescripting regulates a size-function-stratified human genome. *Nat Struct Mol Biol* 2017; 24: 993-999.

110. Berg MG, Singh LN, Younis I, Liu Q, Pinto AM, Kaida D, Zhang Z, Cho S, Sherrill-Mix S, Wan L, Dreyfuss G. U1 snRNP determines mRNA length and regulates isoform expression. *Cell* 2012; 150: 53-64.

111. Yao C, Biesinger J, Wan J, Weng L, Xing Y, Xie X, Shi Y. Transcriptome-wide analyses of CstF64-RNA interactions in global regulation of mRNA alternative polyadenylation. *Proc Natl Acad Sci U S A* 2012; 109: 18773-18778.

112. Masamha CP, Xia Z, Peart N, Collum S, Li W, Wagner EJ, Shyu AB. CFIm25 regulates glutaminase alternative terminal exon definition to modulate miR-23 function. *RNA* 2016; 22: 830-838.

113. Masamha CP, Xia Z, Yang J, Albrecht TR, Li M, Shyu AB, Li W, Wagner EJ. CFIm25 links alternative polyadenylation to glioblastoma tumour suppression. *Nature* 2014; 510: 412-416.

114. Weng T, Ko J, Masamha CP, Xia Z, Xiang Y, Chen NY, Molina JG, Collum S, Mertens TC, Luo F, Philip K, Davies J, Huang J, Wilson C, Thandavarayan RA, Bruckner BA, Jyothula SS, Volcik KA, Li L, Han L, Li W, Assassi S, Karmouty-Quintana H, Wagner EJ, Blackburn MR. Cleavage factor 25 deregulation contributes to pulmonary fibrosis through alternative polyadenylation. *J Clin Invest* 2019; 130.

115. Wang Y, Xu Y, Yan W, Han P, Liu J, Gong J, Li D, Ding X, Wang H, Lin Z, Tian D, Liao J. CFIm25 inhibits hepatocellular carcinoma metastasis by suppressing the p38 and JNK/c-Jun signaling pathways. *Oncotarget* 2018; 9: 11783-11793.

116. Zhu ZJ, Huang P, Chong YX, Kang LX, Huang X, Zhu ZX, Nie L. MicroRNA-181a promotes proliferation and inhibits apoptosis by suppressing CFIm25 in osteosarcoma. *Mol Med Rep* 2016; 14: 4271-4278.

117. Gennarino VA, Alcott CE, Chen CA, Chaudhury A, Gillentine MA, Rosenfeld JA, Parikh S, Wheless JW, Roeder ER, Horovitz DD, Roney EK, Smith JL, Cheung SW, Li W, Neilson JR, Schaaf CP, Zoghbi HY. NUDT21-spanning CNVs lead to neuropsychiatric disease and altered MeCP2 abundance via alternative polyadenylation. *Elife* 2015; 4.

118. Chowdhury B, Xiang B, Liu M, Hemming R, Dolinsky VW, Triggs-Raine B. Hyaluronidase 2 Deficiency Causes Increased Mesenchymal Cells, Congenital Heart Defects, and Heart Failure. *Circ Cardiovasc Genet* 2017; 10.

119. Atmuri V, Martin DC, Hemming R, Gutsol A, Byers S, Sahebjam S, Thliveris JA, Mort JS, Carmona E, Anderson JE, Dakshinamurti S, Triggs-Raine B. Hyaluronidase 3 (HYAL3) knockout mice do not display evidence of hyaluronan accumulation. *Matrix Biol* 2008; 27: 653-660.

120. Triggs-Raine B, Natowicz MR. Biology of hyaluronan: Insights from genetic disorders of hyaluronan metabolism. *World J Biol Chem* 2015; 6: 110-120.

121. Soltes L, Mendichi R, Kogan G, Schiller J, Stankovska M, Arnhold J. Degradative action of reactive oxygen species on hyaluronan. *Biomacromolecules* 2006; 7: 659-668.

122. Evanko SP, Tammi MI, Tammi RH, Wight TN. Hyaluronan-dependent pericellular matrix. *Adv Drug Deliv Rev* 2007; 59: 1351-1365.

123. Suwan K, Choocheep K, Hatano S, Kongtawelert P, Kimata K, Watanabe H. Versican/PG-M Assembles Hyaluronan into Extracellular Matrix and Inhibits CD44-mediated Signaling toward Premature Senescence in Embryonic Fibroblasts. *J Biol Chem* 2009; 284: 8596-8604.

124. Munaim SI, Klagsbrun M, Toole BP. Hyaluronan-dependent pericellular coats of chick embryo limb mesodermal cells: induction by basic fibroblast growth factor. *Dev Biol* 1991; 143: 297-302.

125. Misra S, Obeid LM, Hannun YA, Minamisawa S, Berger FG, Markwald RR, Toole BP, Ghatak S. Hyaluronan constitutively regulates activation of COX-2-mediated cell survival activity in intestinal epithelial and colon carcinoma cells. *J Biol Chem* 2008; 283: 14335-14344.

126. Misra S, Hascall VC, Markwald RR, Ghatak S. Interactions between Hyaluronan and Its Receptors (CD44, RHAMM) Regulate the Activities of Inflammation and Cancer. *Front Immunol* 2015; 6: 201.

127. Goueffic Y, Guilluy C, Guerin P, Patra P, Pacaud P, Loirand G. Hyaluronan induces vascular smooth muscle cell migration through RHAMM-mediated PI3K-dependent Rac activation. *Cardiovasc Res* 2006; 72: 339-348.

128. Hall CL, Yang B, Yang X, Zhang S, Turley M, Samuel S, Lange LA, Wang C, Curpen GD, Savani RC, Greenberg AH, Turley EA. Overexpression of the hyaluronan receptor RHAMM is transforming and is also required for H-ras transformation. *Cell* 1995; 82: 19-26.

129. Harris EN, Kyosseva SV, Weigel JA, Weigel PH. Expression, processing, and glycosaminoglycan binding activity of the recombinant human 315-kDa hyaluronic acid receptor for endocytosis (HARE). *J Biol Chem* 2007; 282: 2785-2797.

130. Bono P, Rubin K, Higgins JM, Hynes RO. Layilin, a novel integral membrane protein, is a hyaluronan receptor. *Mol Biol Cell* 2001; 12: 891-900.

131. Forteza RM, Casalino-Matsuda SM, Falcon NS, Valencia Gattas M, Monzon ME. Hyaluronan and layilin mediate loss of airway epithelial barrier function induced by cigarette smoke by decreasing E-cadherin. *J Biol Chem* 2012; 287: 42288-42298.

132. Litwiniuk M, Krejner A, Speyrer MS, Gauto AR, Grzela T. Hyaluronic Acid in Inflammation and Tissue Regeneration. *Wounds* 2016; 28: 78-88.

133. Kida D, Yoneda M, Miyaura S, Ishimaru T, Yoshida Y, Ito T, Ishiguro N, Iwata H, Kimata K. The SHAP-HA complex in sera from patients with rheumatoid arthritis and osteoarthritis. *J Rheumatol* 1999; 26: 1230-1238.

134. Garantziotis S, Li Z, Potts EN, Kimata K, Zhuo L, Morgan DL, Savani RC, Noble PW, Foster WM, Schwartz DA, Hollingsworth JW. Hyaluronan mediates ozone-induced airway hyperresponsiveness in mice. *J Biol Chem* 2009; 284: 11309-11317.

135. Wiig M, Abrahamsson SO, Lundborg G. Effects of hyaluronan on cell proliferation and collagen synthesis: a study of rabbit flexor tendons in vitro. *J Hand Surg Am* 1996; 21: 599-604.

136. Evanko SP, Angello JC, Wight TN. Formation of hyaluronan- and versican-rich pericellular matrix is required for proliferation and migration of vascular smooth muscle cells. *Arterioscler Thromb Vasc Biol* 1999; 19: 1004-1013.

137. Tolg C, Hamilton SR, Nakrieko KA, Kooshesh F, Walton P, McCarthy JB, Bissell MJ, Turley EA. Rhamm-/- fibroblasts are defective in CD44-mediated ERK1,2 motogenic signaling, leading to defective skin wound repair. *J Cell Biol* 2006; 175: 1017-1028.

138. Lennon FE, Mirzapoiazova T, Mambetsariev N, Mambetsariev B, Salgia R, Singleton PA. Transactivation of the receptor-tyrosine kinase ephrin receptor A2 is required for the low molecular weight hyaluronan-mediated angiogenesis that is implicated in tumor progression. *J Biol Chem* 2014; 289: 24043-24058.

139. Jacobson A, Rahmanian M, Rubin K, Heldin P. Expression of hyaluronan synthase 2 or hyaluronidase 1 differentially affect the growth rate of transplantable colon carcinoma cell tumors. *Int J Cancer* 2002; 102: 212-219.

140. Li Y, Li L, Brown TJ, Heldin P. Silencing of hyaluronan synthase 2 suppresses the malignant phenotype of invasive breast cancer cells. *Int J Cancer* 2007; 120: 2557-2567.

141. Heldin P, Delatorre M, Ytterberg D, Bergh J. Differential synthesis and binding of hyaluronan by human breast cancer cell lines. *Oncol Rep* 1996; 3: 1011-1016.

142. Kodama K, Horikoshi M, Toda K, Yamada S, Hara K, Irie J, Sirota M, Morgan AA, Chen R, Ohtsu H, Maeda S, Kadowaki T, Butte AJ. Expression-based genome-wide association study links the receptor CD44 in adipose tissue with type 2 diabetes. *Proc Natl Acad Sci U S A* 2012; 109: 7049-7054.

143. Mine S, Okada Y, Kawahara C, Tabata T, Tanaka Y. Serum hyaluronan concentration as a marker of angiopathy in patients with diabetes mellitus. *Endocr J* 2006; 53: 761-766.

144. Chai S, Chai Q, Danielsen CC, Hjorth P, Nyengaard JR, Ledet T, Yamaguchi Y, Rasmussen LM, Wogensen L. Overexpression of hyaluronan in the tunica media promotes the development of atherosclerosis. *Circ Res* 2005; 96: 583-591.

145. Zhao L, Lee E, Zukas AM, Middleton MK, Kinder M, Acharya PS, Hall JA, Rader DJ, Pure E. CD44 expressed on both bone marrow-derived and non-bone marrow-derived cells promotes atherogenesis in ApoE-deficient mice. *Arterioscler Thromb Vasc Biol* 2008; 28: 1283-1289.

146. Yatagai Y, Sakamoto T, Yamada H, Masuko H, Kaneko Y, Iijima H, Naito T, Noguchi E, Hirota T, Tamari M, Konno S, Nishimura M, Hizawa N. Genomewide association study identifies HAS2 as a novel susceptibility gene for adult asthma in a Japanese population. *Clin Exp Allergy* 2014; 44: 1327-1334.

147. Bousquet J, Chanez P, Lacoste JY, Enander I, Venge P, Peterson C, Ahlstedt S, Michel FB, Godard P. Indirect evidence of bronchial inflammation assessed by titration of inflammatory mediators in BAL fluid of patients with asthma. *J Allergy Clin Immunol* 1991; 88: 649-660.

148. Liang J, Jiang D, Jung Y, Xie T, Ingram J, Church T, Degan S, Leonard M, Kraft M, Noble PW. Role of hyaluronan and hyaluronan-binding proteins in human asthma. *J Allergy Clin Immunol* 2011; 128: 403-411 e403.

149. Dentener MA, Vernooy JH, Hendriks S, Wouters EF. Enhanced levels of hyaluronan in lungs of patients with COPD: relationship with lung function and local inflammation. *Thorax* 2005; 60: 114-119.

150. Klagas I, Goulet S, Karakiulakis G, Zhong J, Baraket M, Black JL, Papakonstantinou E, Roth M. Decreased hyaluronan in airway smooth muscle cells from patients with asthma and COPD. *Eur Respir J* 2009; 34: 616-628.

151. Cantor J, Armand G, Turino G. Lung hyaluronan levels are decreased in alpha-1 antiprotease deficiency COPD. *Respir Med* 2015; 109: 656-659.

152. Bjermer L, Lundgren R, Hallgren R. Hyaluronan and type III procollagen peptide concentrations in bronchoalveolar lavage fluid in idiopathic pulmonary fibrosis. *Thorax* 1989; 44: 126-131.

153. Li Y, Jiang D, Liang J, Meltzer EB, Gray A, Miura R, Wogensen L, Yamaguchi Y, Noble PW. Severe lung fibrosis requires an invasive fibroblast phenotype regulated by hyaluronan and CD44. *J Exp Med* 2011; 208: 1459-1471.

154. da Silva Bitencourt C, Gelfuso GM, Pereira PA, de Assis PA, Tefe-Silva C, Ramos SG, Arantes EC, Faccioli LH. Hyaluronidase-loaded PLGA microparticles as a new strategy for the treatment of pulmonary fibrosis. *Tissue Eng Part A* 2015; 21: 246-256.

155. Papakonstantinou E, Kouri FM, Karakiulakis G, Klagas I, Eickelberg O. Increased hyaluronic acid content in idiopathic pulmonary arterial hypertension. *Eur Respir J* 2008; 32: 1504-1512.

156. Kalay N, Elcik D, Canatan H, Kaya MG, Yarlioglues M, Oguzhan A, Dweik RA, Aytekin M. Elevated plasma hyaluronan levels in pulmonary hypertension. *Tohoku J Exp Med* 2013; 230: 7-11.

157. Ormiston ML, Slaughter GR, Deng Y, Stewart DJ, Courtman DW. The enzymatic degradation of hyaluronan is associated with disease progression in experimental pulmonary hypertension. *Am J Physiol Lung Cell Mol Physiol* 2010; 298: L148-157.

158. Karmouty-Quintana H, Weng T, Garcia-Morales LJ, Chen NY, Pedroza M, Zhong H, Molina JG, Bunge R, Bruckner BA, Xia Y, Johnston RA, Loebe M, Zeng D, Seethamraju H, Belardinelli L, Blackburn MR. Adenosine A2B receptor and hyaluronan modulate pulmonary hypertension associated with chronic obstructive pulmonary disease. *Am J Respir Cell Mol Biol* 2013; 49: 1038-1047.

159. Cottin V. The impact of emphysema in pulmonary fibrosis. *Eur Respir Rev* 2013; 22: 153-157.

160. Lauer ME, Dweik RA, Garantziotis S, Aronica MA. The Rise and Fall of Hyaluronan in Respiratory Diseases. *Int J Cell Biol* 2015; 2015: 712507.

161. Voelkel NF, Gomez-Arroyo J, Abbate A, Bogaard HJ, Nicolls MR. Pathobiology of pulmonary arterial hypertension and right ventricular failure. *Eur Respir J* 2012; 40: 1555-1565.

162. Liu F, Haeger CM, Dieffenbach PB, Sicard D, Chrobak I, Coronata AM, Suarez Velandia MM, Vitali S, Colas RA, Norris PC, Marinkovic A, Liu X, Ma J, Rose CD, Lee SJ, Comhair SA, Erzurum SC, McDonald JD, Serhan CN, Walsh SR, Tschumperlin DJ, Fredenburgh LE. Distal vessel stiffening is an early and pivotal mechanobiological regulator of vascular remodeling and pulmonary hypertension. *JCI Insight* 2016; 1.

163. Chu Y, Elrod N, Wang C, Li L, Chen T, Routh A, Xia Z, Li W, Wagner EJ, Ji P. Nudt21 regulates the alternative polyadenylation of Pak1 and is predictive in the prognosis of glioblastoma patients. *Oncogene* 2019.

164. Beaudoing E, Freier S, Wyatt JR, Claverie JM, Gautheret D. Patterns of variant polyadenylation signal usage in human genes. *Genome Res* 2000; 10: 1001-1010.

165. Kubo T, Wada T, Yamaguchi Y, Shimizu A, Handa H. Knock-down of 25 kDa subunit of cleavage factor Im in Hela cells alters alternative polyadenylation within 3'-UTRs. *Nucleic acids research* 2006; 34: 6264-6271.

166. Boucherat O, Vitry G, Trinh I, Paulin R, Provencher S, Bonnet S. The cancer theory of pulmonary arterial hypertension. *Pulm Circ* 2017; 7: 285-299.

167. Zhang J, Zhong W, Cui T, Yang M, Hu X, Xu K, Xie C, Xue C, Gibbons GH, Liu C, Li L, Chen YE. Generation of an adult smooth muscle cell-targeted Cre recombinase mouse model. *Arterioscler Thromb Vasc Biol* 2006; 26: e23-24.

168. Justus CR, Leffler N, Ruiz-Echevarria M, Yang LV. In vitro cell migration and invasion assays. *J Vis Exp* 2014.

169. Xia Z, Donehower LA, Cooper TA, Neilson JR, Wheeler DA, Wagner EJ, Li W. Dynamic analyses of alternative polyadenylation from RNA-seq reveal a 3'-UTR landscape across seven tumour types. *Nat Commun* 2014; 5: 5274.

170. Kamburov A, Wierling C, Lehrach H, Herwig R. ConsensusPathDB--a database for integrating human functional interaction networks. *Nucleic Acids Res* 2009; 37: D623-628.

171. Biasin V, Chwalek K, Wilhelm J, Best J, Marsh LM, Ghanim B, Klepetko W, Fink L, Schermuly RT, Weissmann N, Olschewski A, Kwapiszewska G. Endothelin-1 driven proliferation of pulmonary arterial smooth muscle cells is c-fos dependent. *Int J Biochem Cell Biol* 2014; 54: 137-148.

172. Walker J, Undem C, Yun X, Lade J, Jiang H, Shimoda LA. Role of Rho kinase and Na+/H+ exchange in hypoxia-induced pulmonary arterial smooth muscle cell proliferation and migration. *Physiol Rep* 2016; 4.

173. Dai J, Zhou Q, Chen J, Rexius-Hall ML, Rehman J, Zhou G. Alpha-enolase regulates the malignant phenotype of pulmonary artery smooth muscle cells via the AMPK-Akt pathway. *Nat Commun* 2018; 9: 3850.

174. Segura-Ibarra V, Wu S, Hassan N, Moran-Guerrero JA, Ferrari M, Guha A, Karmouty-Quintana H, Blanco E. Nanotherapeutics for Treatment of Pulmonary Arterial Hypertension. *Front Physiol* 2018; 9: 890.

175. McLendon JM, Joshi SR, Sparks J, Matar M, Fewell JG, Abe K, Oka M, McMurtry IF, Gerthoffer WT. Lipid nanoparticle delivery of a microRNA-145 inhibitor improves experimental pulmonary hypertension. *J Control Release* 2015; 210: 67-75.

176. Yang Q, Gilmartin GM, Doublie S. The structure of human cleavage factor I(m) hints at functions beyond UGUA-specific RNA binding: a role in alternative polyadenylation and a potential link to 5' capping and splicing. *RNA Biol* 2011; 8: 748-753.

177. Lorentzen KA, Chai S, Chen H, Danielsen CC, Simonsen U, Wogensen L. Mechanisms involved in extracellular matrix remodeling and arterial stiffness induced by hyaluronan accumulation. *Atherosclerosis* 2016; 244: 195-203.

178. Bensadoun ES, Burke AK, Hogg JC, Roberts CR. Proteoglycan deposition in pulmonary fibrosis. *Am J Respir Crit Care Med* 1996; 154: 1819-1828.

179. Bei Y, Hua-Huy T, Duong-Quy S, Nguyen VH, Chen W, Nicco C, Batteux F, Dinh-Xuan AT. Long-term treatment with fasudil improves bleomycin-induced pulmonary fibrosis and pulmonary hypertension via inhibition of Smad2/3 phosphorylation. *Pulm Pharmacol Ther* 2013; 26: 635-643.

180. Aytekin M, Comhair SA, de la Motte C, Bandyopadhyay SK, Farver CF, Hascall VC, Erzurum SC, Dweik RA. High levels of hyaluronan in idiopathic pulmonary arterial hypertension. *Am J Physiol Lung Cell Mol Physiol* 2008; 295: L789-799.

181. Takeda S, Aburada M. The choleretic mechanism of coumarin compounds and phenolic compounds. *J Pharmacobiodyn* 1981; 4: 724-734.

182. Kakizaki I, Kojima K, Takagaki K, Endo M, Kannagi R, Ito M, Maruo Y, Sato H, Yasuda T, Mita S, Kimata K, Itano N. A novel mechanism for the inhibition of hyaluronan biosynthesis by 4-methylumbelliferone. *J Biol Chem* 2004; 279: 33281-33289.

183. Kultti A, Pasonen-Seppanen S, Jauhiainen M, Rilla KJ, Karna R, Pyoria E, Tammi RH, Tammi MI. 4-Methylumbelliferone inhibits hyaluronan synthesis by depletion of cellular UDP-glucuronic acid and downregulation of hyaluronan synthase 2 and 3. *Exp Cell Res* 2009; 315: 1914-1923.

184. Zhou Y, Schneider DJ, Morschl E, Song L, Pedroza M, Karmouty-Quintana H, Le T, Sun CX, Blackburn MR. Distinct roles for the A2B adenosine receptor in acute and chronic stages of bleomycin-induced lung injury. *J Immunol* 2011; 186: 1097-1106.

185. Ciuclan L, Bonneau O, Hussey M, Duggan N, Holmes AM, Good R, Stringer R, Jones P, Morrell NW, Jarai G, Walker C, Westwick J, Thomas M. A novel murine model of severe pulmonary arterial hypertension. *Am J Respir Crit Care Med* 2011; 184: 1171-1182.

186. Okuda H, Kobayashi A, Xia B, Watabe M, Pai SK, Hirota S, Xing F, Liu W, Pandey PR, Fukuda K, Modur V, Ghosh A, Wilber A, Watabe K. Hyaluronan synthase HAS2 promotes tumor progression in bone by stimulating the interaction of breast cancer stem-like cells with macrophages and stromal cells. *Cancer Res* 2012; 72: 537-547.

187. Esser PR, Wolfle U, Durr C, von Loewenich FD, Schempp CM, Freudenberg MA, Jakob T, Martin SF. Contact sensitizers induce skin inflammation via ROS production and hyaluronic acid degradation. *PLoS One* 2012; 7: e41340.

188. Chowdhury B, Hemming R, Faiyaz S, Triggs-Raine B. Hyaluronidase 2 (HYAL2) is expressed in endothelial cells, as well as some specialized epithelial cells, and is required for normal hyaluronan catabolism. *Histochem Cell Biol* 2016; 145: 53-66.

189. Lennon FE, Singleton PA. Role of hyaluronan and hyaluronan-binding proteins in lung pathobiology. *Am J Physiol Lung Cell Mol Physiol* 2011; 301: L137-147.

190. Karmouty-Quintana H, Zhong H, Acero L, Weng T, Melicoff E, West JD, Hemnes A, Grenz A, Eltzschig HK, Blackwell TS, Xia Y, Johnston RA, Zeng D, Belardinelli L, Blackburn MR. The A2B adenosine receptor modulates pulmonary hypertension associated with interstitial lung disease. *FASEB J* 2012; 26: 2546-2557.

191. Lazo JS, Merrill WW, Pham ET, Lynch TJ, McCallister JD, Ingbar DH. Bleomycin hydrolase activity in pulmonary cells. *J Pharmacol Exp Ther* 1984; 231: 583-588.

192. Bourguignon LY. Hyaluronan-mediated CD44 activation of RhoGTPase signaling and cytoskeleton function promotes tumor progression. *Semin Cancer Biol* 2008; 18: 251-259.

193. Mambetsariev N, Mirzapoiazova T, Mambetsariev B, Sammani S, Lennon FE, Garcia JG, Singleton PA. Hyaluronic Acid binding protein 2 is a novel regulator of vascular integrity. *Arterioscler Thromb Vasc Biol* 2010; 30: 483-490.

194. Momotani K, Artamonov MV, Utepbergenov D, Derewenda U, Derewenda ZS, Somlyo AV. p63RhoGEF couples Galpha(q/11)-mediated signaling to Ca2+ sensitization of vascular smooth muscle contractility. *Circ Res* 2011; 109: 993-1002.

195. Tseng H, Gage JA, Haisler WL, Neeley SK, Shen T, Hebel C, Barthlow HG, Wagoner M, Souza GR. A high-throughput in vitro ring assay for vasoactivity using magnetic 3D bioprinting. *Sci Rep* 2016; 6: 30640.

196. Behr J, Ryu JH. Pulmonary hypertension in interstitial lung disease. *Eur Respir J* 2008; 31: 1357-1367.

197. Garantziotis S, Li Z, Potts EN, Kimata K, Zhuo L, Morgan DL, Savani RC, Noble PW, Foster WM, Schwartz DA, Hollingsworth JW. Hyaluronan mediates ozone-induced airway hyperresponsiveness in mice. *J Biol Chem* 2016; 291: 19257-19258.

198. Li Y, Liang J, Yang T, Monterrosa Mena J, Huan C, Xie T, Kurkciyan A, Liu N, Jiang D, Noble PW. Hyaluronan synthase 2 regulates fibroblast senescence in pulmonary fibrosis. *Matrix Biol* 2016; 55: 35-48.

199. Wang D, Narula N, Azzopardi S, Smith RS, Nasar A, Altorki NK, Mittal V, Somwar R, Stiles BM, Du YN. Expression of the receptor for hyaluronic acid mediated motility (RHAMM) is associated with poor prognosis and metastasis in non-small cell lung carcinoma. *Oncotarget* 2016; 7: 39957-39969.

200. Liang J, Zhang Y, Xie T, Liu N, Chen H, Geng Y, Kurkciyan A, Mena JM, Stripp BR, Jiang D, Noble PW. Hyaluronan and TLR4 promote surfactant-protein-C-

positive alveolar progenitor cell renewal and prevent severe pulmonary fibrosis in mice. *Nat Med* 2016; 22: 1285-1293.

201. Sunitha K, Suresh P, Santhosh MS, Hemshekhar M, Thushara RM, Marathe GK, Thirunavukkarasu C, Kemparaju K, Kumar MS, Girish KS. Inhibition of hyaluronidase by N-acetyl cysteine and glutathione: role of thiol group in hyaluronan protection. *Int J Biol Macromol* 2013; 55: 39-46.

202. Hoffmann J, Wilhelm J, Marsh LM, Ghanim B, Klepetko W, Kovacs G, Olschewski H, Olschewski A, Kwapiszewska G. Distinct differences in gene expression patterns in pulmonary arteries of patients with chronic obstructive pulmonary disease and idiopathic pulmonary fibrosis with pulmonary hypertension. *Am J Respir Crit Care Med* 2014; 190: 98-111.

203. Arai E, Nishida Y, Wasa J, Urakawa H, Zhuo L, Kimata K, Kozawa E, Futamura N, Ishiguro N. Inhibition of hyaluronan retention by 4-methylumbelliferone suppresses osteosarcoma cells in vitro and lung metastasis in vivo. *Br J Cancer* 2011; 105: 1839-1849.

204. McKallip RJ, Hagele HF, Uchakina ON. Treatment with the hyaluronic acid synthesis inhibitor 4-methylumbelliferone suppresses SEB-induced lung inflammation. *Toxins (Basel)* 2013; 5: 1814-1826.

205. McKallip RJ, Ban H, Uchakina ON. Treatment with the hyaluronic Acid synthesis inhibitor 4-methylumbelliferone suppresses LPS-induced lung inflammation. *Inflammation* 2015; 38: 1250-1259.

206. Hoeper MM, Apitz C, Grunig E, Halank M, Ewert R, Kaemmerer H, Kabitz HJ, Kahler C, Klose H, Leuchte H, Ulrich S, Olsson KM, Distler O, Rosenkranz S,

Ghofrani HA. Targeted therapy of pulmonary arterial hypertension: Updated recommendations from the Cologne Consensus Conference 2018. *Int J Cardiol* 2018; 272S: 37-45.

207. Kuipers HF, Nagy N, Ruppert SM, Sunkari VG, Marshall PL, Gebe JA, Ishak HD, Keswani SG, Bollyky J, Frymoyer AR, Wight TN, Steinman L, Bollyky PL. The pharmacokinetics and dosing of oral 4-methylumbelliferone for inhibition of hyaluronan synthesis in mice. *Clin Exp Immunol* 2016; 185: 372-381.

208. Abate A, Dimartino V, Spina P, Costa PL, Lombardo C, Santini A, Del Piano M, Alimonti P. Hymecromone in the treatment of motor disorders of the bile ducts: a multicenter, double-blind, placebo-controlled clinical study. *Drugs Exp Clin Res* 2001; 27: 223-231.

209. Gadang V, Konaniah E, Hui DY, Jaeschke A. Mixed-lineage kinase 3 deficiency promotes neointima formation through increased activation of the RhoA pathway in vascular smooth muscle cells. *Arterioscler Thromb Vasc Biol* 2014; 34: 1429-1436.

210. Papakonstantinou E, Karakiulakis G. The 'sweet' and 'bitter' involvement of glycosaminoglycans in lung diseases: pharmacotherapeutic relevance. *Br J Pharmacol* 2009; 157: 1111-1127.

211. Antoniu SA. Targeting RhoA/ROCK pathway in pulmonary arterial hypertension. *Expert Opin Ther Targets* 2012; 16: 355-363.

212. Jiang C, Huang H, Liu J, Wang Y, Lu Z, Xu Z. Fasudil, a Rho-kinase inhibitor, attenuates bleomycin-induced pulmonary fibrosis in mice. *Int J Mol Sci* 2012; 13: 8293-8307.

213. Mirzapoiazova T, Mambetsariev N, Lennon FE, Mambetsariev B, Berlind JE, Salgia R, Singleton PA. HABP2 is a Novel Regulator of Hyaluronan-Mediated Human Lung Cancer Progression. *Front Oncol* 2015; 5: 164.

214. Bjermer L, Engstrom-Laurent A, Lundgren R, Rosenhall L, Hallgren R. Hyaluronate and type III procollagen peptide concentrations in bronchoalveolar lavage fluid as markers of disease activity in farmer's lung. *Br Med J (Clin Res Ed)* 1987; 295: 803-806.

215. Papakonstantinou E, Bonovolias I, Roth M, Tamm M, Schumann D, Baty F, Louis R, Milenkovic B, Boersma W, Stieltjes B, Kostikas K, Blasi F, Aerts JG, Rohde GGU, Lacoma A, Torres A, Welte T, Stolz D. Serum levels of hyaluronic acid are associated with COPD severity and predict survival. *Eur Respir J* 2019; 53.

216. Auerbach O, Garfinkel L, Hammond EC. Relation of smoking and age to findings in lung parenchyma: a microscopic study. *Chest* 1974; 65: 29-35.

217. Cottin V, Nunes H, Brillet PY, Delaval P, Devouassoux G, Tillie-Leblond I, Israel-Biet D, Court-Fortune I, Valeyre D, Cordier JF, Groupe d'Etude et de Recherche sur les Maladies Orphelines P. Combined pulmonary fibrosis and emphysema: a distinct underrecognised entity. *Eur Respir J* 2005; 26: 586-593.

218. Jankowich MD, Rounds S. Combined pulmonary fibrosis and emphysema alters physiology but has similar mortality to pulmonary fibrosis without emphysema. *Lung* 2010; 188: 365-373.

219. Jankowich MD, Rounds SIS. Combined pulmonary fibrosis and emphysema syndrome: a review. *Chest* 2012; 141: 222-231.

220. Archer SL, Weir EK, Wilkins MR. Basic science of pulmonary arterial hypertension for clinicians: new concepts and experimental therapies. *Circulation* 2010; 121: 2045-2066.

221. Garcia-Morales LJ, Chen NY, Weng T, Luo F, Davies J, Philip K, Volcik KA, Melicoff E, Amione-Guerra J, Bunge RR, Bruckner BA, Loebe M, Eltzschig HK, Pandit LM, Blackburn MR, Karmouty-Quintana H. Altered Hypoxic-Adenosine Axis and Metabolism in Group III Pulmonary Hypertension. *American journal of respiratory cell and molecular biology* 2016; 54: 574-583.

222. Karmouty-Quintana H, Philip K, Acero LF, Chen NY, Weng T, Molina JG, Luo F, Davies J, Le NB, Bunge I, Volcik KA, Le TT, Johnston RA, Xia Y, Eltzschig HK, Blackburn MR. Deletion of ADORA2B from myeloid cells dampens lung fibrosis and pulmonary hypertension. *FASEB journal : official publication of the Federation of American Societies for Experimental Biology* 2015; 29: 50-60.

223. Philip K, Mills TW, Davies J, Chen NY, Karmouty-Quintana H, Luo F, Molina JG, Amione-Guerra J, Sinha N, Guha A, Eltzschig HK, Blackburn MR. HIF1A up-regulates the ADORA2B receptor on alternatively activated macrophages and contributes to pulmonary fibrosis. *FASEB journal : official publication of the Federation of American Societies for Experimental Biology* 2017; 31: 4745-4758.

224. Chunn JL, Molina JG, Mi T, Xia Y, Kellems RE, Blackburn MR. Adenosine-dependent pulmonary fibrosis in adenosine deaminase-deficient mice. *Journal of immunology (Baltimore, Md : 1950)* 2005; 175: 1937-1946.

225. Karmouty-Quintana H, Xia Y, Blackburn MR. Adenosine signaling during acute and chronic disease states. *J Mol Med (Berl)* 2013; 91: 173-181.

226. Collum SD, Chen NY, Hernandez AM, Hanmandlu A, Sweeney H, Mertens TCJ, Weng T, Luo F, Molina JG, Davies J, Horan IP, Morrell NW, Amione-Guerra J, Al-Jabbari O, Youker K, Sun W, Rajadas J, Bollyky PL, Akkanti BH, Jyothula S, Sinha N, Guha A, Karmouty-Quintana H. Inhibition of hyaluronan synthesis attenuates pulmonary hypertension associated with lung fibrosis. *Br J Pharmacol* 2017; 174: 3284-3301.

227. Le TT, Karmouty-Quintana H, Melicoff E, Le TT, Weng T, Chen NY, Pedroza M, Zhou Y, Davies J, Philip K, Molina J, Luo F, George AT, Garcia-Morales LJ, Bunge RR, Bruckner BA, Loebe M, Seethamraju H, Agarwal SK, Blackburn MR. Blockade of IL-6 Trans signaling attenuates pulmonary fibrosis. *Journal of immunology (Baltimore, Md : 1950)* 2014; 193: 3755-3768.

228. Luo F, Le N-B, Mills T, Chen N-Y, Karmouty-Quintana H, Molina JG, Davies J, Philip K, Volcik KA, Liu H, Xia Y, Eltzschig HK, Blackburn MR. Extracellular adenosine levels are associated with the progression and exacerbation of pulmonary fibrosis. *FASEB journal : official publication of the Federation of American Societies for Experimental Biology* 2016; 30: 874-883.

229. Burgstaller G, Oehrle B, Gerckens M, White ES, Schiller HB, Eickelberg O. The instructive extracellular matrix of the lung: basic composition and alterations in chronic lung disease. *Eur Respir J* 2017; 50.

230. The Lancet Respiratory M. Lung disease left out in the cold. *The Lancet Respiratory medicine* 2016; 4: 527.

231. Vlahos R, Bozinovski S. Preclinical murine models of Chronic Obstructive Pulmonary Disease. *European journal of pharmacology* 2015; 759: 265-271.

232. Cattani-Cavalieri I, Reis AG, Kennedy-Feitosa E, Pinho-Ribeiro V, Lanzetti M, Gitirana LB, Romana-Souza B, Porto LC, Valença SS. Pulmonary Emphysema Cross-Linking with Pulmonary Fibrosis and Vice Versa: a Non-usual Experimental Intervention with Elastase and Bleomycin. *Inflammation* 2017; 40: 1487-1496.

233. Trajano LA, Trajano ET, Lanzetti M, Mendonca MS, Guilherme RF, Figueiredo RT, Benjamim CF, Valenca SS, Costa AM, Porto LC. Elastase modifies bleomycin-induced pulmonary fibrosis in mice. *Acta histochemica* 2016; 118: 203-212.

234. Zhang W-G, Wu S-S, He L, Yang Q, Feng Y-K, Chen Y-T, Zhen G-H, Xu Y-J, Zhang Z-X, Zhao J-P, Zhang H-L. Comparative study of two models of combined pulmonary fibrosis and emphysema in mice. *Acta histochemica* 2017; 119: 244-251.

235. Aggarwal S, Ahmad I, Lam A, Carlisle MA, Li C, Wells JM, Raju SV, Athar M, Rowe SM, Dransfield MT, Matalon S. Heme scavenging reduces pulmonary endoplasmic reticulum stress, fibrosis, and emphysema. *JCI insight* 2018; 3.

236. Blackburn MR, Datta SK, Kellems RE. Adenosine deaminase-deficient mice generated using a two-stage genetic engineering strategy exhibit a combined immunodeficiency. *The Journal of biological chemistry* 1998; 273: 5093-5100.

237. Blackburn MR, Volmer JB, Thrasher JL, Zhong H, Crosby JR, Lee JJ, Kellems RE. Metabolic consequences of adenosine deaminase deficiency in mice are associated with defects in alveogenesis, pulmonary inflammation, and airway obstruction. *The Journal of experimental medicine* 2000; 192: 159-170.

238. Schneider DJ, Lindsay JC, Zhou Y, Molina JG, Blackburn MR. Adenosine and osteopontin contribute to the development of chronic obstructive pulmonary disease. *FASEB journal : official publication of the Federation of American Societies for Experimental Biology* 2010; 24: 70-80.

239. Sun CX, Zhong H, Mohsenin A, Morschl E, Chunn JL, Molina JG, Belardinelli L, Zeng D, Blackburn MR. Role of A2B adenosine receptor signaling in adenosine-dependent pulmonary inflammation and injury. *The Journal of clinical investigation* 2006; 116: 2173-2182.

240. Bracke KR, Dentener MA, Papakonstantinou E, Vernooy JHJ, Demoor T, Pauwels NS, Cleutjens J, Suylen RJv, Joos GF, Brusselle GG, Wouters EFM. Enhanced Deposition of Low-Molecular-Weight Hyaluronan in Lungs of Cigarette Smoke–Exposed Mice. *American journal of respiratory cell and molecular biology* 2010; 42: 753-761.

241. Chen NY, S DC, Luo F, Weng T, Le TT, A MH, Philip K, Molina JG, Garcia-Morales LJ, Cao Y, Ko TC, Amione-Guerra J, Al-Jabbari O, Bunge RR, Youker K, Bruckner BA, Hamid R, Davies J, Sinha N, Karmouty-Quintana H. Macrophage bone morphogenic protein receptor 2 depletion in idiopathic pulmonary fibrosis and Group III pulmonary hypertension. *American journal of physiology Lung cellular and molecular physiology* 2016; 311: L238-254.

242. Pedroza M, Schneider DJ, Karmouty-Quintana H, Coote J, Shaw S, Corrigan R, Molina JG, Alcorn JL, Galas D, Gelinas R, Blackburn MR. Interleukin-6 Contributes to Inflammation and Remodeling in a Model of Adenosine Mediated Lung Injury. *PloS one* 2011; 6: e22667.

243. Itano N, Sawai T, Yoshida M, Lenas P, Yamada Y, Imagawa M, Shinomura T, Hamaguchi M, Yoshida Y, Ohnuki Y, Miyauchi S, Spicer AP, McDonald JA, Kimata K. Three isoforms of mammalian hyaluronan synthases have distinct enzymatic properties. *The Journal of biological chemistry* 1999; 274: 25085-25092.

244. Colgan SP, Eltzschig HK, Eckle T, Thompson LF. Physiological roles for ecto-5'-nucleotidase (CD73). *Purinergic signalling* 2006; 2: 351-360.

245. Fredholm BB, AP IJ, Jacobson KA, Klotz KN, Linden J. International Union of Pharmacology. XXV. Nomenclature and classification of adenosine receptors. *Pharmacol Rev* 2001; 53: 527-552.

246. Zhou Y, Schneider DJ, Blackburn MR. Adenosine signaling and the regulation of chronic lung disease. *Pharmacology & therapeutics* 2009; 123: 105-116.

247. Zhou Y, Murthy JN, Zeng D, Belardinelli L, Blackburn MR. Alterations in adenosine metabolism and signaling in patients with chronic obstructive pulmonary disease and idiopathic pulmonary fibrosis. *PloS one* 2010; 5: e9224.

248. Mustafa SJ, Nadeem A, Fan M, Zhong H, Belardinelli L, Zeng D. Effect of a specific and selective A(2B) adenosine receptor antagonist on adenosine agonist AMP and allergen-induced airway responsiveness and cellular influx in a mouse model of asthma. *The Journal of pharmacology and experimental therapeutics* 2007; 320: 1246-1251.

249. Weng T, Karmouty-Quintana H, Garcia-Morales LJ, Molina JG, Pedroza M, Bunge RR, Bruckner BA, Loebe M, Seethamraju H, Blackburn MR. Hypoxia-induced

deoxycytidine kinase expression contributes to apoptosis in chronic lung disease. *FASEB J* 2013; 27: 2013-2026.

250. Plataki M, Tzortzaki E, Rytila P, Demosthenes M, Koutsopoulos A, Siafakas NM. Apoptotic mechanisms in the pathogenesis of COPD. *Int J Chron Obstruct Pulmon Dis* 2006; 1: 161-171.

251. Liang OD, So EY, Egan PC, Goldberg LR, Aliotta JM, Wu KQ, Dubielecka PM, Ventetuolo CE, Reginato AM, Quesenberry PJ, Klinger JR. Endothelial to haematopoietic transition contributes to pulmonary arterial hypertension. *Cardiovasc Res* 2017; 113: 1560-1573.

252. Kurokawa M, Hirai H. Role of AML1/Runx1 in the pathogenesis of hematological malignancies. *Cancer Sci* 2003; 94: 841-846.

253. Ruffenach G, Chabot S, Tanguay VF, Courboulin A, Boucherat O, Potus F, Meloche J, Pflieger A, Breuils-Bonnet S, Nadeau V, Paradis R, Tremblay E, Girerd B, Hautefort A, Montani D, Fadel E, Dorfmuller P, Humbert M, Perros F, Paulin R, Provencher S, Bonnet S. Role for Runt-related Transcription Factor 2 in Proliferative and Calcified Vascular Lesions in Pulmonary Arterial Hypertension. *Am J Respir Crit Care Med* 2016; 194: 1273-1285.

254. Negi V, Chan SY. Discerning functional hierarchies of microRNAs in pulmonary hypertension. *JCI Insight* 2017; 2: e91327.

255. Sartini BL, Wang H, Wang W, Millette CF, Kilpatrick DL. Pre-messenger RNA cleavage factor I (CFIm): potential role in alternative polyadenylation during spermatogenesis. *Biol Reprod* 2008; 78: 472-482.

256. Garrett ER, Venitz J. Comparisons of detections, stabilities, and kinetics of degradation of hymecromone and its glucuronide and sulfate metabolites. *J Pharm Sci* 1994; 83: 115-116.

257. Trabucchi E, Baratti C, Centemero A, Zuin M, Rizzitelli E, Colombo R. Controlled study of the effects of tiropramide on biliary dyskinesia. *Pharmatherapeutica* 1986; 4: 541-550.

258. Kudo D, Kon A, Yoshihara S, Kakizaki I, Sasaki M, Endo M, Takagaki K. Effect of a hyaluronan synthase suppressor, 4-methylumbelliferone, on B16F-10 melanoma cell adhesion and locomotion. *Biochem Biophys Res Commun* 2004; 321: 783-787.

259. Nakazawa H, Yoshihara S, Kudo D, Morohashi H, Kakizaki I, Kon A, Takagaki K, Sasaki M. 4-methylumbelliferone, a hyaluronan synthase suppressor, enhances the anticancer activity of gemcitabine in human pancreatic cancer cells. *Cancer Chemother Pharmacol* 2006; 57: 165-170.

260. Jenkins RG, Moore BB, Chambers RC, Eickelberg O, Konigshoff M, Kolb M, Laurent GJ, Nanthakumar CB, Olman MA, Pardo A, Selman M, Sheppard D, Sime PJ, Tager AM, Tatler AL, Thannickal VJ, White ES. An Official American Thoracic Society Workshop Report: Use of Animal Models for the Preclinical Assessment of Potential Therapies for Pulmonary Fibrosis. *Am J Respir Cell Mol Biol* 2017; 56: 667-679.

261. King TE, Jr., Pardo A, Selman M. Idiopathic pulmonary fibrosis. *Lancet* 2011; 378: 1949-1961.

262. Lederer DJ, Martinez FJ. Idiopathic Pulmonary Fibrosis. *New England Journal of Medicine* 2018; 378: 1811-1823.

263. Redente EF, Jacobsen KM, Solomon JJ, Lara AR, Faubel S, Keith RC, Henson PM, Downey GP, Riches DW. Age and sex dimorphisms contribute to the severity of bleomycin-induced lung injury and fibrosis. *American journal of physiology Lung cellular and molecular physiology* 2011; 301: L510-518.

264. Malli F, Papakosta D, Antoniou K, Dimadi M, Polychronopoulos V, Malagari K, Oikonomou A, Bouros DE, Daniil Z. Combined pulmonary fibrosis and emphysema characteristics in a Greek cohort. *ERJ Open Res* 2019; 5.

Vita

Scott Dale Collum was born in Stephenville, Texas. After graduating from Huckabay High School in 2008, Scott pursued his Bachelor of Science in Biochemistry at Texas A&M University, graduating in 2012. He began the PhD program in the Department of Biochemistry and Molecular Biology at The University of Texas MD Anderson Cancer Center UTHealth Graduate School of Biomedical Sciences in 2012.

Permanent Address:

740 Cr 435

Stephenville, TX 76401

Publications

Collum SD, Chen NY, Hernandez AM, Hanmandlu A, Sweeney H, Mertens TCJ, Weng T, Luo F, Molina JG, Davies J, Horan IP, Morrell NW, Amione-Guerra J, Al-Jabbari O, Youker K, Sun W, Rajadas J, Bollyky PL, Akkanti BH, Jyothula S, Sinha N, Guha A, Karmouty-Quintana H. Inhibition of hyaluronan synthesis attenuates pulmonary hypertension associated with lung fibrosis. *Br J Pharmacol* 2017

Collum SD, Molina JG, Hanmandlu A, Bi W, Pedroza M, Mertens TCJ, Wareing N, Wei W, Wilson C, Sun W, Rajadas J, Bollyky PL, Philip KM, Ren D, Thandavarayan RA, Bruckner BA, Xia Y, Blackburn MR, Karmouty-Quintana H. Adenosine and

hyaluronan modulate lung fibrosis and pulmonary hypertension in combined pulmonary fibrosis and emphysema (CPFE). *Dis Model Mech* 2019.

Collum SD, Amione-Guerra J, Cruz-Solbes AS, DiFrancesco A, Hernandez AM, Hanmandlu A, Youker K, Guha A, Karmouty-Quintana H. Pulmonary Hypertension Associated with Idiopathic Pulmonary Fibrosis: Current and Future Perspectives. *Can Respir J* 2017

Masamha CP, Xia Z, Peart N, **Collum S**, Li W, Wagner EJ, Shyu AB. CFIm25 regulates glutaminase alternative terminal exon definition to modulate miR-23 function. *RNA* 2016

Mertens TCJ, Hanmandlu A, Tu L, Phan C, **Collum SD**, Chen NY, Weng T, Davies J, Liu C, Eltzschig HK, Jyothula SSK, Rajagopal K, Xia Y, Guha A, Bruckner BA, Blackburn MR, Guignabert C, Karmouty-Quintana H. Switching-Off Adora2b in Vascular Smooth Muscle Cells Halts the Development of Pulmonary Hypertension. *Front Physiol* 2018

Headley L, Bi W, Wilson C, **Collum SD**, Chavez M, Darwiche T, Mertens TCJ, Hernandez AM, Siddiqui SR, Rosenbaum S, Johnston RA, Karmouty-Quintana H. Low-dose administration of bleomycin leads to early alterations in lung mechanics. *Exp Physiol* 2018

Karmouty-Quintana H, Molina JG, Philip K, Bellocchi C, Gudenkauf B, Wu M, Chen NY, **Collum SD**, Ko J, Agarwal SK, Assassi S, Zhong H, Blackburn MR, Weng T. The Antifibrotic Effect of A2B Adenosine Receptor Antagonism in a Mouse Model of Dermal Fibrosis. *Arthritis Rheumatol* 2018

Weng T, Ko J, Masamha CP, Xia Z, Xiang Y, Chen NY, Molina JG, **Collum S**, Mertens TC, Luo F, Philip K, Davies J, Huang J, Wilson C, Thandavarayan RA, Bruckner BA, Jyothula SS, Volcik KA, Li L, Han L, Li W, Assassi S, Karmouty-Quintana H, Wagner EJ, Blackburn MR. Cleavage factor 25 deregulation contributes to pulmonary fibrosis through alternative polyadenylation. *J Clin Invest* 2019

Darwiche T, **Collum SD**, Bi W, Reynolds JO, Wilson C, Wareing N, Hernandez AM, Mertens TCJ, Zhou Z, Pandit LM, Karmouty-Quintana H. Alterations in cardiovascular function in an experimental model of lung fibrosis and pulmonary hypertension. *Exp Physiol* 2019